Effect of the Interphase on the Thermo-Mechanical Response of Unidirectional Fiber-Reinforced Epoxies: Modeling, Analyses and Experiments

by

Krishnan Jayaraman

Dissertation submitted to the Faculty of the

Virginia Polytechnic Institute and State University

in partial fulfillment of the requirements for the degree of

Doctor of Philosophy

in

Engineering Mechanics

APPROVED:

Kenneth L. Reifsnider, Chairman

Charles W. Smith

Edmund G. Henneke II

Junuthula N. Reddy

Mark S. Cramer

David A. Dillard

August, 1992

Blacksburg, Virginia

Effect of the Interphase on the Thermo-Mechanical Response of Unidirectional Fiber-Reinforced Epoxies: Modeling, Analyses and Experiments

by

Krishnan Jayaraman

Kenneth L. Reifsnider, Chairman

Engineering Mechanics

(ABSTRACT)

The complexity of the fiber-matrix interphase in a composite is largely due to the myriad of variables (material, processing, and design) that affect its formation. The interphase, thus formed, has to be characterized at several levels (micro-structural, chemical, and mechanical) in order for one to fully understand the nature of the bond between the fiber and matrix and in order to perform a stress analysis of the fiber-interphase-matrix assemblage.

A thorough thermo-mechanical characterization of the interphase is difficult, at present, due to the necessity of studying the interphase *in situ*, its small dimension (usually on the order of a micrometer), and its general complexity. However, a cursory glance at the literature shows that great progress has been made in all of the three levels of characterization mentioned above for various composite systems. Several recent attempts have focused on the physical characterization (evaluation of volume fraction, thickness, Young's modulus, shear modulus and coefficient of thermal expansion) of the interphase.

Models of physical properties (thickness, Young's modulus, Poisson's ratio and coefficient of thermal expansion) of the interphase have been considered by several researchers in an effort to study the influence of the interphase on overall composite properties and behavior. Hypotheses on interphase formation and properties have been proposed and tested by some researchers. Both experimental characterization as well as modeling studies are necessary to achieve a more profound understanding of the interphase and its behavior.

The interphase, in a composite, is usually modeled as a homogeneous region, despite the fact that it may have spatial property variations. However, it is important to the

understanding of composite behavior to incorporate a realistic interphasial region into the analysis and testing of composite material systems. A new thermo-elastic model for the interphase properties in fiber-reinforced thermosets is proposed. The Young's modulus and coefficient of thermal expansion of the interphase are assumed to be functions of distance from the fiber in this model. The Poisson's ratio of the interphase is assumed to be the same as that of the matrix.

The new model is used in a concentric cylinder assemblage analysis for the determination of the residual thermal stresses in unidirectional fiber-reinforced epoxies. The governing field equations in terms of displacements are solved in "closed form". It is found that, although the solution is *dilute*, the property variations in the interphase have a distinct effect on the residual thermal stresses. This is significant, considering the fact that residual thermal stresses play an important role in controlling the structural performance of a composite.

The new model is used in Mori-Tanaka analyses for the determination of *non-dilute* local stress fields in unidirectional fiber-reinforced epoxies under thermo-mechanical loading situations. The governing field equations in terms of displacements are solved in "closed form". It is found that property variations in the interphase have a distinct effect on the local stresses. This is also significant, considering the fact that local stresses play an important role in controlling the structural performance of a composite.

A model composite system consisting of a coated glass rod embedded in Epon 828 is considered; coatings are applied to the glass rod in succession to simulate two different interphase types. The model composite specimens are loaded in transverse compression and transverse shear, and the resulting in-plane displacements are measured by the use of the Moire interferometry technique. Differences in displacement fields between the various specimens, due to the presence of interphasial regions, are found to be minimal. More sensitive measurements are needed to measure pointwise displacements in the interphasial (coatings) region.

Acknowledgements

The author acknowledges with gratitude the efforts of the members of his committee in providing help in this difficult undertaking. Specifically, he expresses his appreciation to:

- Dr. K. L. Reifsnider for assistance in defining the materials and mechanics aspects of the "interphase problem", and for providing financial assistance through the National Science Foundation Science & Technology Center for High Performance Polymeric Adhesives and Composites,
- Prof. C. W. Smith for educating the author about elasticity theory and applications, and for sharing anecdotes about various elasticians,
- Dr. D. A. Dillard for helpful discussions regarding specimen preparation, and for permission to use the facilities of the Georgia Pacific Adhesion Laboratory, and
- Dr. E. G. Henneke, Dr. J. N. Reddy and Dr. M. S. Cramer for their suggestions and support.

Sincere thanks are due to:

- Ms. B. Wengert, Ms. S. Collins and Ms. M. Morrozoff for taking care of the necessary bureaucratic work with good humor,
- Dr. Z. Gao for patiently explaining the ideas behind the research work of Eshelby and Mori and Tanaka,

- Mr. R. Ramchander for helping me get familiar with personal computers,
- Dr. G. S. Haldankar and Dr. A. Garton (Department of Chemistry, University of Connecticut) for making model composite samples,
- Mr. R. Davis (Machine Shop, Department of Engineering Science and Mechanics, Virginia Polytechnic Institute and State University) for cutting the specimens,
- Dr. P. Ifju and Dr. B-T. Han (Photomechanics Laboratory, Department of Engineering Science and Mechanics, Virginia Polytechnic Institute and State University) for help with the Moire interferometry experiments,
- Mr. A. Tiwari, Dr. R. E. Swain, Dr. A. Razvan and Mr. S. S. Lee for helping the author find his way around the laboratories, and
- All those who have come and gone through the Patton Hall graduate students office.

Finally the author extends his warm appreciation to members of his family for being a constant source of strength and inspiration.

Table of Contents

List of Illustrations

List of Tables

1.0 Introduction

Modifications to the glass fiber-resin interface in reinforced plastics have been attempted since 1942 in order to improve the properties of such composites [1]. By 1963, it was clear that the mechanical performance of reinforced plastics depended not only on the fiber and matrix, but also on the effectiveness of the fiber-matrix bond in transferring the stresses across the interface. Systematic examinations of the types of interfaces in tungsten-reinforced copper alloys were performed by Petrasek and Weeton [2] in 1964; the tensile strength and ductility of this composite was found to be dependent on the interface reaction. A general scheme for interface classification was also developed for metal matrix composites around this time, based on the type of chemical reaction occurring between the fiber and matrix. Brennan [3] has recently (1986) examined the interface in a Nicalon/lithium aluminosilicate (LAS-III) composite using the Scanning Auger Microprobe analysis. It was concluded, based on this analysis, that the interfacial chemistry determined, to a large extent, the toughness of this composite. The above references clearly show that the importance of interfaces to composite behavior has long been recognized. But, over the years, applied developmental work seems to have provided the major impetus for the study of interphases. The knowledge obtained from the fields of material science, chemistry, mechanics, and chemical engineering

about the nature of the interaction between the fiber and matrix has not resulted in a mechanistic characterization of the interphase suitable for local failure analysis in composites.

In the past, the word "interface" was used to refer to both an imaginary entity between the fiber and matrix (a curved plane to which certain mechanical properties were sometimes attributed), and a finite region between the fiber and matrix (a cylindrical shell having certain definite properties). But, of late, the words "interface", and "interphase" are both being used, sometimes to refer to the same entity. Hence, the precise definitions of the words *phase, interphase, interface, surface treatment, sizing, finish* and *coating* as applied to unidirectional fiber reinforced composite micromechanics are a necessary first step in the study of fiber-matrix bonds. They are:

Phase A phase is a physically distinct and a mechanically separable entity with a given chemical composition and micro-structure; the fiber and matrix are examples of a solid phase.

Interphase The interphase is defined as the region that is formed due to the bonding between the fiber and matrix; it has a significantly distinct morphology or chemical composition as compared to the bulk fiber and/or the bulk matrix. The interphase may be a diffusion zone, a nucleation zone, a chemical reaction zone, etc., or any combination of the above [4].

Interface An interface is defined as a two-dimensional boundary separating distinct phases like the fiber, matrix, and the interphase [4]. When the interphase becomes vanishingly thin, in the limit, it becomes an interface.

Surface Treatment Fiber surface treatments are designed to promote fiber-matrix adhesion by removing a weak outer layer initially present on the fiber and adding surface chemical groups which increase interaction with the matrix [5].

Sizing A sizing is a mixture of a lubricant and a binder applied to the fiber after manufacture to protect its surface and aid the process of handling and fabrication. The sizing is usually removed by heat-cleaning before the finish is applied [6].

Finish A finish is a mixture of processing aids (lubricant, wetting agent, and coupling agent) applied to the fiber surface to enhance fiber-matrix adhesion. The finish protects the fiber from abrasive damage during handling, improves the wettability of the fiber and protects fiber surface reactivity [6, 7].

Coating A coating is a material applied to the fiber surface, as in the case of metal matrix and ceramic matrix composites, to reduce and/or control the reaction between the fiber and matrix.

The reader is reminded that the words "sizing" and "finish" are used interchangeably by some authors [7].

All the factors that affect the formation of a composite may also affect the formation of the interphase. These factors can be classified into :

- Choice of materials
  - Fiber -- material, surface treatment, sizing, diameter, shape, volume fraction, manufacturing methods.
  - Matrix -- material, additives, morphology, processing methods.
- Processing variables -- cure temperature, cure time, cure pressure, prepregging methods, fabrication methods.
- Lamination scheme -- presence of interleaves, number of plies.
- History -- history of exposure to mechanical, thermal and chemical environments.

The interphase that results consists of several "components" or "layers", as illustrated by a schematic representation for polymeric composites adapted from Verpoest, *et al.* [8]. The components can be identified as follows (see Figure 1):

a. The bulk fiber.

b. A fiber surface layer possessing a different micro-structure or chemical composition compared to the bulk fiber.

c. An outer fiber layer altered by fiber surface treatments.

d. A layer where the fiber bonds to the sizing.

e. A sizing or coupling agent layer.

f. A layer where the matrix micro-structure and/or chemical composition gradually changes from that of the sizing to that of the bulk matrix.

g. The bulk matrix.

Drzal [9] has presented a similar schematic for a polymeric composite interphase and has discussed the characteristics of the various components. Schematic representations of the interphase in metal matrix composites [10] and ceramic matrix composites [11] have also been discussed in the literature.

A multicomponent interphase has a complex micro-structure and/or chemical composition which may have an effect on the physical and thermo-mechanical properties of the interphase. This fact has been discussed by several researchers [8, 9, 12-16]:

- Erickson, *et al.* [12] note that: " The deformable resin layer (interphase layer) in glass fiber reinforced plastics may have thicknesses of several hundred Angstroms. The modulus properties of this deformable resin layer are presumed to vary with distance from the glass (fiber) surface. Many other properties of the layer, such as toughness, ductility, and plasticity, may and probably do, vary in an analogous manner."
- Metcalfe [13] points out that the interaction compound in boron-titanium composites will possess an elastic modulus different from that of the fiber and matrix.
- Sharpe [14] suggests that " ... the boundary layers (interphase) differ structurally from the bulk materials with which they are in contact. They must, therefore, differ mechanically."
- Drzal [9] states that: "Depending on the (composite) system, the interphase itself can extend from a few to a few hundred nanometers in depth. The structure of this region can have profound effects on the performance of the composite."
- Sottos, *et al.* [15] feel that " ... it is reasonable to assume that in most composite systems, the fiber/matrix interactions create a gradient in resin properties near the interface."
- Verpoest, *et al.* [8] express the opinion that: " ... the interface could be considered to have its own stiffness. Fracture, for instance, can occur in any of the layers, as each of them has a different strength or fracture behavior."

- Tsai, *et al.* [16] recognize that "the true interphase region has radially varying properties and can also exhibit circumferential property gradients."

The author concludes, based on the publications quoted above, that the interphase may possess such features as:

- a finite dimension or thickness,
- elastic or inelastic response,
- a degree of anisotropy,
- tensorial bond strength associated with adhesion to the fibers,
- tensorial bond strength associated with adhesion to the matrix, and
- tensorial values of modulus, coefficient of thermal expansion, Poisson's ratio, and cohesive strength (possibly functions of position in the radial and azimuthal directions).

Hence, the interphase has to be characterized and/or modeled in a manner similar to the characterization of the fiber and matrix if it is to be incorporated into micromechanical models.

This dissertation addresses the following issues relating to the interphase in fiber-reinforced epoxies:

- a review of characterization methods,
- a review of modeling studies,
- a new model for interphase properties,
- a study of the effect of a distinct interphase on residual thermal stresses,
- a study of the effect of a distinct interphase on local stresses under thermo-mechanical loading, and
- an experimental study of interphasial effects.

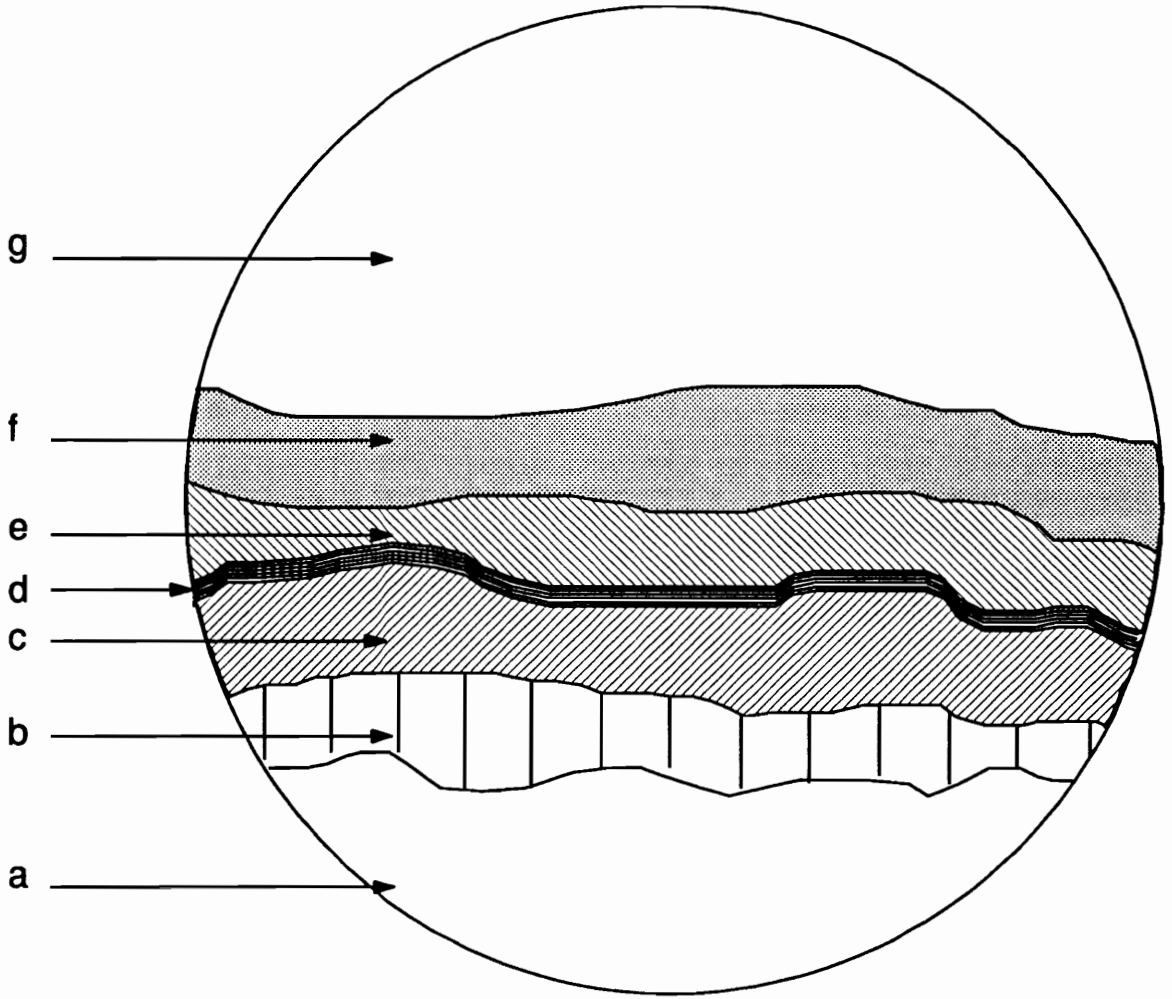

Figure 1. Schematic representation of the interphase region in polymeric composites based on the schematics of Verpoest, et al. [8] and Drzal [9]: See page 3 for a description of the components a to g.

2.0 Characterization Methods

Published work regarding the structure and role of the fiber/matrix interphase has been growing in quantity and quality in recent years [17-19]. However, study of the thermo-mechanical properties of the interphase has not received much attention due to the difficulties involved in interphasial property measurements; most of the research efforts have been confined to polymeric composites. This chapter provides a brief review of the principal characterization methods and discusses recent attempts at physical characterization (evaluation of volume fraction, thickness, Young's modulus, shear modulus, and coefficient of thermal expansion) of the interphase.

2.1 Principal Methods of Interphase Characterization

As research in the area of interphase characterization grows, new methods come into existence and older ones are modified. It would be a formidable task to review all the current methods available. This section deals with only three principal characterization

methods that are being used extensively by researchers: micro-structural, chemical, and mechanical methods. The following three sub-sections describe these methods.

2.1.1 Micro-structural Characterization

It would be desirable to have a means to directly image the physical structure and environment of the interphase. Several types of microscopes are available for direct imaging, such as the Optical Microscope, Scanning Electron Microscope (SEM), Transmission Electron Microscope (TEM), and Scanning Tunneling Microscope (STM). While the SEM and TEM are currently the workhorses of the interphase research community, the STM may be used for interphase imaging in the future.

Lerch, *et al.* [20] have recently used a technique called "interference layering" that accentuates the differences between the various phases in a SiC/Ti-15-3 composite as seen through an optical microscope. An interference layer of platinum was deposited on the specimen surface and the surface was viewed under visible light. The light waves incident on the specimen surface were attenuated by multiple reflections at the specimen/platinum and the platinum/air interfaces resulting in contrast enhancement and color separation for each phase. The interference layered specimen clearly revealed the presence of the following phases: carbon core, the pyrolitic coating, the mid-radius grain size change, the individual coatings on the fiber surface, the reaction zone and the various matrix features.

PEEK is a semi-crystalline polymer whose partly crystalline morphology can affect its properties. The crystalline morphology consists mainly of closely packed spherulites, which are structures that start at nucleation points and grow radially outward. Peacock, *et al.* [21] have used the SEM in their study of crystallization in AS4/PEEK (APC-2) composites. The composite sample was polished and chemically etched to reveal the presence of fibers and the underlying crystalline structure as shown in Figure 2. Nucleation from the carbon fibers dominated the morphology, with spherulites growing from the fiber surface into the matrix.

Peacock, *et al.* [21] have concluded that this controlled, crystalline interphasial morphology resulted in good fiber-matrix adhesion in APC-2 composites.

Brennan [22, 23] has used the TEM extensively to study the interphases in a variety of glass-ceramic matrix/silicon carbide fiber composites using replicas of polished composite cross-sections and ion-beam thinned sections. Figure 3 shows a TEM thin foil micrograph of a Nicalon/LAS-III composite; a carbon rich, light colored zone and a dark Niobium Carbide layer were identified between the fiber and matrix using Energy Dispersive X-ray Spectroscopy (EDXS) analysis. Brennan [22] has concluded that the interphasial carbon rich layer, being weaker than the fiber or matrix, contributed to the ability of Nicalon/LAS-III to deflect matrix cracks, thus increasing the material's fracture toughness.

The STM is a relatively new technique that measures surface topography with a vertical resolution of 0.1 Å and a horizontal resolution of 2.6 Å, approximately [24]. The STM consists of a needle, usually made from tungsten, whose tip is either ground or etched until it is one atom wide. This tip is lowered within a billionth of an inch from the surface to be imaged and a small voltage is applied. Electrons tunnel between the tip and the surface creating a measurable current. In the *constant current mode*, the current between the tip and the surface is sensed; a feedback network changes the height of the tip to keep the current constant. An image consists of a map of the tip height versus the lateral position. In the *constant height mode*, the tip is moved across a surface at a nearly constant height and constant voltage while the current is sensed; a feedback network keeps the average current constant. The image consists of the rapid variations in current plotted against lateral position. The remarkable precision of the instrument is due to the exponential variation of the tunneling current with the distance between the tip and the surface. Hansma and Tersoff [24] have speculated about the future of STM and some of these ideas have a direct bearing on interphase studies. These ideas include:

- Determination of accurate surface structure,
- Potential in molecular vibrational spectroscopy, and
- Potential for atomic scale manipulation.

2.1.2 Chemical Characterization

Several techniques are currently being used to improve fiber-matrix adhesion in composites; the chemistry of the resulting interphases needs to be studied in order to understand the factors that contribute to the improved adhesion. The characterization techniques that are typically used to study the chemical constitution of the interphase started out as surface analytical methods that have evolved over the years; Feldman and Mayer [25] have discussed the fundamentals of many of these techniques. These techniques are numerous and offer a variety of choices between depth sensitivity, x-y spatial resolution (or spot size) and concentration limits as shown in Figure 4 [26]. The four most widely used techniques with commercially available instrumentation are: XPS, AES, ISS and SIMS (see Figure 4 for acronym description). Occhiello, *et al.*, [27] while providing an excellent review of the spectroscopic methods that can be used to study the chemistry of interphases in polymer composites, have also declared that "most of the work has been performed to study the modification of fillers to improve adhesion, since it is less difficult than looking at the real interface."

Brennan [23] has used the Scanning Auger Microprobe to study the elemental composition in the fiber and matrix of a Nicalon/LAS-III composite. The probe used had a minimum electron beam spot size of less than 500 Å and a typical electron emission depth of 10-30 Å; Argon-ion beam *in situ* sputtering was used to obtain the depth profile. The surfaces of unsized fibers, fibers from a fracture surface parallel to the fiber direction, and matrix troughs from which fibers have been pulled away were studied. The findings can be summarized as follows :

- The surface of the unsized fiber was high in oxygen and low in carbon content (see Figure 5).

- The surface of the fiber from a longitudinal fracture surface showed a carbon rich layer of the order of 500 Å in thickness. The composition stabilized out to the bulk fiber composition at a depth of about 3000 Å (see Figure 6).
- The composition down through the matrix trough stabilized out to the bulk matrix composition at a depth of about 5000 Å.

Thus, a region of approximately 8000 Å was found between the fiber and matrix where the chemical composition was neither that of the bulk fiber nor that of the bulk matrix.

Lerch, *et al.* [20] have utilized the Electron Microprobe Analysis, in a Wavelength Dispersive Spectroscopy mode, to study the elemental composition in the fiber and matrix of a SiC/Ti-15-3 composite. The specimen was cut longitudinally, almost parallel to the fibers, so that the thickness of the interphase region would be exaggerated. The relative changes in the element concentrations, obtained as elemental X-ray intensities, were recorded as an electron beam moved across the specimen, from the fiber into the matrix. Plots of elemental X-ray intensity with respect to position revealed a reaction zone of approximately 0.10 to 0.35 μm between the fiber and matrix.

Thomason and Morsink [28] have investigated the chemical nature of the interphase in glass/Epikote 828 (with 32 phr Epikure 113) composites using Scanning Secondary Ion Mass Spectrometry (SSIMS). The T_g of the fiber sizing (54.2 °C) was used as a control parameter in the production of laminates with the same fiber and matrix but with different interphases. This was carried out as follows:

- A laminate, designated as composite 157, was prepared and initially cured at 23 °C for 18 hours, in order to localize the sizing around the fiber.
- A laminate, designated as composite 161, was prepared and initially cured at 50 °C for 18 hours, in an attempt to disperse the sizing around the fiber.
- Both laminates were then postcured at increasing temperature steps of 25 °C per hour ending with a 2 hour postcure at 150 °C.

Samples for SSIMS investigation were prepared from each of the laminates by taking cross-sections perpendicular to the fibers and then polishing them. Figure 7 shows maps of O^- and

CN^- ions from composite 157. The highest intensity of the O^- signal comes from the glass fiber whose edge can be clearly seen in the map; the CN^- signal of the highest intensity emanates from a region of 1 μm thickness around the fiber. Figure 8 shows maps of O^- and CN^- ions from composite 161. Again the highest intensity of the O^- signal comes from the glass fiber, but the CN^- signal does not show any inhomogeneity around the fiber. Based on the SSIMS results, Thomason and Morsink [28] speculate that an interphase region, rich in CN^- producing material, surrounds the fibers in composite 157 and that such a region is absent in composite 161.

Bacon, *et al.* [29] have used Micro-Raman Spectroscopy to characterize the changes in chemical structure of the interphase in a carbon/epoxy composite. Spectra were collected from selected regions in the epoxy; the intensity variations in the spectra indicated the existence of a region (interphase) surrounding the fiber whose chemical properties were different from the chemical properties of regions distant from the fiber.

2.1.3 Mechanical Characterization

Mechanical (or structural) properties have to be assigned to the interphase if the interphase is to be introduced into micromechanical analyses. At present, there are no test methods available to directly measure interphasial tensorial stiffness, strength and thermal properties. However, there are several test methods in the literature that purport to measure *interface strength*; the interface strength is then attributed to the interphase as a whole [8]. The reader is referred to [8, 30-32] for excellent reviews of many of these techniques.

Interphasial shear strength tests can be divided into single fiber tests (fiber pull-out, fiber fragmentation, micro-indentation and micro-debonding) and laminate tests (short beam shear, transverse tension, transverse flexure and Dynamic Mechanical Analysis (DMA)). *Single fiber tests* do not reflect the complex stress state around the fiber in a "real" composite; in a "real" composite the fiber is influenced by the surrounding fibers, irregular fiber spacing,

and variations in matrix morphology. Other drawbacks in such single fiber tests include difficulties in test specimen preparation, data scatter, and difficulties in data interpretation. *Laminate tests* attempt to infer a local strength from a global laminate failure. The fact that the strength of the interphase may not coincide with the failure strength of the specimen may make the global failure-local failure correlation quite difficult. In spite of drawbacks, some of these tests are widely used and generally accepted by the interphase research community.

2.2 Physical Characterization of the Interphase

The idea of an interphase region existing between the fiber and matrix, with its own set of properties, is not new. However, it is still quite difficult to evaluate the physical properties of this region. The use of the word "physical" is deliberate in this context, since it is a catchall word that includes the dimensional properties (volume fraction and thickness), the elastic constants (Young's modulus and shear modulus) and the thermal constants (coefficient of thermal expansion).

Several studies [16, 34, 36, 38, 40 and 41] in which the interphase properties are "backed out" from experimentally measurable properties of composite systems and one study [42] in which the interphase Young's modulus is directly evaluated using a micro-indentation test are discussed in this section. Each of these studies makes a simplifying assumption of isotropy of the interphase for the evaluation of properties. While these studies show promise, more work needs to be done before rigorous conclusions regarding their limitations and their usefulness can be reached.

2.2.1 Tensile test on short fiber composites

Sanadi and Piggott [33] have investigated the effect of the interphase on Young's modulus and the strength of short fiber composites made of carbon fibers and Epon-815 epoxy. Different composite samples were produced by varying the following:

- fiber length (0.5 to 5 mm),
- fiber surface (presence of sizing, absence of sizing, nitric acid etching and silicone oil coating), and,
- fiber volume fraction (0.15 to 0.4).

Tensile tests showed that Young's modulus and the strength of the short fiber composite were dependent on all the above factors.

Piggott [34], in a later publication, "backed out" the shear modulus of the interphase (G_i) in carbon/Epon-815 composites by using the results of Sanadi and Piggott [33]. The expressions for Young's modulus and the strength of the composites obtained by a "shear lag" analysis were equated to the nominal values obtained by Sanadi and Piggott [33]; these equations resulted in relationships between the shear modulus of the interphase and its volume fraction. *G_i was found to be several hundred times less than the shear modulus of the matrix for interphasial volume fractions on the order of 0.01* (see Table 1). The values of G_i "backed out" from the Young's modulus comparison were found to be three to four times higher than those "backed out" from the strength comparison. Piggott [34] has speculated that the disagreement in results could be due to the statistical variation in fiber strength and the imperfections introduced during the composite manufacturing process.

2.2.2 Fiber indentation technique

Mandell, *et al.* [35] have used a micro-indentation test (called micro-debonding test in [35]) to measure the interfacial shear strength of S-glass and graphite-reinforced epoxies. A step-wise compressive load was applied to a fiber oriented normal to a polished surface. Microscopic visualization was used to detect debonding; the force needed to produce debonding of the fiber was measured. A finite element analysis was performed to reduce the experimental data to a nominal interfacial shear strength.

Tsai, *et al.* [16] have "backed out" the shear modulus of the interphase (G_i) in S-glass and graphite-reinforced epoxies by using the results of Mandell, *et al.* [35]. The expression for interfacial shear strength of the composites obtained by a "shear lag" analysis was equated to the nominal value of the interfacial shear strength obtained by Mandell, *et al.* [35]; this equation resulted in a relationship between the shear modulus of the interphase and its thickness. *G_i was calculated for values of interphasial thickness ranging from 10 nm to 1000 nm. It was found to be several hundred times less than the shear modulus of the matrix* (see Table 2).

2.2.3 Fiber fragmentation test

Asloun, *et al.* [36] have investigated the stress transfer in single fiber composites using a fiber fragmentation test. They have experimentally determined the critical fiber length to fiber diameter ratio (l_c/d) for a PAN-based carbon fiber embedded in DGEBA-DDS epoxy and polyethylene-vinyl-acetate (EVA). The l_c/d ratio for carbon/epoxy, and that of several other thermosets and thermoplastics, obeyed the equation: $l_c/d \simeq 4.7\,(E_f/E_m)^{1/2}$. But, the ratio for carbon/EVA obeyed the equation: $l_c/d \simeq 0.65\,(E_f/E_m)^{1/2}$. In an attempt to explain this difference,

it was concluded that the nature of the matrix layer next to the fiber surface (interphase) in carbon/EVA composites may be different from that of the bulk matrix.

Asloun, *et al.* [36] have hypothesized that the mobility of the polymer chains in the interphase layer of carbon/EVA composites may be restricted by the presence of the fiber, and hence, may have a higher elastic modulus compared to the bulk matrix. As a first approximation, the mechanical behavior of the interphase was considered to be equivalent to that of the matrix in its glassy state, even at temperatures much higher than the glass transition temperature (T_g). The Young's modulus of the interphase (E_m^*) was found by extrapolating the linear relationship observed between $log\,(E_m/T)$ and T at temperatures below T_g, to temperatures beyond T_g (see Table 3). The l_c/d values of carbon/EVA were found to agree well with $l_c/d \simeq 4.7\,(E_f/E_m)^{1/2}$, once E_m^* was used instead of E_m.

2.2.4 Laser micro-interferometric technique

Sottos, *et al.* [37] have used a laser micro-interferometric technique to map the surface of single fiber composites, before and after heating, to find relative thermal displacements. Specimens were cut from samples made by embedding pitch-base carbon fibers (30 μm in diameter) in a "pool" of Epon-828 resin *(Young's modulus = 2.5 GPa, and coefficient of thermal expansion = 68 ppm/°C).* The radius and length of the cylindrical specimen were measured to be 1.5875 cm and 2 cm, respectively. The faces of the specimen were polished metallographically to ensure reflectivity. Leads were attached to the specimen faces; a 1000 Å thick layer of gold was sputtered on to the front face to provide a current conduction path to the fiber.

The specimen was heated by passing controlled, low levels of electric current through the fiber. The surface map obtained before heating was "subtracted" from the surface map obtained after heating. Figure 9 shows the axial thermal displacements in the single fiber composite surface. Displacements have been normalized by subtracting the value of the

displacement at a distance 30 fiber radii away from the center of the fiber from each measurement. The theoretical axial displacement profile of a carbon fiber - interphase *(Young's modulus = 0.1 GPa, coefficient of thermal expansion = 160 ppm/°C, and thickness = 0.175 times fiber radius)* - Epon-828 matrix assemblage was found to be in good agreement with the experimentally obtained axial displacement profile [38]. The Young's modulus and coefficient of thermal expansion of the interphase have been "backed out" in this study and the interphasial properties are found to be different from the bulk matrix properties, as can be seen from the highlighted values.

2.2.5 High Accuracy Strain-field Mapper --- Tensioned-fiber test

Stereoscopic analysis techniques compare optical or scanning electron micrographs of a surface obtained before and after deformation to find relative displacements. James, *et al.* [39] have applied digital image processing techniques to stereoscopic analysis resulting in a computer-automated high-spatial-resolution displacement-measurement system called the High Accuracy Strain-field Mapper (HASMAP). HASMAP measures relative displacements by cross-correlation analysis of the relative positions of visible surface texture on the pre-deformation and post-deformation micrographs. Displacement accuracy ranges from $\pm$60 Å for optical micrographs to $\pm$10 Å for scanning electron micrographs. Both in-plane and out-of-plane displacements are determined depending on the angle at which the specimen is viewed in the microscope.

James, *et al.* [40] have applied the HASMAP to measure surface displacements of a mechanically-loaded single fiber AS4-G/Epon-828 *(Young's modulus = 3.3 GPa, and coefficient of thermal expansion = 48 ppm/°C)* composite specimen. The experimental setup consists of a C-frame with a screw to apply the load to the fiber as shown in Figure 10. The fiber is threaded through the lower and upper holes in the frame; it is fixed at the lower end and cured in resin at the top. The fiber is cut at the upper surface with a sharp blade and the resin

surface is polished. The sample thickness and the sample diameter are of the order of 150 μm and 500 μm, respectively.

The fiber was taken through one complete loading and unloading cycle; the out-of-plane displacements of the matrix relative to the fiber along the radial direction are shown in Figure 11. The displacements obtained were non-symmetric and non-uniform and there was no recovery of the vertical displacements. The sample holder was then transferred to a heating stage and heated to 100 °C (the resin cure temperature) and substantial recovery of the displacements occurred. The deepest offset, it is claimed, could be due to micro-cracking. The same sample was re-polished to remove the near surface damage and cycled at an amplitude of 0.4% fiber strain. The displacements near the interface completely recovered while non-elastic irreversible displacement was noticed at distances of 3 μm from the interface.

Tsai, *et al.* [16] have performed a finite element analysis with an axisymmetric model that includes an interphase to study the effect of the interphase on out-of-plane displacements. The theoretical out-of-plane displacement profile of a AS4-G fiber - interphase *(Young's modulus = 0.8 GPa, and thickness = 700 nm)* - Epon-828 matrix assemblage was found to be in good agreement with the Tensioned-fiber test data of James, *et al.* [40]. A similar experimental-cum-finite element analysis performed on a sized AS4-G fiber/Epon-828 composite revealed an interphase region with a Young's modulus of 0.65 GPa and a thickness of 3000 nm [41].

2.2.6 Matrix indentation technique

Williams, *et al.* [42] have used a micro-indentation test (called nano-hardness test in [42]) to measure the Young's modulus of Epon-828 matrix surrounding a single AS4-G fiber. The technique involves the determination of the load-displacement relationship as the indenter is forced into the surface of a material. Forces and displacements are measured with resolutions of 0.3 μN and 0.16 nm, respectively. The indenter causes both elastic and plastic

deformation as it is forced into the surface. The geometry of the tip of the indenter, the slope of the unloading portion of the load-displacement curve, and the properties of the indenter are used to determine the Young's modulus of the surface being tested.

The fiber in the specimen was cut at an angle of 6° to the horizontal and the resultant elliptical cross-section of the fiber and the adjacent matrix regions were polished; indentation tests were carried out in the interphase/matrix adjacent to the fiber. Figure 12 shows the variation of the Young's modulus (called pseudo-modulus in [42]) as a function of distance from the fiber. Indentation tests run on a neat resin specimen for comparison provided a Young's modulus value of 3.8 GPa. In spite of some shortcomings, the method shows promise and is probably the only direct method available for the measurement of the interphase modulus.

Both the Tensioned-fiber test and the micro-indentation test use similar single fiber composite samples made of AS4-G fiber cured in a "pool" of Epon-828 matrix. While the Tensioned-fiber test predicts an interphase thickness of 700 nm and Young's modulus of 0.8 GPa, the micro-indentation test predicts an interphase thickness of 1000 nm and a Young's modulus gradient. Williams, *et al.* [42] favor the results from the Tensioned-fiber test; they explain that the apparent increase in Young's modulus predicted by the micro-indentation test may be due to the proximity of the reinforcing fiber to the indenter.

2.3 Summary

The main issues addressed herein can be summarized as follows:

1. The evaluation of interphasial volume fraction, thickness, Young's modulus, shear modulus and coefficient of thermal expansion has been limited mainly to polymeric composites, while interphasial shear strength characterization has been attempted for polymeric [31, 32], metal [43] and ceramic matrix [11, 43] composites.

2. Characterization methods for interphasial properties are far from satisfactory due to the following reasons:
    - Simplifying assumptions are usually made in the evaluation of properties.
    - Property values evaluated by the various techniques show a wide scatter.
    - Most of the techniques (except the Matrix indentation technique) are indirect methods that "back out" properties from other measured quantities.
3. Simple tests and interpretations are appropriate for exploratory studies. However, the design and optimization of interphases will require more sophisticated test methods and models to evaluate micro-level tensorial properties of the interphase. The reader is referred to the following within this context:
    - Ultrasonic techniques for the measurement of shear modulus of the interphase as a function of distance in an aluminum-epoxy bond [44] and measurement of the orthotropic stiffness coefficients of a bovine bone [45], which may provide a good starting point for sophisticated interphasial test methods.
    - Chapter 3, wherein a review of interphase property models is presented.

Table 1. Interphasial shear modulus of carbon/epoxy composites [34].

Fiber length (mm)	Fiber Surface treatment	G_m / G_i by modulus comparison	G_m / G_i by strength comparison
2	sized	300	
	desized	2,700	700
	etched	2,700	700
	coated	12,000	4,000
5	sized		
	desized	8,500	
	etched	2,500	
	coated	62,000	15,000

Table 2. Interphasial shear modulus of S-glass/epoxy and graphite/epoxy composites [16].

Interphase thickness (nm)	G_m/G_i for S-glass/epoxy	G_m/G_i for graphite/epoxy
10	922	724
50	184	145
100	92	74
500	18	15
1,000	9	7

Table 3. The bulk matrix and the interphase values of the Young's modulus of carbon/EVA composites [36].

Temperature (°C)	E_m (MPa)	E_m^* (MPa)
- 20	30.5	524
0	12.9	307
20	6.6	179
40	1.7	104

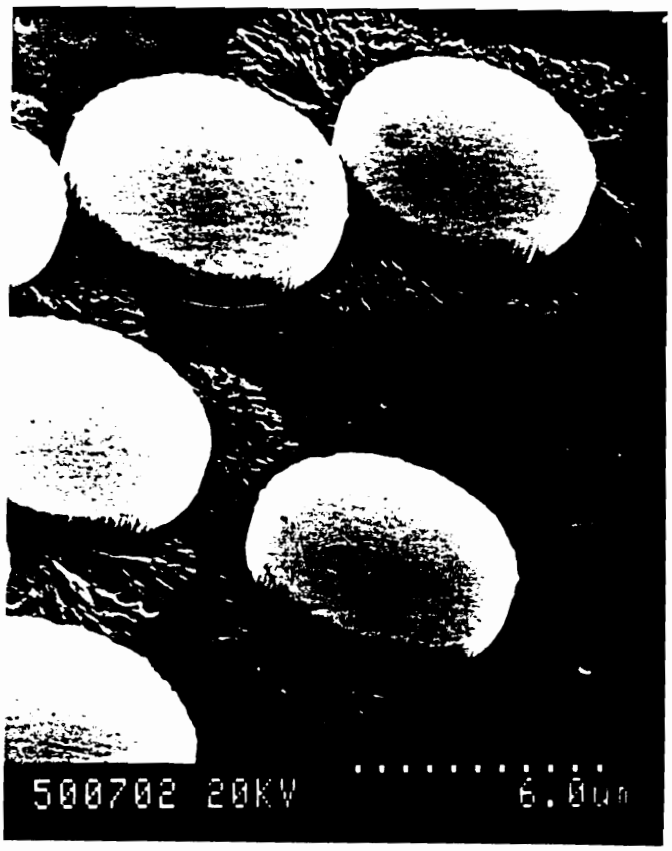

Figure 2. Scanning electron micrograph of the etched cross-section of a partially crystallized APC-2 showing spherulitic growth [21].

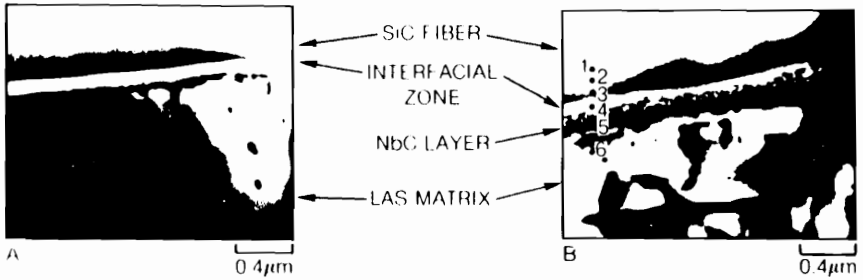

Figure 3. Transmission electron micrographs of Nicalon/LAS-III composite [22].

AES—AUGER ELECTRON

EELS—ELECTRON ENERGY LOSS

ISS—ION SCATTERING

LEED—LOW ENERGY ELECTRON DIFFRACTION

SAM—SCANNING AUGER MICROPROBE

SIMS—SECONDARY ION MASS

SXAPS—SOFT X-RAY APPEARANCE POTENTIAL

UPS—ULTRAVIOLET PHOTOELECTRON

XPS—X-RAY PHOTOELECTRON

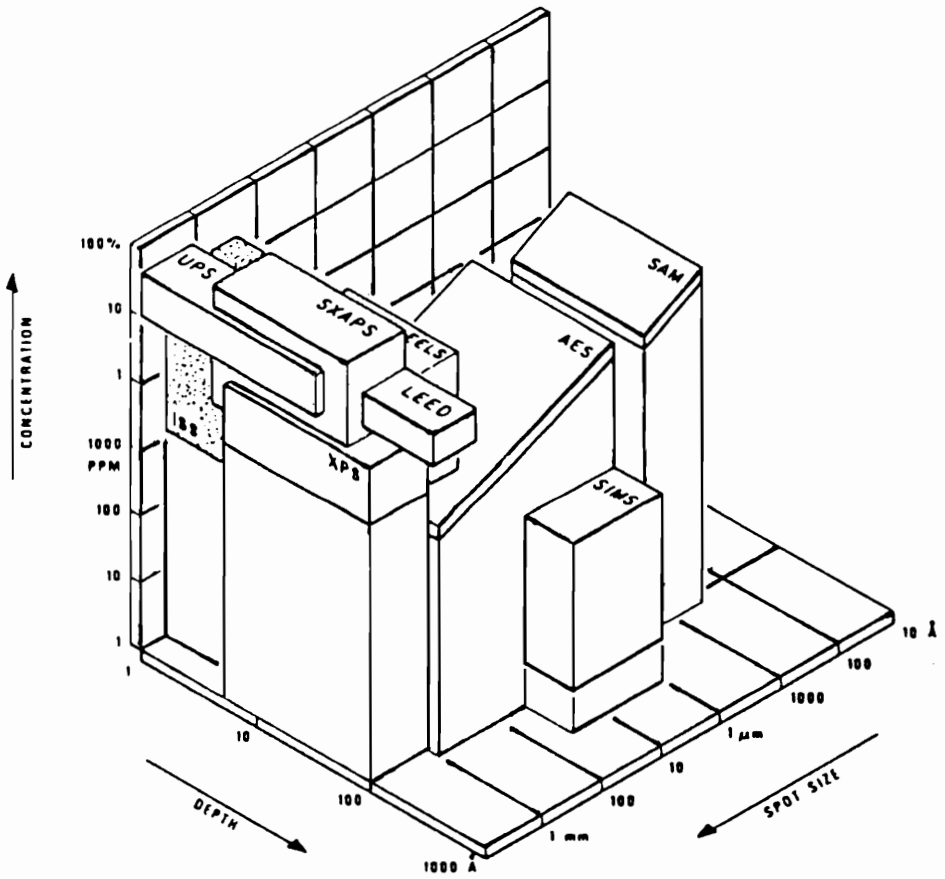

Figure 4. Surface analysis techniques represented as a function of depth sensitivity, concentration limit, and spot size [26].

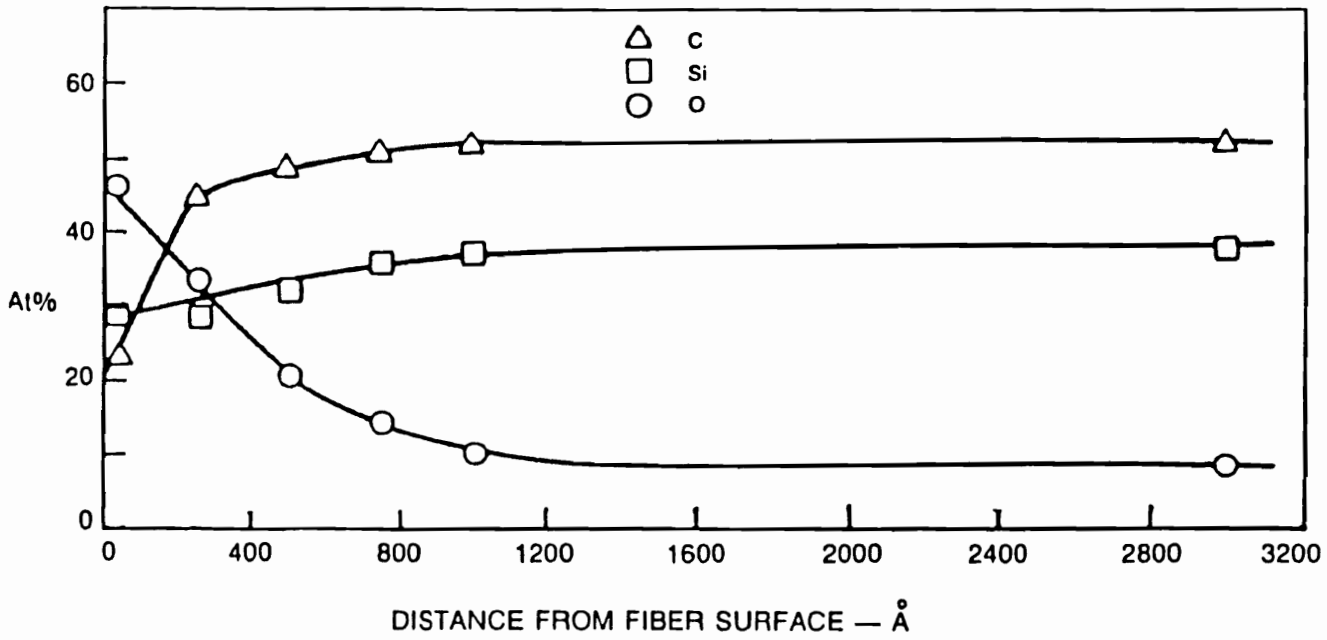

Figure 5. Scanning Auger depth profile of as-received, flame de-sized Nicalon fiber [23].

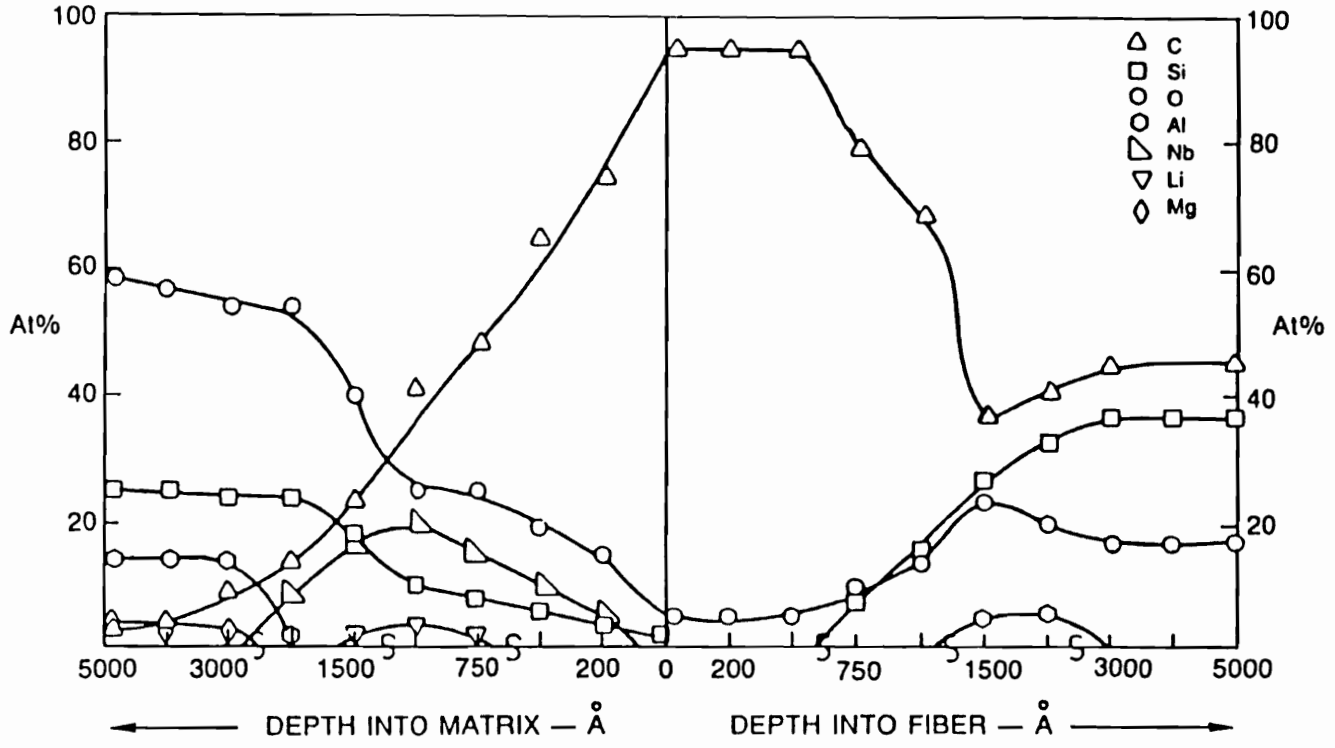

Figure 6. Scanning Auger depth profile of the interphase in a Nicalon/LAS-III composite [23].

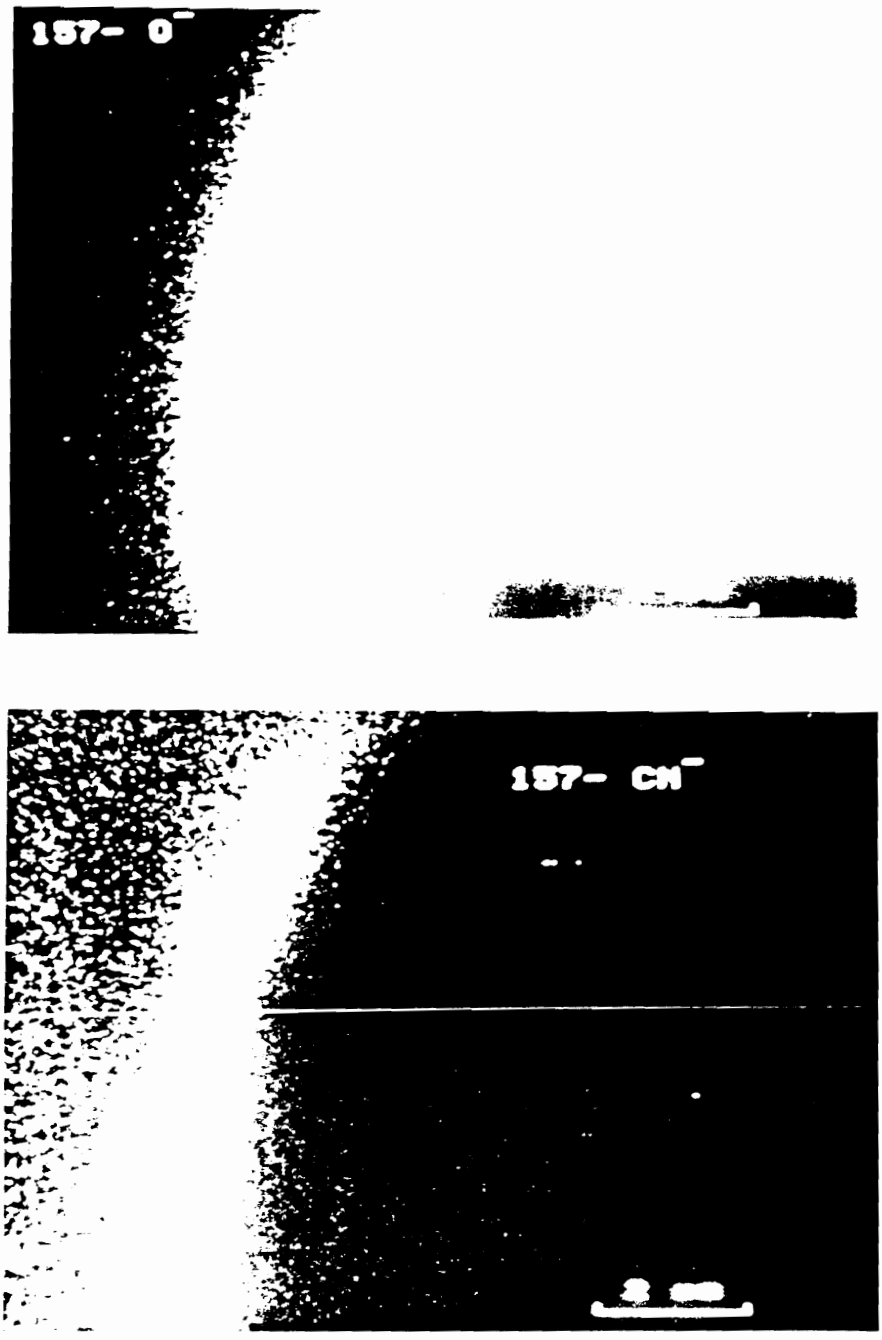

Figure 7. Scanning Secondary Ion Mass Spectrometry maps from composite 157 [28].

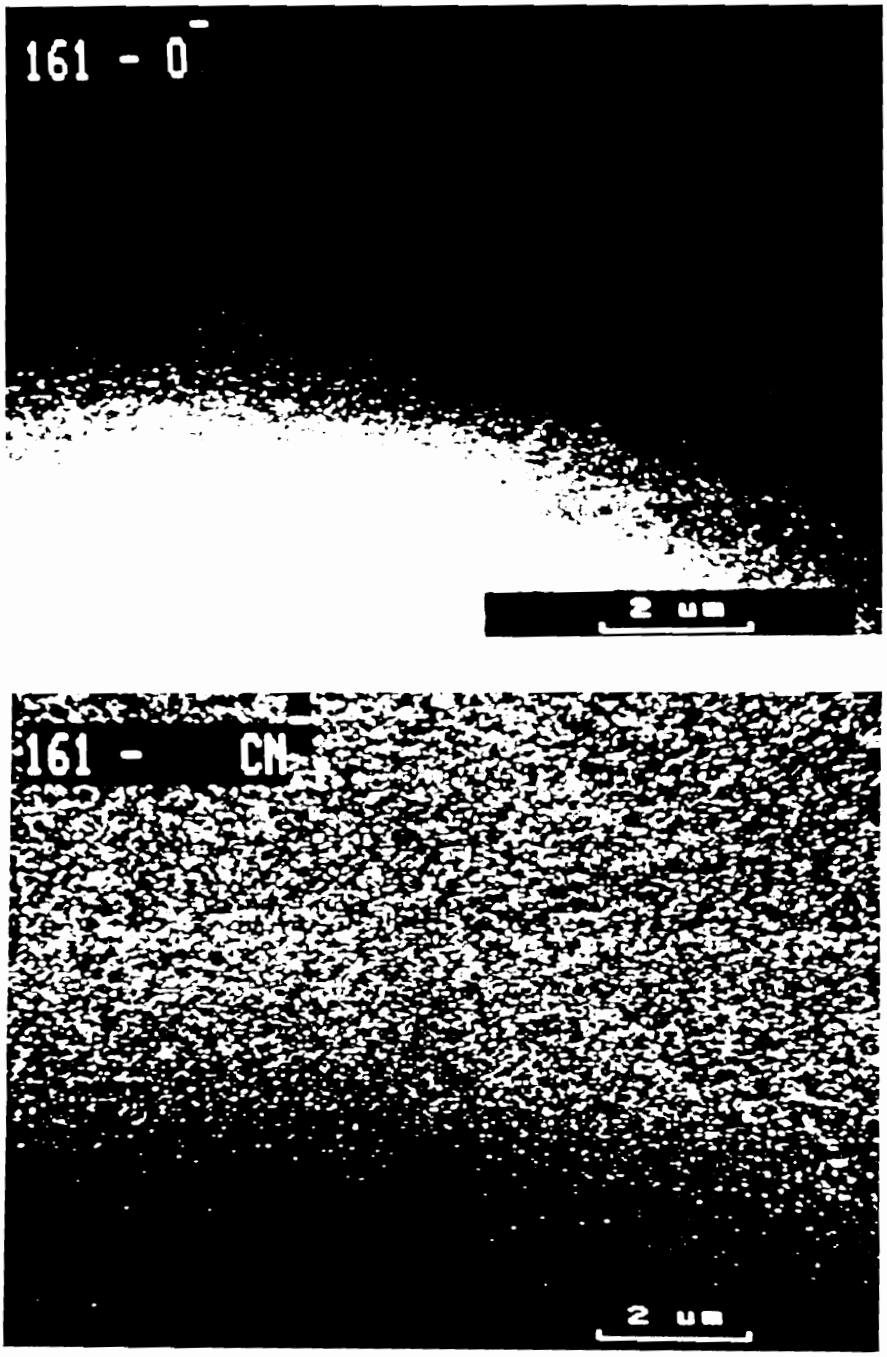

Figure 8. Scanning Secondary Ion Mass Spectrometry maps from composite 161 [28].

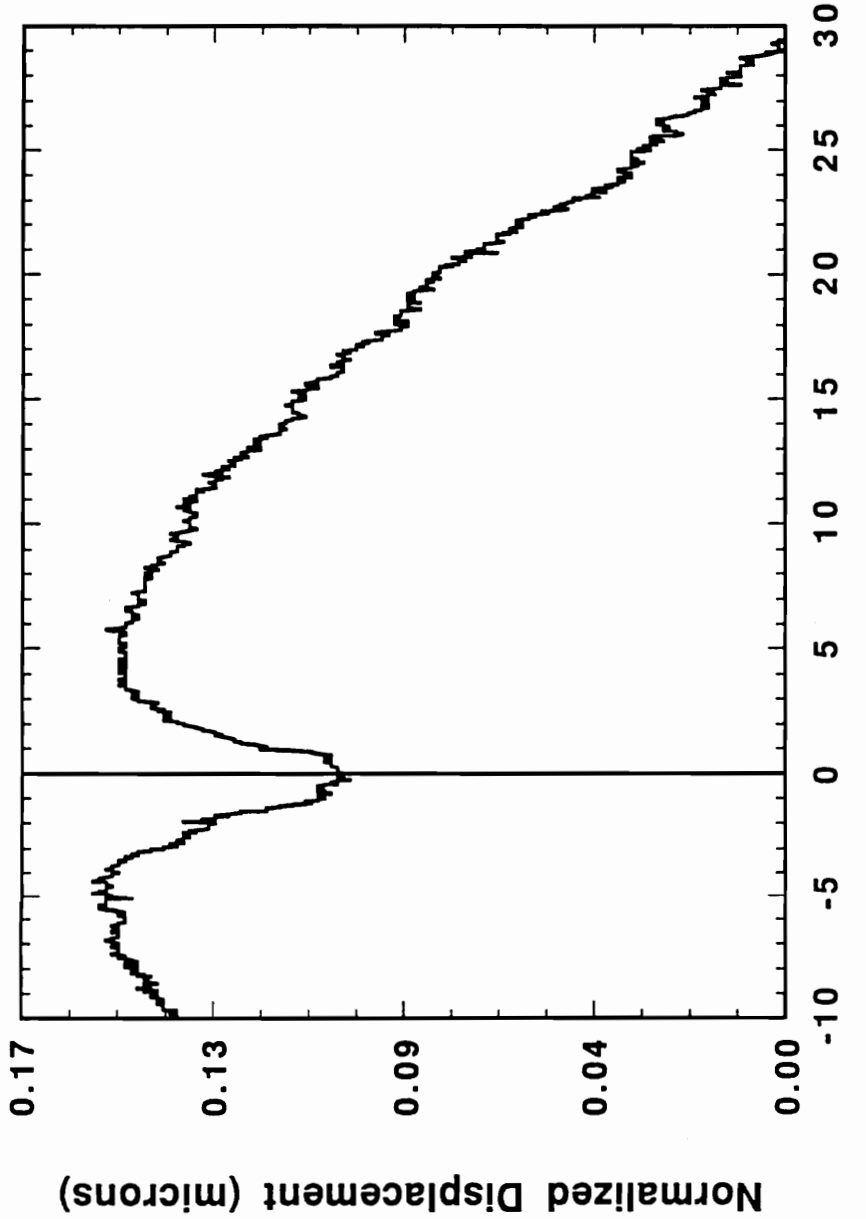

Figure 9. Normalized, out-of-plane displacement profile of a carbon/Epon-828, single fiber composite due to thermal expansion; the central indentation marks the location of the fiber [37].

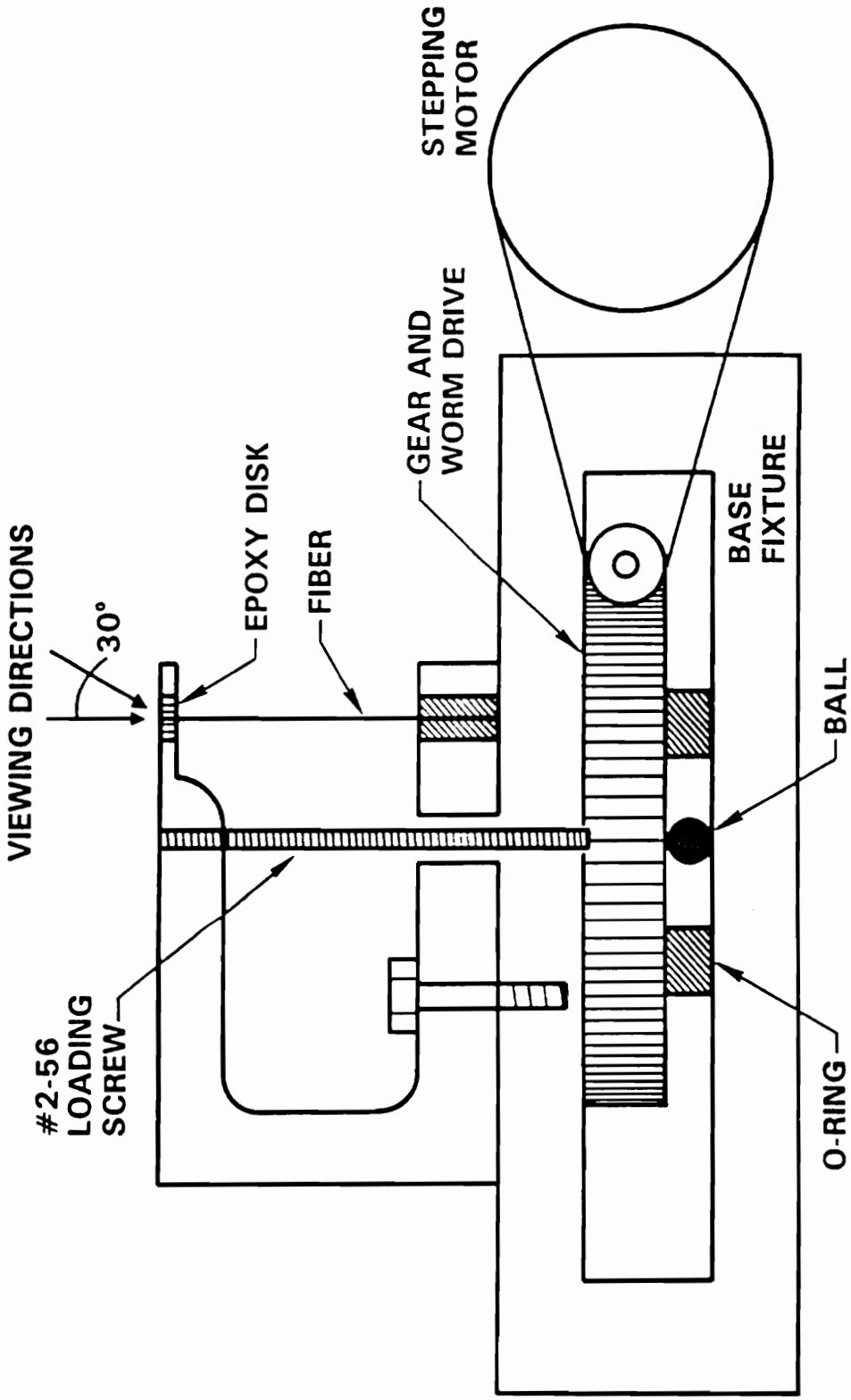

Figure 10. The in situ loading frame and the sample for the Tensioned-fiber test [40].

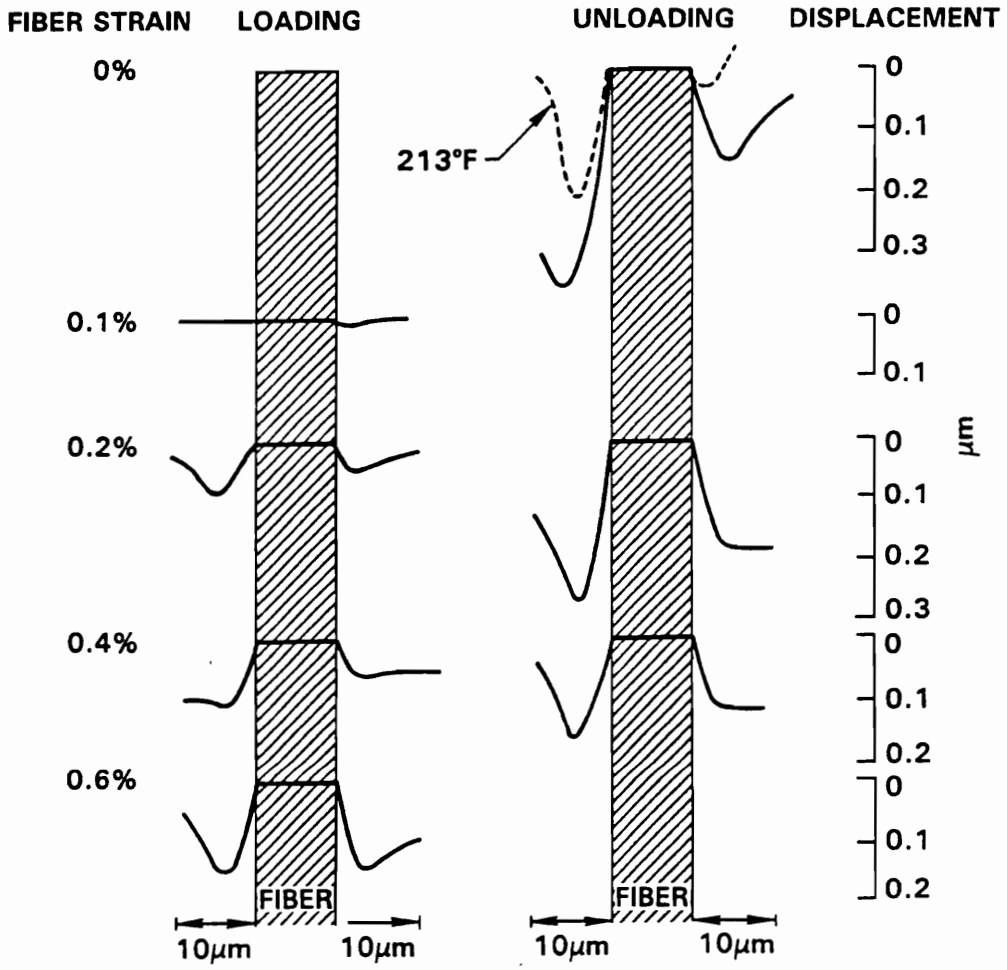

Figure 11. Normalized, out-of-plane displacement profile of a AS-4G/Epon-828, single fiber composite through the first loading and unloading cycle [40].

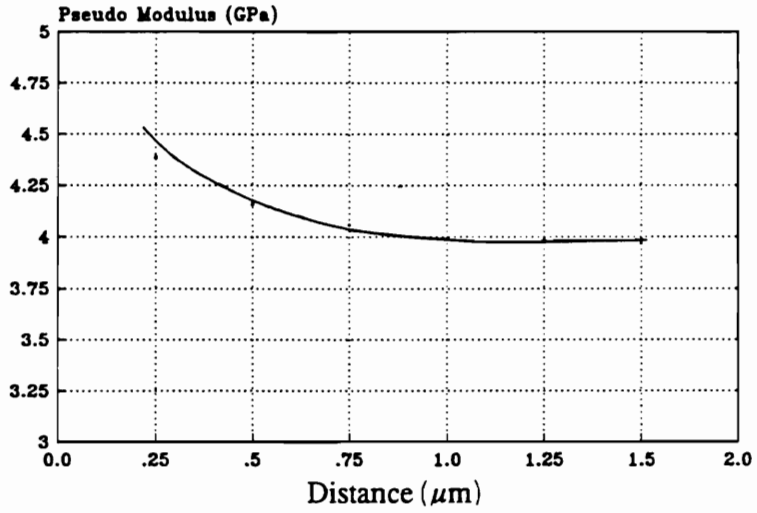

Figure 12. Young's modulus profile of Epon-828 as a function of distance from the fiber in a AS-4G/Epon-828, single fiber composite obtained by the micro-indentation test [42].

3.0 Modeling Studies

Various models have been considered for the physical properties (thickness, Young's modulus, Poisson's ratio and coefficient of thermal expansion) of the interphase in an effort to study the effect of the interphase on residual thermal stresses, stress distribution under thermo-mechanical loading situations, elastic moduli, etc., in a composite. Models have also been proposed, for the formation of the interphase and the resulting interphasial properties, and substantiated in a limited manner through experiments. These models range from hypothetical to semi-empirical and provide approximate representations of the interphase. Although the representations provided by both experiments and models are approximate, the models take into account some of the complexities of the interphase that are usually not considered in the interpretation of the experiments. This chapter presents a review of several models available for the characterization of the physical properties of the interphase.

3.1 Interphase Models

The idea of an interphase with its own set of constant properties existing between the fiber and matrix is not new. This section discusses several studies where the presence of an interphase is assumed and its physical properties (thickness, Young's modulus, Poisson's ratio and coefficient of thermal expansion) are modeled. Interphase models can be broadly classified into *spring layer* models [46, 47] and *interphase layer* models [48-58, 62-71, 73-79].

The *spring layer* model considers a very thin interfacial zone of unspecified thickness existing between the fiber and matrix. The model can be explained through the following assumptions:

- The tractions are continuous across the interface.
- The normal and tangential displacements are discontinuous across the interface.
- The jumps in the normal and tangential displacements at the interface are proportional to the associated normal and shear tractions, respectively.
- These proportionality constants characterize the properties of the interphase as well as the fiber-matrix bonding.

Studies dealing with the *spring layer* model will not be reviewed here; the reader is urged to refer to Jasiuk and Tong [46] and Achenbach and Zhu [47] for a concise review of articles utilizing this model.

The *interphase layer* model considers an interphase layer between the fiber and matrix, of specified thickness and thermo-elastic properties different from those of the fiber and matrix. Some of the significant features of this model are:

- The interphase layer models can be divided into uniform models [48-58, 62-67] (properties are spatially uniform) and non-uniform models [68-71, 73-79] (properties are spatially non-uniform functions of radius — in the present case).

- Although the *in situ* properties of the constituents may be strongly influenced by processing conditions, the uniform models have routinely neglected this effect due to the lack of definitive data.
- All the non-uniform models consider the interphase in polymeric matrix composites only.
- The interphase is assumed to be isotropic, linear elastic and perfectly bonded to the fiber and matrix.
- The perfect bonding implies continuity of tractions and displacements at the fiber-interphase and interphase-matrix interfaces.
- The degree of fiber-matrix debonding or damage in the interphase can be simulated by adjusting the elastic properties and thickness of the interphase region.
- In some studies, coatings applied to the fibers have been considered as a separate phase (akin to the interphase) existing between the fiber and matrix.

Representative studies which bring out all the different aspects of interphase layer models will be discussed in the following sections.

3.1.1 Uniform interphase layer model --- Organic matrix composites

Nairn [48] has considered a separate interphase region in an AS/3501-6 epoxy composite, in order to determine residual thermal stresses using an elasticity solution based on an axisymmetric three-phase model (fiber/interphase/matrix). The interphase properties were assumed to be identical to that of the matrix except for the coefficient of thermal expansion. The coefficient of thermal expansion of the interphase was treated as a variable (in the range 0 to 250 ppm/°C compared to a matrix value of 40 ppm/°C) and its effect on the stress field was studied. It was found that increasing the coefficient of thermal expansion of the interphase region caused a decrease in the in-plane residual thermal stresses in the matrix, but also increased the residual stresses in the interphase.

Lo, *et al.* [49] have considered an elasticity solution based on an axisymmetric four-phase model (fiber/flexible interlayer/matrix/surrounding body) to investigate the constituent stresses in a glass/epoxy composite under a transverse tensile load applied perpendicular to the fiber direction. The interlayer modulus and thickness were treated as variables and their effect on the constituent stresses was examined. The optimal interlayer thickness and modulus that caused the smallest radial stress to develop at the interlayer/matrix interface were determined, based on the results of a parametric study.

Zhang [50] has developed an elasticity formulation for the determination of constituent stresses in a unidirectional *n*-layered composite subjected to mechanical loading conditions. The composite was idealized by a single fiber surrounded by *n* concentric cylindrical, anisotropic matrices and was subjected to two different loading conditions — uniaxial strain applied parallel to the fiber direction and equal biaxial stresses applied perpendicular to the fiber direction. The original problem, requiring the solution of a linear system of equations of the order $2n+2$, was reduced to a problem of finding the inverse of a *nxn* matrix, using the matrix resolution technique. Numerical results were not reported. This formulation is ideal for models that treat the interphase as a series of cylindrical layers with successively different properties. Further, this formulation can be easily extended to include the case of a composite subjected to an applied thermal load.

Bowles [51] has considered a three-phase model (fiber/interphase/matrix) with a linear finite element analysis to investigate the thermally induced stress fields in P75/934 composites at temperatures typical of spacecraft operating environments. The Young's modulus and coefficient of thermal expansion of the interphase region were treated as variables and their influence on constituent stresses was investigated. Tailoring the interphase region was found to cause modest changes in the interphase and matrix stresses.

Sullivan and Hashin [52] have used both the composite cylinders assemblage and the generalized self-consistent scheme for determining the following for an AS4/epoxy composite:

- Effective elastic constants of a three-phase (fiber/interphase/matrix) unidirectional fiber-reinforced composite given the elastic properties and volume fractions of the fiber, interphase and matrix.
- Elastic properties of the interphase, given the elastic properties of the fiber, matrix and composite, and the volume fractions of the fiber, interphase and matrix.

Qiu and Weng [53] have used similar formulations to study the effect of an interphase on the thermo-elastic properties of composites.

3.1.2 Uniform interphase layer model --- Metal and Ceramic matrix composites

Mikata and Taya [54] have used an elasticity solution based on an axisymmetric four-phase model (fiber/coating/matrix/surrounding body) to evaluate the constituent stresses in coated fiber composites (Ni-coated T300/Al 6061 and SiC-coated T300/Al 6061) under thermo-mechanical loading situations. The composite was subjected to three independent loading conditions — axisymmetric temperature change, uniaxial stress applied parallel to the fiber direction, and equal biaxial stresses applied perpendicular to the fiber direction; the properties of the surrounding body were obtained using the rule-of-mixtures. It was shown that an increase in fiber volume fraction and thickness of the coating resulted in a decrease in the thermal stresses (axial and hoop) at the fiber-coating interface.

Tandon and Pagano [55] and Pagano and Tandon [56, 57] have predicted the thermo-elastic properties and the constituent stresses under thermo-mechanical loading conditions of a coated Nicalon/BMAS composite. An elasticity formulation based on a three-phase model (fiber/coating/matrix) was used and the conditions on the radial boundary of the concentric cylinder assemblage were approximated by the applied boundary conditions on the composite. The Young's modulus, coefficient of thermal expansion and thickness of the coat-

ing were treated as variables and their effect on the thermo-elastic properties and constituent stresses was studied. The following conclusions were reached based on parametric studies:

- A proper choice of the coating thickness, Young's modulus and coefficient of thermal expansion can be used to control the stress components of interest.
- Thermo-elastic properties of the composite in the transverse direction are much more sensitive than the longitudinal properties to the variation of coating modulus and thickness.

Benveniste, *et al.* [58] have used a three-phase model (fiber/coating/matrix) to predict the thermo-elastic properties and the local stresses under thermo-mechanical loading situations in a carbon-coated SiC/Titanium Aluminate composite. A simple variation of the formulations of Eshelby [59, 60] and Mori and Tanaka [61], called the *Equivalent Inclusion - Average Stress (EIAS) concept*, was used and the composite was subjected to six different loading conditions — uniform change in temperature, axial normal stress, transverse hydrostatic stress, longitudinal shear stress, transverse shear stress, and transverse normal stress. The conditions inside the composite were approximated by the elasticity solution for a single coated fiber in infinite matrix subjected to average matrix stresses. The average matrix stresses approximately account for the fiber-fiber interaction in the composite. Jasiuk and Tong [46] and Tong and Jasiuk [62] have also evaluated the thermo-elastic properties of composites using a variation of the Mori-Tanaka formulation called the *Successive Iteration* method.

The compliant (or compensating) layer concept deals with the insertion of an interface material between the fiber and matrix in metal matrix composites. This layer reduces the micro-damage development in the constituents during cool-down and during mechanical loading by modifying the residual stress field. Elasticity solutions [63, 64, 65] and finite element analyses [66, 67] have been used to predict the properties of the optimal compliant layer in a variety of composites.

Vedula, *et al.* [63] have used an elasticity solution based on an axisymmetric three-phase model (fiber/interphase/matrix) to predict the residual thermal stresses in a Pitch

55/A 201 composite. The Young's modulus of the interphase was treated as a variable (over a range of values above and below the value of the fiber modulus) and the Poisson's ratio and the coefficient of thermal expansion of the interphase were assumed to be identical to that of the matrix. It was found that a compliant interphasial layer reduced the tensile residual stresses in the matrix. Arnold, *et al.* [64] have investigated the viability of the compliant layer concept in a unidirectional metal matrix composite (SiC/Ti_3Al+Nb) using an elasticity solution based on an axisymmetric three-phase model (fiber/interphase/matrix). A parametric study was conducted and the following guidelines were given for the selection of materials for the compliant layer:

- The two parameters that are most responsible for a reduction in the matrix in-plane stresses are the thickness and coefficient of thermal expansion of the compensating layer.
- The thickness of the compensating layer should be as large as other thermo-mechanical considerations will allow.
- The coefficient of thermal expansion of the compensating layer should be greater than the coefficient of thermal expansion of the matrix.

Ghosn and Lerch [65] have used an elasticity solution based on an axisymmetric three-phase (fiber/interphase/matrix) model to predict the properties of an interphasial layer which would minimize the residual thermal stresses in a variety of metal matrix composites. Two different fibers (SiC and TiB_2) and three different matrices (Ti-15-3, Ti_3Al and NiAl) were considered. The Young's modulus, coefficient of thermal expansion and thickness of the interphase were considered as the decision variables; the sum of the average distortional energies in the matrix and the interphase was minimized as a means of reducing the tensile residual stresses. Ghosn and Lerch [65] were also able to show, through a survey of common coating materials, that very few coating materials conformed to the optimized property values.

Caruso, *et al.* [66] have treated the properties of a hypothetical compliant layer as variables, in order to determine their influence on the behavior of unidirectional metal matrix composites (SiC/Ti_3Al+Nb and SiC/Ti-15-3). A linear, three-dimensional finite element analy-

sis of a nine-fiber unidirectional composite system was used to calculate the residual stresses in the constituents; a parametric study was conducted to determine the properties of the optimum compliant layer which would reduce the residual stresses in the matrix. The optimum compliant layer was found to have a modulus value that was 15% of the modulus value of the matrix and a coefficient of thermal expansion roughly equal to that of the composite system without the compliant layer. Morel, *et al.* [67] have attempted to optimize the properties of the interphase layer in P100/Copper and SiC/Ti-15-3 composites, in order to reduce the residual stresses in the matrix. The constituent stresses were predicted using a non-linear micromechanics-based numerical method; the interphase optimization was carried out, with and without the fabrication considerations, using the non-linear programming method. A strong coupling was found between interphase and fabrication tailoring, which resulted in significant residual stress reductions.

3.1.3 Non-uniform interphase layer model --- Erickson-Volpe-Cooper

Erickson, *et al.* [68] have claimed that "preferential adsorption" occurs in the regions adjacent to the glass fibers in glass fiber-reinforced plastics. Their attempt to attribute properties to the "deformable resin layer" (interphase) can be explained in the following steps:

- Several additives are necessary for the complete curing of the resin in a glass fiber-reinforced plastic.
- Fiber sizings adsorb one or more of the additives necessary for resin cure out of the liquid resin.
- The stoichiometric balance needed for the optimal cure of the resin is disturbed by such an adsorption; this disturbance is dominant in a layer of several hundred angstroms thickness around the fiber.

- In turn, this leads to an interphase possessing an elastic modulus (and possibly fracture toughness) different from that of the fully cured resin. This hypothetical modulus has a lower value (lower than the resin modulus) at the fiber surface and increases with radial distance into the bulk resin.

Erickson, *et al.* [68] have also attempted to prove the validity of the "preferential adsorption" theory by performing adsorption experiments with different types of powdered glass having different sizings. The powdered glass with sizing was packed in a 10 ml burette in sufficient amount to give a total surface area of 4.25 m^2; a small pad of Pyrex glass-wool was placed below the powder to prevent it from being carried out of the burette. A solution of carbon tetrachloride with 1% Epon-826 epoxy and 1% of a curing agent identified as "A" was synthesized and an infra-red spectrum of the solution was obtained; this was deemed the "before" spectrum. The solution was poured on top of the powdered glass in the burette and 0.5 ml of the solution coming through the burette was collected. An infra-red spectrum of this solution was obtained; this was deemed the "after" spectrum. An analysis of the "before" and "after" spectra was performed to determine the percent concentration of the resin and curing agent adsorbed by the sizing on the glass powder. The data clearly show that the resin and curing agent adsorption are different for different glass powders and different sizings; Erickson *et al.* [68] consider this as a reasonable validation of the "preferential adsorption" theory in the case of fiber reinforced plastics.

3.1.4 Non-uniform interphase layer model --- Van Fo Fy

Van Fo Fy [69] has used the work of Erickson *et al.* [68] to conclude that "the physicomechanical properties, specifically the intermediate phase (interphase) moduli, vary continuously with distance from the fiber surface." Two different expressions for the shear modulus of the interphase in a glass fiber-reinforced plastic were considered. The expressions for stresses in the composite, represented by a hexagonal fiber arrangement, were evaluated

for an applied longitudinal shear load; numerical results were not presented. The expressions used for the shear modulus of the interphase (G_i) were:

$$G_i = G_0 e^{g(\lambda - \rho)} \quad (1)$$

$$G_i = G_0 e^{-g(\lambda - \rho)} \quad (2)$$

where λ represents the radius of the fiber, ρ represents the radial coordinate, g represents a constant, and G_0 represents the value of the interphase shear moduli at $\rho = \lambda$. Equation (1) characterizes an interphase where the shear modulus decreases as a function of distance from the fiber surface, while Equation (2) characterizes the opposite of the above case.

3.1.5 Non-uniform interphase layer model --- Drzal-Rich-Koenig-Lloyd

Drzal, *et al.* [70] have considered a hypothesis similar to that of Erickson, *et al.* [68], while studying the effect of fiber finish on the adhesion of graphite fibers to epoxy matrix. The details about the constituents used in this study can be summarized as follows:

- Fiber — graphite
- Finish — diglycidyl ether of bisphenol-A (DGEBA) of 100-200 nm thickness
- Matrix — stoichiometric mixture of DGEBA with 14.5 parts per hundred meta-phenylene diamine (mPDA)

Drzal, *et al.* [70] have hypothesized that:

- During the period before gelation the amine in the epoxy diffuses into the finish and reacts with the epoxy functionalities.
- This reaction retards the further diffusion of the amine into the finish.
- An interphase layer with a gradient in amine concentration decreasing from 14.5 parts per hundred in the bulk resin to a very low value near the fiber surface is formed.

- This interphase layer has less than the stoichiometric amount of amine necessary for full cure.
- As a result, the properties of the interphase are different from that of the bulk resin.

An attempt was made to test this hypothesis by measuring the properties of DGEBA, with varying amounts of mPDA, cast and cured under conditions identical to those used to fabricate single fiber specimens. When the amine content was reduced from 14.5 parts per hundred, the resulting material had a higher modulus, lower strength and lower fracture toughness. While Drzal, *et al.* [70] have not claimed that physical property gradients exist in the interphase, it is possible to reach that conclusion based on the data available from their experiments (See Figure 13).

3.1.6 Non-uniform interphase layer model --- Theocaris

Theocaris [71] has developed an interphase model for unidirectional glass-reinforced epoxies based on hypotheses and calorimetric measurements. The Young's modulus of the interphase (E_i) was assumed to vary continuously between that of the fiber and that of the matrix and possess the form:

$$E_i(r) = E_m + E_f\left(\frac{r_f}{r}\right)^{\eta_1} - E_m\left(\frac{r_f}{r}\right)^{\eta_2} \qquad (3)$$

where E denotes the Young's modulus, η_1, η_2 are adhesion exponents that depend on the quality of adhesion existing between the fiber and the matrix, and the subscripts f, i, and m denote the fiber, interphase and matrix, respectively. The adhesion exponents were evaluated by using the following sequence of steps:

- Choice of a representative volume element for the composite,
- Evaluation of the thickness of the interphase by calorimetric analysis,
- Choice of interface conditions for the interphase Young's modulus,

- Derivation of the "average interphase modulus condition", and,
- Determination of the adhesion exponents.

Representative volume element: A three-cylinder model was considered as the representative volume element of the composite; the cylinders represent the matrix, the interphase and the fiber. The following relations hold for the representative volume element (See Figure 14):

$$v_f = \left(\frac{r_f^2}{r_m^2} \right); \quad v_i = \left(\frac{r_i^2 - r_f^2}{r_m^2} \right); \quad v_m = \left(\frac{r_m^2 - r_i^2}{r_m^2} \right) \tag{4}$$

where r refers to radius, and v refers to volume fraction.

Calorimetric analysis: Calorimetric analysis of fiber reinforced epoxies reveals that heat capacity jumps occur in the temperature regime near the glass transition temperature, T_g. Theocaris [71] has claimed that these jumps are sensitive to both the thickness of the interphase region around the fiber and the volume fraction of the fiber in the composite. Furthermore, based on the experimental data and analysis of Lipatov [72] for particulate composites, Theocaris [71] has proposed the following relationship involving heat capacity jumps, volume fraction of the fiber and the extent of the interphase for unidirectional reinforced epoxies:

$$\left(\frac{r_i}{r_f} \right)^2 - 1 = \left(1 - \frac{\Delta C_p^f}{\Delta C_p^o} \right) \left(\frac{v_f}{1 - v_f} \right) \tag{5}$$

Here ΔC_p^f and ΔC_p^o represent the jumps in the heat capacity of the composite and polymer, respectively.

Samples of pure epoxy and samples of unidirectional E-glass/epoxy with known fiber volume fractions were tested in a Differential Scanning Calorimeter (DSC) over a range of temperatures including the T_g. Heat capacity jumps were determined for each sample as shown in Figure 15. Once the heat capacity jumps were determined, the radius of the inter-

phase was determined from Equation (5) and the interphase and matrix volume fractions were determined from Equation (4).

Interface conditions: The interface conditions for the interphase modulus at the fiber-interphase and interphase-matrix boundaries were assumed to be:

$$E_i(r_f) = E_f; \qquad E_i(r_i) = E_m \tag{6}$$

The condition at the fiber-interphase interface was automatically satisfied. Satisfaction of the condition at the interphase-matrix interface required that :

$$\frac{E_f}{E_m} = \left(\frac{r_i}{r_f}\right)^{(\eta_1 - \eta_2)} \tag{7}$$

Average interphase modulus condition: The rule-of-mixtures for the longitudinal modulus of the composite was assumed to be:

$$E_c = E_f v_f + E_i^a v_i + E_m v_m \tag{8}$$

where E_i^a represents the average value of the interphase modulus. Furthermore, using Equation (3), the average value of the interphase modulus was derived as:

$$E_i^a = \left(\frac{1}{r_i - r_f}\right)\left[E_m \int_{r_f}^{r_i} dr + E_f \int_{r_f}^{r_i} \left(\frac{r_f}{r}\right)^{\eta_1} dr - E_m \int_{r_f}^{r_i} \left(\frac{r_f}{r}\right)^{\eta_2} dr\right] \tag{9}$$

Using the measured values of the longitudinal modulus of the composite, the modulus of the fiber, the modulus of the matrix and the necessary volume fractions, E_i^a was calculated from Equation (8) for each sample and its value was substituted in Equation (9).

Adhesion exponents: The values of η_1 and η_2 were now determined using the interface condition (Equation (7)) and the "average interphase modulus condition" (Equation (9)). Figure

16 shows the variation in the interphase modulus for a E-glass/epoxy composite with a 65% fiber volume fraction.

Theocaris, *et al.* [73] have also considered the following hypothetical variations for the Young's modulus and Poisson's ratio (ν_i) of the interphase:

- Linear — $E_i = A + Br$; $\nu_i = A' + B'r$
- Parabolic — $E_i = Ar^2 + Br + C$; $\nu_i = A'r^2 + B'r + C'$
- Hyperbolic — $E_i = A + \left(\frac{B}{r}\right)$; $\nu_i = A' + \left(\frac{B'}{r}\right)$
- Logarithmic — $E_i = A \ln\left(\frac{B}{r}\right)$; $\nu_i = A' \ln\left(\frac{B'}{r}\right)$

where A, A', B, and B' are constants and a variation for the coefficient of thermal expansion of the interphase [74]. A number of articles by Theocaris and co-workers [73, 75-77] have predicted the moduli of unidirectional fiber-reinforced composites with interphasial property gradients and a more recent publication of Theocaris [78] has dealt with interphase models for reinforced epoxies taking into account the presence of coupling agents on the fibers.

3.1.7 Non-uniform interphase layer model --- Sottos-McCullough-Güçeri

Sottos, *et al.* [15, 38] have adopted a linear relationship for the property gradients in the fiber-matrix interphase of polymeric matrix composites and have used the model in a numerical scheme (Boundary Fitted Coordinates Technique) to study the effect of the interphase on residual thermal stresses. Three different fiber types (carbon, Kevlar 49 and E-glass) and two matrices (IMHS epoxy and polycarbonate) were considered in the study. It was concluded, based on a parametric study, that the interphase in high-performance composites can be tailored to reduce local residual stresses.

A schematic of the model interphase used for this study is shown in Figure 17. Parameters λ and ψ_j characterize the model; λ is the ratio of the width of the affected zone (*radial* distance from the fiber surface to the point in the matrix where the properties return to the bulk value) to the radius of the fiber and ψ_j is the ratio of the value of the j^{th} property

at the fiber-interphase interface to the bulk value in the matrix. The elastic modulus was denoted by the subscript j=m and the coefficient of thermal expansion was denoted by the subscript j=a.

Many interphase types were modeled by varying λ and ψ_j. A reinforced thermoset, for example, with a cure chemistry that resulted in a higher cross-linking density at the fiber-interphase interface than in the bulk matrix was assumed to have :

- a higher elastic modulus at the fiber-interphase interface decreasing along the radial distance into the bulk matrix, and
- a lower coefficient of thermal expansion at the fiber-interphase interface increasing along the radial distance into the bulk matrix.

Such an interphase was modeled by choosing $\psi_m > 1$ and $\psi_a < 1$.

3.1.8 Non-uniform interphase layer model --- Palmese

Palmese [79] has extensively studied the structural modifications of a Epon 828/PACM 20 epoxy in the presence of carbon fibers. Development of a stoichiometric imbalance of epoxy resin and amine curing agent is hypothesized near the carbon fiber surfaces, causing the formation of structural and chemical gradients; variation in structure and chemistry is assumed to lead to gradients in material properties.

Palmese [79] has predicted the interphase modulus profile of a 72% fiber volume fraction carbon-Epon 828/PACM 20 composite using the following methodology:

- A thermodynamic model, that describes the equilibrium behavior of a binary mixture in contact with a surface, was used to predict epoxy and amine concentrations as functions of radial distance from the fiber surface.
- A series of homogeneous epoxy/amine samples were synthesized to match the predicted local interphase composition.

- The modulus and glass transition temperature of the samples were measured by fixed frequency (1 Hz) dynamic mechanical analysis.

The modulus gradient plotted as a function of the radial distance from the fiber surface is shown in Figure 18. The modulus at the fiber-interphase interface starts out at a value lower than for the neat resin, increases sharply, reaches a maximum, and then decreases back to the value of the neat resin. The interphase width for this modulus profile can be estimated from Figure 18 to be about 0.3 μm.

3.2 Summary

The main issues addressed herein can be summarized as follows:

1. Models of physical properties (thickness, Young's modulus, Poisson's ratio and coefficient of thermal expansion) of the interphase have been considered by several researchers in an effort to study the influence of the interphase on overall composite properties or behavior.
2. Hypotheses on interphase formation and properties have been proposed and tested.
3. The models range from hypothetical to semi-empirical and provide approximate representations of the interphase.
4. Non-uniform interphase layer models have been considered only for fiber reinforced-epoxies, while uniform interphase layer models have been used for polymeric, metal and ceramic matrix composites.
5. The models have been used in analyses to study the effect of an interphasial region on:
   - residual thermal stresses in a composite,
   - local stresses in a composite under thermo-mechanical loading situations, and
   - elastic moduli of a composite.

6. The models have been utilized to optimize interphasial behavior and thereby enhance the overall performance of composites.

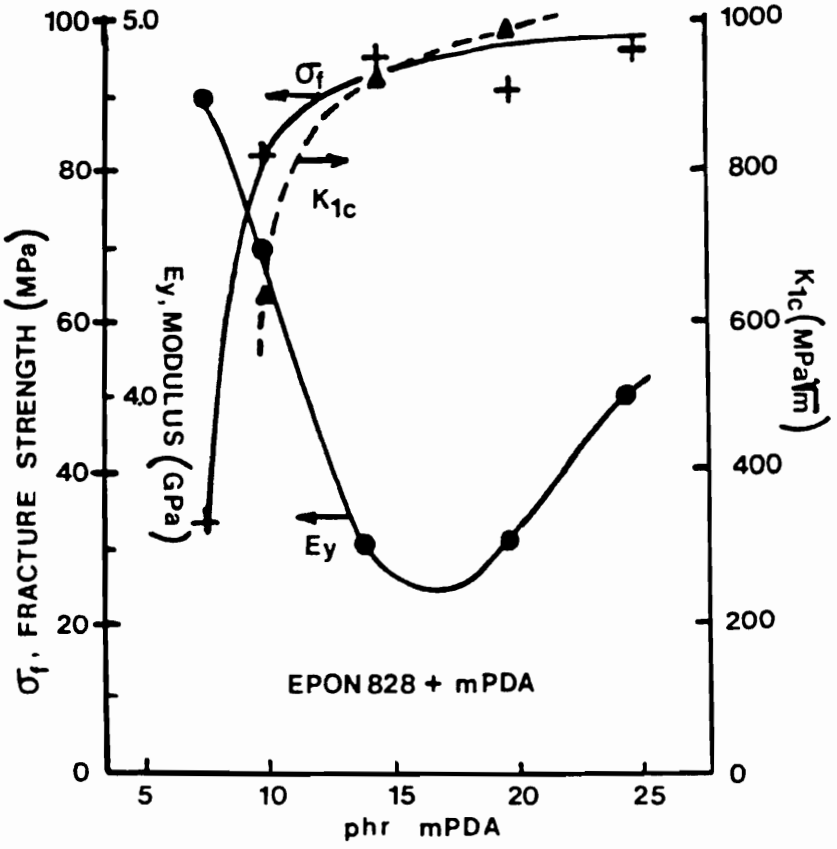

Figure 13. Tensile modulus, Fracture strength, and Fracture toughness of Epon 828/mPDA mixtures as a function of parts per hundred resin (phr) of mPDA [70].

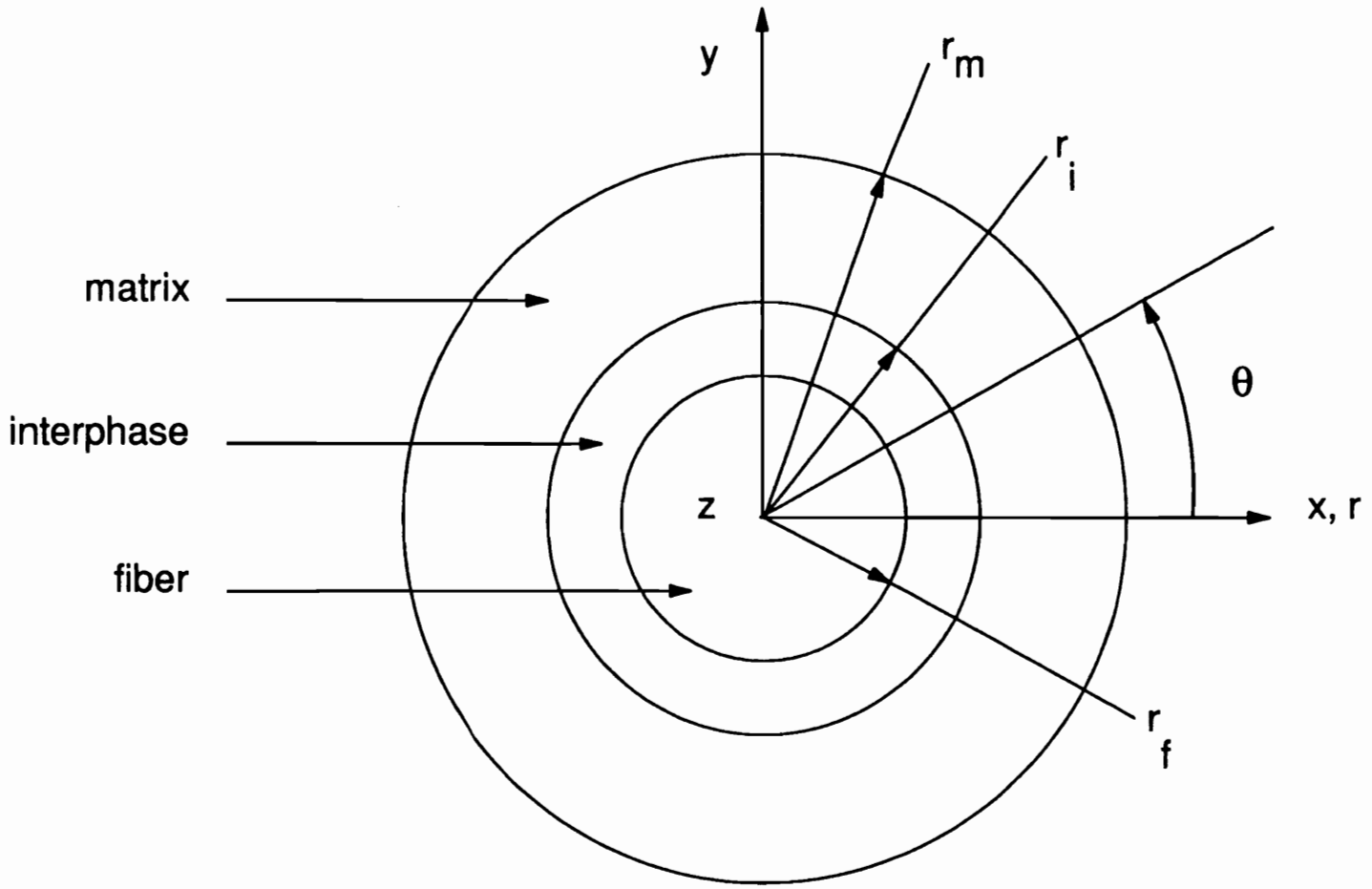

Figure 14. Representative volume element used in the model of Theocaris [71].

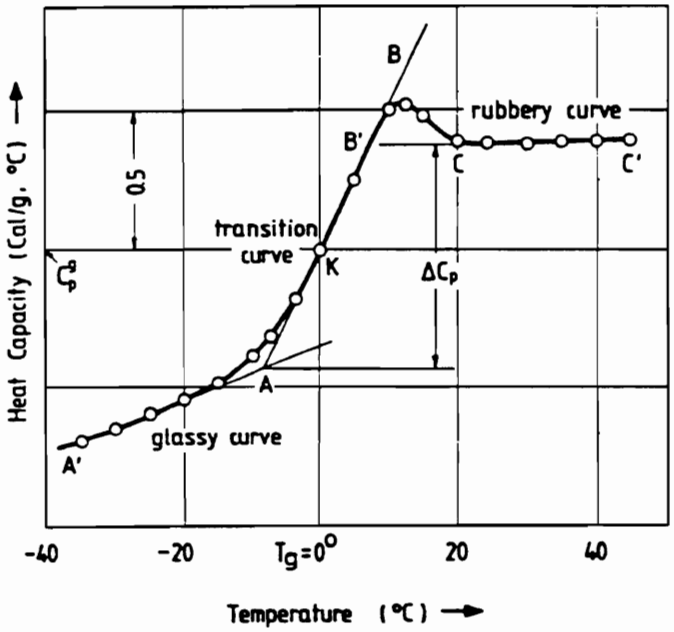

Figure 15. A typical DSC trace for the specific heat jump in E-glass/epoxy [71].

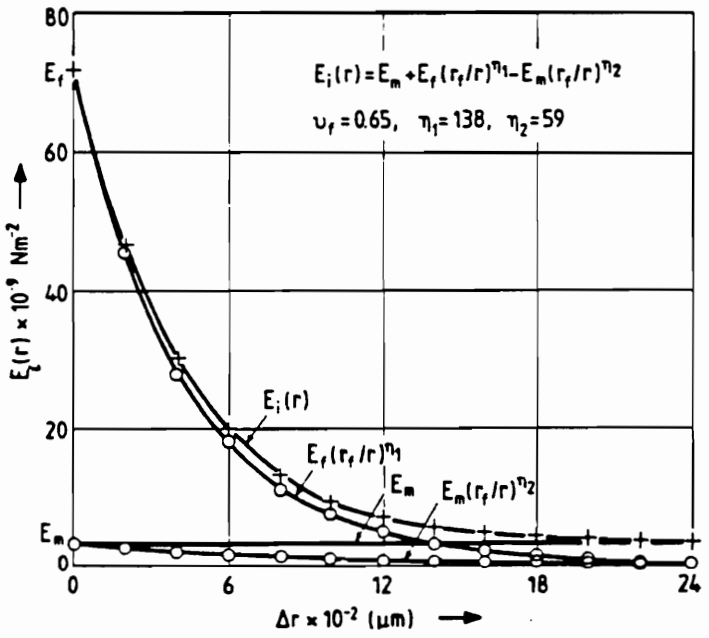

Figure 16. Theoretical interphase Young's modulus profile of a E-glass/epoxy composite with a 65% fiber volume fraction [71].

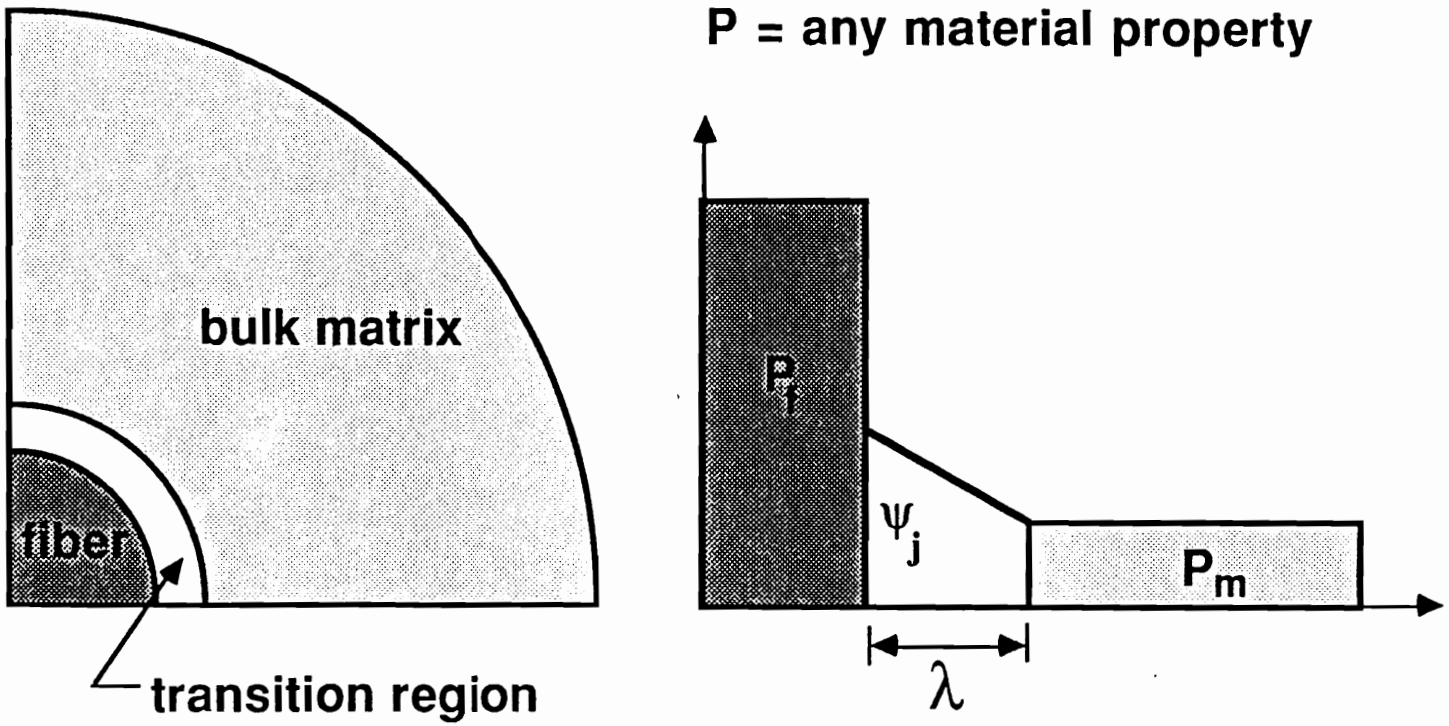

Figure 17. A schematic diagram of the interphase model used by Sottos, et al. [15].

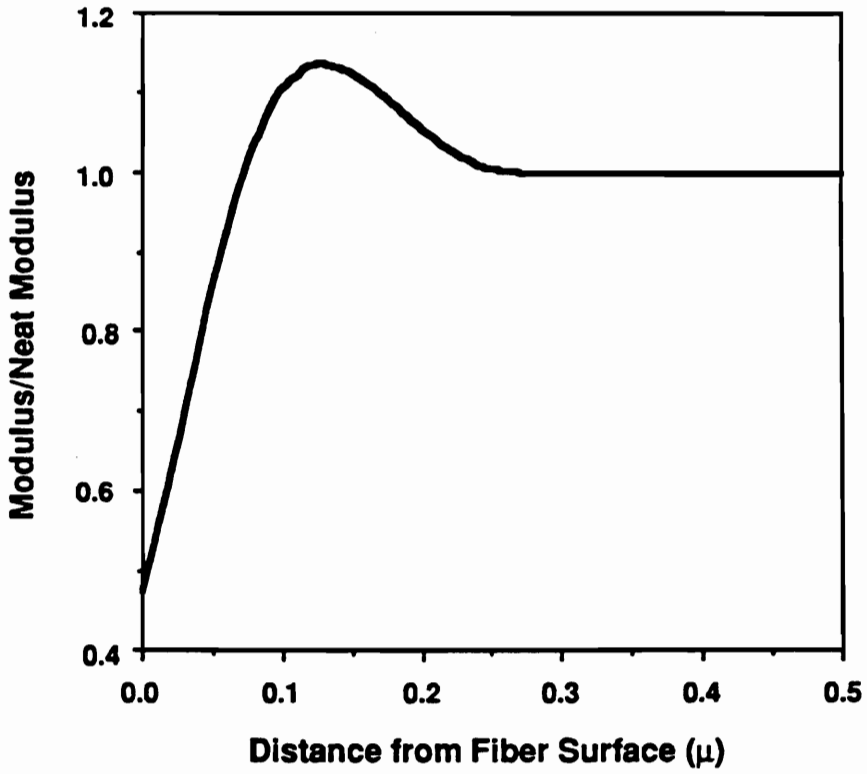

Figure 18. Theoretical interphase modulus profile of a carbon/Epon 828-PACM 20 composite with a 72% fiber volume fraction [79].

4.0 Fiber-Interphase-Matrix Model

The present model considers the interphase in a fiber-reinforced epoxy; the model follows some of the ideas set forth in the models available in the literature and includes the following assumptions:

- The interphase is simulated by a circular cylindrical shell of inner radius, r_f (also the radius of the fiber) and outer radius, r_i as shown in Figure 19(a); the fiber, simulated by a solid circular cylinder of radius, r_f lies inside the shell, while the matrix lies outside. The matrix, interphase and the fiber are denoted by m, i and f, respectively. The properties of the matrix, interphase and the fiber are denoted by subscripts m, i and f, respectively. The interphase thickness and fiber diameter are denoted by c and d, respectively. The variable ϕ is defined as the ratio of the interphase thickness to the fiber diameter.
- The fiber is transversely isotropic (or isotropic) and linearly elastic.
- The interphase and the matrix are isotropic and linearly elastic.
- The values of the Young's modulus (E_i) and the coefficient of thermal expansion (α_i) at the interphase-matrix interface are equal to the bulk matrix values (E_m and α_m).
- The values of the Young's modulus and the coefficient of thermal expansion at the fiber-interphase interface are ratios of the values in the bulk matrix. These ratios are repres-

ented by ξ_y and ξ_c, where subscripts y and c indicate the modulus ratio and the coefficient of thermal expansion ratio respectively (See Figure 19(b)).

- The ratios are, to a certain extent, suggested by the cure chemistry of epoxy.
  - If a higher cross-linking density is present at the fiber-interphase interface than in the bulk matrix, then this is expected to result in a higher elastic modulus and a lower coefficient of thermal expansion at that interface. Thus, if $\xi_y > 1$, then $\xi_c < 1$. The Young's modulus of the interphase in this case will resemble the interphasial Young's modulus predicted by Williams, *et al.* [42] and Theocaris [71].
  - If a lower cross-linking density is present at the fiber-interphase interface than in the bulk matrix, then this is expected to result in a lower elastic modulus and a higher coefficient of thermal expansion at that interface. Thus, if $\xi_y < 1$, then $\xi_c > 1$. The Young's modulus of the interphase in this case will resemble the interphasial Young's modulus predicted by Erickson, *et al.* [68], Drzal, *et al.* [70] and Palmese [79].
- The Young's modulus and the coefficient of thermal expansion of the interphase are functions of the radial coordinate.
- The Young's modulus and the coefficient of thermal expansion of the interphase follow the same functional form. Different surface treatments, sizings, etc., applied to the fiber and different manufacturing processes alter the nature of the interphase differently; this, in turn, may cause the interphase properties to follow different functional forms. The functional forms chosen to represent the Young's modulus and the coefficient of thermal expansion of the interphase are:
  - Power variation — $P\left(\frac{r}{r_f}\right)^Q$
  - Reciprocal variation — $\frac{P}{\left(\frac{r}{r_f}\right)-Q}$
  - Cubic variation — $P\left(\frac{r}{r_f}\right)^3+Q\left(\frac{r}{r_f}\right)^2+R\left(\frac{r}{r_f}\right)+S$

P, Q, R and S are constants that have to be determined from the interface conditions for the properties; subscripts y and c on these constants would indicate if a particular variation represents Young's modulus or coefficient of thermal expansion. For example, $P_y\left(\frac{r}{r_f}\right)^{Q_y}$ represents the Young's modulus of the interphase modeled by the Power variation.

- The interface conditions for the Young's modulus and coefficient of thermal expansion are given by :

$$E_i(r_i) = E_m\,; \quad E_i(r_f) = \xi_y E_m\,; \quad \alpha_i(r_i) = \alpha_m\,; \quad \alpha_i(r_f) = \xi_c \alpha_m \tag{10}$$

Additional conditions that have to be used in the case of cubic variations are "zero-slope conditions" given by:

$$\frac{dE_i}{dr}\Big|_{r=r_i} = 0\,; \quad \frac{dE_i}{dr}\Big|_{r=r_f} = 0\,; \quad \frac{d\alpha_i}{dr}\Big|_{r=r_i} = 0\,; \quad \frac{d\alpha_i}{dr}\Big|_{r=r_f} = 0 \tag{11}$$

or "intra-interphase conditions" given by:

$$E_i(r_1') = E_1'\,; \quad E_i(r_2') = E_2'\,; \quad \alpha_i(r_1') = \alpha_1'\,; \quad \alpha_i(r_2') = \alpha_2' \tag{12}$$

where r_1' and r_2' are radial points inside the interphase ($r_f < r_1', r_2' < r_i$) and E_1', E_2', α_1', and α_2' are constant values of the properties. The "zero-slope" conditions have been used for the cubic variations in this study.

- The Poisson's ratio of the interphase (ν_i) is assumed to be constant and the same as that of the matrix.
- The bonding between the phases is perfect.

Many different interphases can be modeled by varying the parameters ϕ (representing the interphase thickness), ξ (representing the values of the properties at the fiber-interphase interface), and the type of spatial variation (Power, Reciprocal and Cubic).

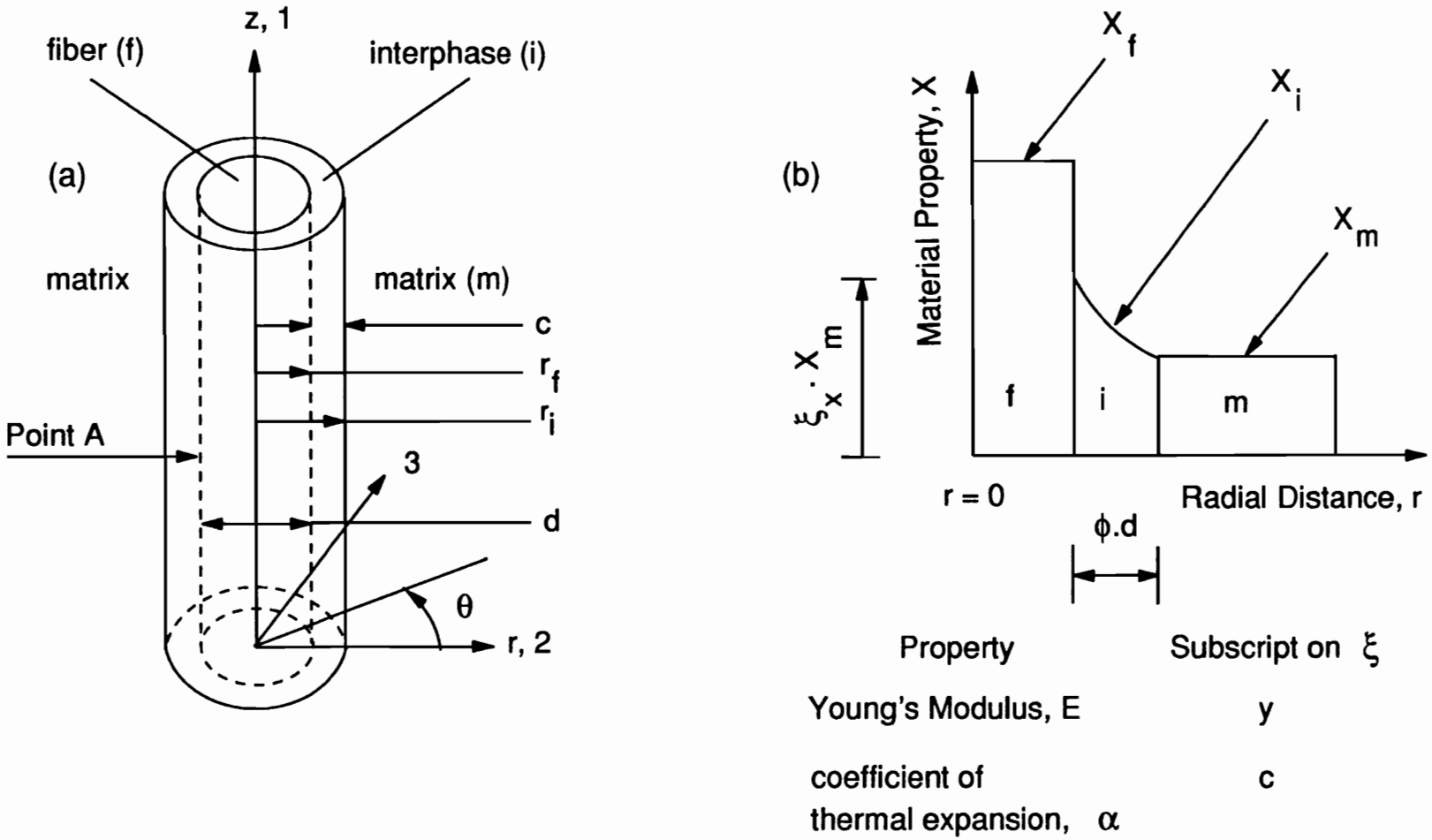

Figure 19. Schematic of the interphase: (a) Location, and (b) Property variation.

5.0 Effect on Residual Thermal Stresses

In general, large residual stresses may develop in the interphase during composite processing due to:

- differences in the thermal expansion coefficients of the fiber and matrix,
- differential cure shrinkage and spatial variations in morphology in thermosetting matrices,
- melting/solidification in thermoplastics, and
- phase transformations with accompanying volume changes in metallic matrices.

Depending on their nature, these stresses for example, can enhance surface contact between the fiber and matrix, cause debonding, or initiate matrix cracking. The connection between residual stresses and fiber/matrix adhesion has been studied by a number of researchers [80-84].

Penn, *et al.* [80] have attempted to find the reasons behind the difference in interfacial shear strength, observed in single fiber pull-out tests, between graphite/epoxy and aramid/epoxy systems. It was concluded that the smaller coefficient of thermal expansion mismatch between fiber and matrix in aramid/epoxy resulted in a lower level of thermal stresses and relatively weaker interfacial adhesion in aramid/epoxy. It was also shown that the interfacial shear strength increased with cure temperature for both systems. Jang, *et al.*

[81] have also evaluated the effect of cure temperature on the debonding load of polypropylene/epoxy and nylon/epoxy as measured by pull-out tests. The debonding load increased with cure temperature in the case of polypropylene/epoxy but, there were no clear trends in the case of nylon/epoxy. Kalantar and Drzal [82] have verified the trend in the results of Penn, *et al.* [80] for the dependence of interfacial shear strength of graphite/epoxy on cure temperature; however, no significant dependence of the interfacial shear strength of aramid/epoxy on cure temperature was found. Banbaji [83, 84] has shown that increasing the compressive stresses normal to the fiber in a polypropylene/cement composite results in higher interfacial shear strength; shrinkage stresses and curing stresses are given as reasons for the study. Thus, the residual thermal stress field is one of the factors that control the structural performance of a composite by controlling the interfacial adhesion.

In this chapter, a variation of the concentric cylinder assemblage analysis of Hashin and Rosen [85] is employed to evaluate the constituent stresses in a unidirectional fiber-reinforced composite subjected to a uniform temperature change, T^0. The composite consists of three phases — the fiber, interphase and matrix; the interphase Young's modulus and coefficient of thermal expansion are modeled as outlined in Chapter 4. The formulation of the problem, the solution methods, and the results are presented in the following sections.

5.1 Problem Formulation

5.1.2 Assumptions

- The continuous fiber composite is simulated by a representative volume element consisting of three concentric, long, circular cylinders. The three cylinders represent the

matrix, the interphase and the fiber — the three domains of the problem and their radii are denoted by r_m, r_i, and r_f, respectively.

- The composite end conditions are considered only in the St.Venant sense.
- The temperature change is uniform in all the phases.
- The composite experiences axisymmetric generalized plane-strain.

5.1.2 Displacement Field

A cylindrical coordinate system (r, θ, z) is considered with z as the axial coordinate and r-θ as the transverse plane. Due to axisymmetry and the absence of shear in the concentric cylinder assemblage model, the displacement field in the n-th domain (n = m, i, f) can be expressed by

$$u_r^{(n)} = u^{(n)}(r); \quad u_\theta^{(n)} = 0; \quad u_z^{(n)} = w^{(n)}(z) \tag{13}$$

where $u_j^{(n)}$ are the components of displacement.

5.1.3 Fiber (n=f) and Matrix (n=m) Domains

The Navier's equations of elasticity are :

$$\frac{d^2 w^{(n)}}{dz^2} = 0 \tag{14}$$

$$\frac{d^2 u^{(n)}}{dr^2} + \frac{1}{r}\frac{du^{(n)}}{dr} - \frac{u^{(n)}}{r^2} = 0 \tag{15}$$

The general solution to Equation (14) is given by

$$w^{(n)}(z) = C^{(n)}z + D^{(n)} \tag{16}$$

and the general solution to Equation (15) is found by the Cauchy-Euler method (see section on Solution Methods) to be

$$u^{(n)}(r) = A^{(n)}r + \frac{B^{(n)}}{r} \tag{17}$$

$A^{(n)}, B^{(n)}, C^{(n)}$ and $D^{(n)}$ are unknown constants which will be determined by the boundary/interface conditions.

5.1.4 Interphasial Domain (n=i)

Model 1: The Young's modulus and the coefficient of thermal expansion of the interphase are given by

$$E_i = P_y\left(\frac{r}{r_f}\right)^{Q_y}; \quad \alpha_i = P_c\left(\frac{r}{r_f}\right)^{Q_c} \tag{18}$$

The Navier's equations of elasticity are:

$$\frac{d^2w^{(i)}}{dz^2} = 0 \tag{19}$$

$$\frac{d^2u^{(i)}}{dr^2} + \left[\frac{Q_y + 1}{r}\right]\frac{du^{(i)}}{dr} + \left[\frac{Q_y\frac{\nu_i}{1-\nu_i} - 1}{r^2}\right]u^{(i)} + \left[\frac{\nu_i}{1-\nu_i}\frac{Q_y}{r}\right]\frac{dw^{(i)}}{dz}$$

$$-\left[\frac{1+\nu_i}{1-\nu_i}\frac{P_c(Q_y + Q_c)r^{Q_c - 1}}{r_f^{Q_c}}\right]T^0 = 0 \tag{20}$$

The general solution to Equation (19) is given by

$$w^{(i)}(z) = C^{(i)}z + D^{(i)} \tag{21}$$

and the general solution to Equation (20) is found by the Cauchy-Euler method to be

$$u^{(i)}(r) = A^{(i)}r^{m_1} + B^{(i)}r^{m_2} - C^{(i)}\nu_i r + \frac{\frac{1+\nu_i}{1-\nu_i}P_c(Q_y+Q_c)r^{Q_c+1}T^0}{\left\{Q_c{}^2 + 2Q_c + Q_yQ_c + Q_y + Q_y\frac{\nu_i}{1-\nu_i}\right\}r_f{}^{Q_c}} \tag{22}$$

where

$$m_1, m_2 = \frac{1}{2}\left[-Q_y \pm \sqrt{\frac{Q_y{}^2(1-\nu_i) - 4\nu_i(Q_y+1)+4}{1-\nu_i}}\right]$$

$A^{(i)}$, $B^{(i)}$, $C^{(i)}$ and $D^{(i)}$ are unknown constants which will be determined by the boundary/interface conditions.

Model 2: The Young's modulus and the coefficient of thermal expansion of the interphase are given by

$$E_i = \frac{P_y}{\left(\frac{r}{r_f} - Q_y\right)}; \quad \alpha_i = \frac{P_c}{\left(\frac{r}{r_f} - Q_c\right)} \tag{23}$$

The Navier's equations of elasticity are:

$$\frac{d^2w^{(i)}}{dz^2} = 0 \tag{24}$$

$$\frac{d^2u^{(i)}}{dr^2} + \left[\frac{Q_yr_f}{r(Q_yr_f - r)}\right]\frac{du^{(i)}}{dr} + \left[\frac{r\left(\frac{1}{1-\nu_i}\right) - Q_yr_f}{r^2(Q_yr_f - r)}\right]u^{(i)} + \left[\frac{\frac{\nu_i}{1-\nu_i}}{Q_yr_f - r}\right]\frac{dw^{(i)}}{dz}$$

$$+\left[\frac{1+\nu_i}{1-\nu_i}\frac{P_c r_f^2(Q_y+Q_c)-2P_c r_f r}{(Q_y r_f-r)(Q_c r_f-r)^2}\right]T^0=0 \tag{25}$$

The general solution to Equation (24) is given by

$$w^{(i)}(z)=C^{(i)}z+D^{(i)} \tag{26}$$

where $C^{(i)}$ and $D^{(i)}$ are unknown constants. The general solution to Equation (25) is found by the Series Solution method (see section on Solution Methods) resulting in an expression for $u^{(i)}$ with unknown constants $A^{(i)}, B^{(i)}$ and $C^{(i)}$. The constants $A^{(i)}, B^{(i)}, C^{(i)}$ and $D^{(i)}$ will be determined by the boundary/interface conditions.

Model 3: The Young's modulus and the coefficient of thermal expansion are given by

$$E_i=P_y\left(\frac{r}{r_f}\right)^3+Q_y\left(\frac{r}{r_f}\right)^2+R_y\left(\frac{r}{r_f}\right)+S_y;\quad \alpha_i=P_c\left(\frac{r}{r_f}\right)^3+Q_c\left(\frac{r}{r_f}\right)^2+R_c\left(\frac{r}{r_f}\right)+S_c \tag{27}$$

The Navier's equations of elasticity are:

$$\frac{d^2w^{(i)}}{dz^2}=0 \tag{28}$$

$$\frac{d^2u^{(i)}}{dr^2}+\left[\frac{4\frac{P_y}{r_f^3}r^3+3\frac{Q_y}{r_f^2}r^2+2\frac{R_y}{r_f}r+S_y}{r\left(\frac{P_y}{r_f^3}r^3+\frac{Q_y}{r_f^2}r^2+\frac{R_y}{r_f}r+S_y\right)}\right]\frac{du^{(i)}}{dr}$$

$$+\left[\frac{\left(3\frac{\nu_i}{1-\nu_i}-1\right)\frac{P_y}{r_f^3}r^3+\left(2\frac{\nu_i}{1-\nu_i}-1\right)\frac{Q_y}{r_f^2}r^2+\left(\frac{\nu_i}{1-\nu_i}-1\right)\frac{R_y}{r_f}r-S_y}{r^2\left(\frac{P_y}{r_f^3}r^3+\frac{Q_y}{r_f^2}r^2+\frac{R_y}{r_f}r+S_y\right)}\right]u^{(i)}$$

$$+\left[\frac{\nu_i}{1-\nu_i}\frac{3\frac{P_y}{r_f^3}r^2+2\frac{Q_y}{r_f^2}r+\frac{R_y}{r_f}}{\frac{P_y}{r_f^3}r^3+\frac{Q_y}{r_f^2}r^2+\frac{R_y}{r_f}r+S_y}\right]\frac{dw^{(i)}}{dz}-\left[\frac{1+\nu_i}{1-\nu_i}\left\{3\frac{P_c}{r_f^3}r^2+2\frac{Q_c}{r_f^2}r+\frac{R_c}{r_f}\right\}\right]T^0$$

$$-\left[\frac{1+\nu_i}{1-\nu_i}\frac{\left\{\frac{P_c}{r_f^3}r^3+\frac{Q_c}{r_f^2}r^2+\frac{R_c}{r_f}r+S_c\right\}\left\{3\frac{P_y}{r_f^3}r^2+2\frac{Q_y}{r_f^2}r+\frac{R_y}{r_f}\right\}}{\frac{P_y}{r_f^3}r^3+\frac{Q_y}{r_f^2}r^2+\frac{R_y}{r_f}r+S_y}\right]T^0=0 \tag{29}$$

The general solution to Equation (28) is given by

$$w^{(i)}(z)=C^{(i)}z+D^{(i)} \tag{30}$$

where $C^{(i)}$ and $D^{(i)}$ are unknown constants. The general solution to Equation (29) is found by the Series Solution method resulting in an expression for $u^{(i)}$ with unknown constants $A^{(i)}$, $B^{(i)}$ and $C^{(i)}$. The constants $A^{(i)}$, $B^{(i)}$, $C^{(i)}$ and $D^{(i)}$ will be determined by the boundary/interface conditions.

5.1.5 Comments on Navier's Equations

- The Navier's equations in axial displacement (w) for the fiber, matrix and interphasial domains are of the same form.
- The Navier's equations in radial displacement (u) for the fiber and matrix domains are of the same form.
- The Navier's equations in radial displacement (u) for the interphasial domain are affected by the material property variations in the interphase as follows:
  - A coupling term (dw/dz) and a forcing function term ($T°$) are introduced.

- The interphase material constants (P_y, Q_y, R_y and S_y) and the fiber radius (r_f) appear in the coefficients of du/dr and u.

5.2 Solution Methods

5.2.1 Solution Methods for the Governing Differential Equations

Equations (15) and (20) are solved by the Cauchy-Euler method. The equations are transformed into equations with constant coefficients after making a change of variables

$$r = e^x \tag{31}$$

where x is the transformed independent variable. The differential equations are then solved by one of the basic methods [86].

Equation (25) has singularities at $r = 0$, $r = Q_y r_f$ and $r = Q_c r_f$, while Equation (29) has singularities at $r = 0$ and at the roots of $P_y\left(\frac{r}{r_f}\right)^3 + Q_y\left(\frac{r}{r_f}\right)^2 + R_y\left(\frac{r}{r_f}\right) + S_y = 0$. The singularity at $r = 0$ occurs at the center of the fiber and therefore, is not of physical interest in the interphase. It can be shown that the other singularities in the cases under consideration also lie outside the interphase. Hence, an ordinary point, r_o, is chosen at the middle of the interphase and the differential equations are solved about this ordinary point by the Series Solution method. The radial displacement is chosen to be :

$$u^{(i)}(r) = \sum_{k=0}^{\infty} F_k x^k \tag{32}$$

$$x = (r - r_o) \tag{33}$$

where x is the transformed independent variable and F_k are the coefficients of the power series. Equation (32) and Equation (33) are substituted into the differential equations and the coefficients of like powers of r are equated to find F_k in terms of constants $A^{(i)}$, $B^{(i)}$ and $C^{(i)}$. $u^{(i)}$ is now found in terms of $A^{(i)}$, $B^{(i)}$, $C^{(i)}$ and powers of r [87]. The software package MACSYMA [88] was used to write a symbolic program that determines $u^{(i)}$.

Since the boundary conditions of the interphasial domain are actually the interface conditions of the concentric cylinder assemblage problem (See next section), $u^{(i)}$ can be determined only after the concentric cylinder assemblage problem is solved. The convergence of the series representing $u^{(i)}$ is met by solving the concentric cylinder assemblage problem for successive values of k and examining the values of $u^{(i)}$ at different points along the interphasial domain. Hence, the convergence of $u^{(i)}$ has to be proved individually for each case being considered.

5.2.2 Solution Method for the Concentric Cylinder Assemblage Problem

The following three cases of concentric cylinder assemblages are considered:

- CCA 1 --- Fiber/Interphase Model 1/Matrix.
- CCA 2 --- Fiber/Interphase Model 2/Matrix.
- CCA 3 --- Fiber/Interphase Model 3/Matrix.

The displacements in the constituents in each of the above cases are given by the solutions of the governing differential equations valid in that particular domain. The strains and the stresses in the constituents are determined by making use of the strain-displacement and the constitutive relations, respectively. The displacement, the strain and the stress fields of the problem are then given by twelve constants ($A^{(n)}$, $B^{(n)}$, $C^{(n)}$, $D^{(n)}$, n = m, i, f) which are determined by the boundary/interface conditions.

The boundary and interface conditions for this problem are given by

$$\int_0^{r_f} \sigma_{zz}^{(f)} r dr + \int_{r_f}^{r_i} \sigma_{zz}^{(i)} r dr + \int_{r_i}^{r_m} \sigma_{zz}^{(m)} r dr = 0 \tag{34}$$

$$\sigma_{rr}^{(m)} = 0 \quad at \quad r = r_m \tag{35}$$

$$u^{(m)} = u^{(i)} \quad w^{(m)} = w^{(i)} \quad \sigma_{rr}^{(m)} = \sigma_{rr}^{(i)} \quad at \quad r = r_i \tag{36}$$

$$u^{(i)} = u^{(f)} \quad w^{(i)} = w^{(f)} \quad \sigma_{rr}^{(i)} = \sigma_{rr}^{(f)} \quad at \quad r = r_f \tag{37}$$

where σ_{rr} and σ_{zz} represent the radial and axial stresses, respectively.

The required end conditions are given by:

$$\sigma_{zz}^{(m)}(r, \pm l/2) = \sigma_{zz}^{(i)}(r, \pm l/2) = \sigma_{zz}^{(f)}(r, \pm l/2) = 0 \tag{38}$$

where l is the length of the cylinder assemblage. Since end conditions (38) are difficult to enforce, condition (34), "equivalent in the St.Venant sense" to conditions (38) is enforced. The concentric cylinder assemblage analysis does not take into account fiber-fiber interaction; boundary condition (35) is a direct consequence of this assumption. Interface conditions (36) and (37) are dictated by the assumption of perfect bonding at the fiber-interphase and interphase-matrix interfaces.

The interface conditions on w dictate that $C^{(m)} = C^{(i)} = C^{(f)} = C$ and $D^{(m)} = D^{(i)} = D^{(f)} = D$. Since D represents a rigid body displacement, it can be set to zero without loss of generality. Thus, we have

$$w^{(m)}(z) = w^{(i)}(z) = w^{(f)}(z) = Cz \tag{39}$$

$B^{(f)}$ must be set equal to zero, since $|u^{(f)}(0)| < \infty$. The remaining six boundary/interface conditions are used to solve for the remaining constants $A^{(m)}$, $A^{(i)}$, $A^{(f)}$, $B^{(m)}$, $B^{(i)}$ and C. The dis-

placements, the strains and the stresses in each of the constituents are determined using the values of the above constants.

5.2.3 Check on the Solution Methods

The following two methods were employed to check the solution methods and the numerical calculations:

- The non-uniform interphase region in the case of the concentric cylinder assemblage CCA 1 was replaced by a region made up of n uniform cylinders each possessing a progressively different Young's modulus and coefficient of thermal expansion. The thermal stress analysis was performed for this n+2 cylinder assemblage and compared to the stresses obtained from CCA 1.
- By selectively specifying values of P, Q, R and S, one may reduce Equations (25) and (29) into forms that may be readily solved by the Cauchy-Euler method. This fact was employed to partially check the algorithms used in the symbolic manipulation programs that solve Equations (25) and (29). For example, setting $P_y = Q_y = R_y = 0$ and $P_c = Q_c = R_c = 0$ in Equation (29) results in Equation (15) for which the general solution is given by Equation (17). Equation (29) was solved using the symbolic program for $P_y = Q_y = R_y = 0$ and $P_c = Q_c = R_c = 0$ and the results were compared with Equation (17).

Good agreements were found in these checks.

5.3 Results and Discussion

E-glass/IMHS epoxy, carbon/IMHS epoxy and Kevlar 49/IMHS epoxy are considered in this discussion; typical bulk property values of E-glass fiber [15], carbon fiber [15, 89],

Kevlar 49 fiber [15, 90], and IMHS epoxy [15, 89] are given in Table 4. Parametric studies were performed by varying the functional form of the interphase properties, fiber volume fraction, V_f and parameters ϕ, ξ_y, and ξ_c and the results are presented. A uniform temperature change of -1 °C was assumed for all the results; the total buildup of residual stresses can be found by multiplying the results by the actual temperature change.

Figures 20, 21, and 22 present the constituent stresses in E-glass/IMHS epoxy composites for different interphasial properties. Figures 23, 24, and 25 present the constituent stresses in carbon/IMHS epoxy composites modeled by the concentric cylinder assemblages CCA 1, CCA 2 and CCA 3. The magnitude of the radial stress and the hoop stress ($\sigma_{\theta\theta}$) in the fiber are the same in Figures 20, 21, 22, 23, 24, and 25. The figures clearly bring out the fact that the constituent stresses depend on:

- the presence or absence of an interphase region (Figure 20 vs. Figure 22),
- the presence or absence of an interphase region with one or more properties following a certain functional form (Figure 21 vs. Figure 22), and
- the presence of an interphase region with the properties following different functional forms, to a smaller extent (Figures 23, 24, and 25).

Changing the type of property variation results in modest changes to the property profile, for a given set of similar conditions. This results in small changes in the stress state, as can be seen by a comparison of Figures 23, 24, and 25. Figures 26, 27, and 28 show the redistribution of the stresses in the interphasial region of Kevlar 49/IMHS epoxy (modeled by the concentric cylinder assemblage CCA 1) as a function of ξ_y.

Table 5 presents the stresses at the fiber-interphase interface (point A in Figure 19) in carbon/IMHS epoxy and Kevlar 49/IMHS epoxy composites as a function of the various parameters indicated; the composites are modeled by the concentric cylinder assemblage CCA 1. The following observations can be made based on Table 5:

- The radial stresses in carbon/IMHS epoxy are more compressive than those in Kevlar 49/IMHS epoxy for all cases considered. A similar trend was considered by Penn, *et al.*

[80] as a possible reason for the higher interphasial shear strength observed in graphite/epoxy as compared to aramid/epoxy.

- Both composites show an increase in compressive radial stresses with a decrease in V_f, increase in ϕ, increase in ξ_y and increase in ξ_c; similar trends have been reported by Sottos, *et al.* [15].
- Assuming that
  - room temperature - cure temperature = T^0 = -100 °C, and
  - interphase tensile strength = matrix tensile strength = 103.43 MPa [89],

  some of the hoop stress and axial stress values may produce preferential failure at the fiber-interphase interface.

Rojstaczer, *et al.* [91] have experimentally determined the coefficients of thermal expansion of Kevlar 49 fiber to be:

- axial coefficient = α_{11} = - 5.7 ppm/°C, and
- transverse coefficient = α_{22} = 66.3 ppm/°C.

The transverse coefficient of thermal expansion is considerably different from the value reported in the "Data Manual for Kevlar 49 Aramid" [90]. The radial stresses in Kevlar 49/IMHS epoxy will be much less compressive than the values reported in Table 5 if the coefficients of thermal expansion obtained by Rojstaczer, *et al.* [91] are used.

Several functional forms are used to simulate the interphase properties; the reciprocal and the cubic variations require the use of the Series Solution method to solve the resulting governing differential equations for the interphasial domain. The convergence requirement for the solutions to these governing differential equations requires that the concentric cylinder assemblage problem be solved multiple times, for consecutive numbers of terms in the series. This is a drawback in using the reciprocal and cubic variations and this solution method to simulate the interphasial behavior.

Table 4. Material properties.

Property	E-glass	carbon	Kevlar 49	IMHS epoxy
E_{11}(GPa)	76.00	214.00	124.00	3.50
E_{22}(GPa)	76.00	14.00	6.90	3.50
G_{12}(GPa)	31.15	14.00	2.80	1.30
α_{11} (ppm/ ℃)	4.90	-1.00	- 5.20	65.00
α_{22} (ppm/ ℃)	4.90	10.10	41.50	65.00
ν_{12}	0.22	0.20	0.36	0.35
ν_{23}	0.22	0.25	0.30	0.35

Table 5. Residual thermal stresses (in KPa) at point A in carbon/IMHS epoxy and Kevlar 49/IMHS epoxy composites.

		carbon/IMHS epoxy			Kevlar 49/IMHS epoxy		
	Variable	σ_{rr}	$\sigma_{\theta\theta}$	σ_{zz}	σ_{rr}	$\sigma_{\theta\theta}$	σ_{zz}
$\phi = 0.06$, $\xi_y = 3$, $\xi_c = 0.75$	$V_f = 0.4$	-117.35	529.58	646.97	-64.95	200.87	581.66
	$V_f = 0.5$	- 99.31	551.74	666.70	-54.79	218.32	600.92
	$V_f = 0.6$	- 81.76	573.03	684.20	-44.75	235.58	617.02
	$V_f = 0.7$	- 64.71	593.56	700.23	-34.83	252.65	631.21
$V_f = 0.4$, $\xi_y = 3$, $\xi_c = 0.75$	$\phi = 0.1$	-126.22	518.98	639.07	-68.01	195.61	577.02
	$\phi = 0.14$	-133.67	510.04	632.26	-70.41	191.47	572.98
	$\phi = 0.18$	-139.97	502.45	626.32	-72.30	188.24	569.43
	$\phi = 0.22$	-145.34	495.96	621.10	-73.76	185.74	566.26
$V_f = 0.4$, $\phi = 0.06$, $\xi_c = 0.75$	$\xi_y = 2$	-108.73	340.40	416.82	-61.18	127.26	380.13
	$\xi_y = 4$	-124.96	716.42	876.16	-68.21	272.59	781.94
	$\xi_y = 6$	-138.42	1,083.39	1,331.48	-73.83	410.89	1,178.96
	$\xi_y = 8$	-150.38	1,442.01	1,782.80	-78.71	543.09	1,571.62
$V_f = 0.4$, $\phi = 0.06$, $\xi_y = 0.75$	$\xi_c = 2$	-101.88	423.96	451.93	-61.59	354.91	449.84
	$\xi_c = 4$	-110.44	942.92	971.40	-69.72	873.13	968.97
	$\xi_c = 6$	-117.70	1,462.80	1,491.71	-76.61	1,392.38	1,488.98
	$\xi_c = 8$	-124.27	1,983.15	2,012.46	-82.85	1,912.17	2,009.46

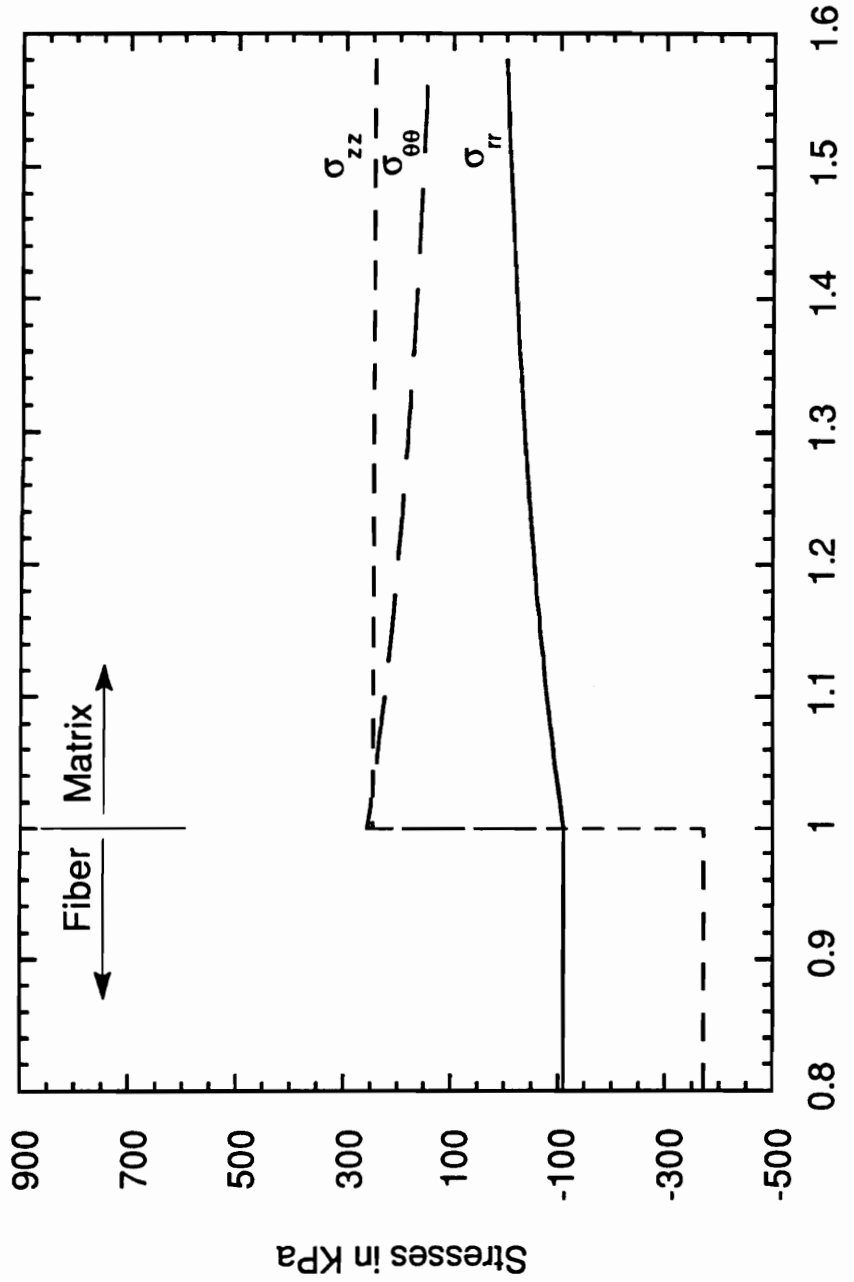

Figure 20. Constituent stresses in a E-glass/IMHS epoxy composite with no interphase: $V_f = 0.4$

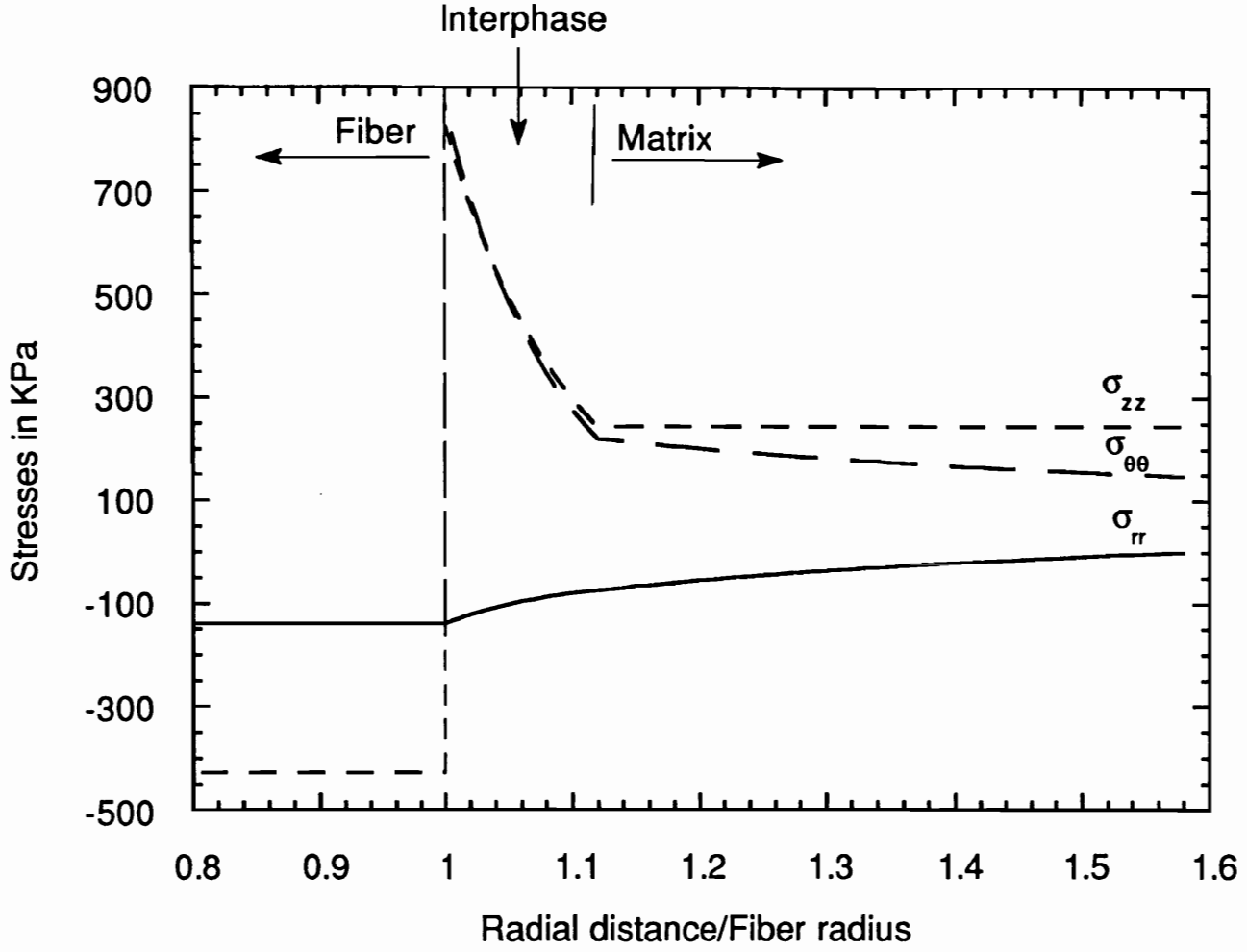

Figure 21. Constituent stresses in a E-glass/IMHS epoxy composite with an interphase possessing gradients in Young's modulus only: $V_f = 0.4$; $\phi = 0.06$; $\xi_y = 3.0$; $E_i = P_y \left(\frac{r}{r_f} \right)^{Q_y}$; $\alpha_i = \alpha_m$.

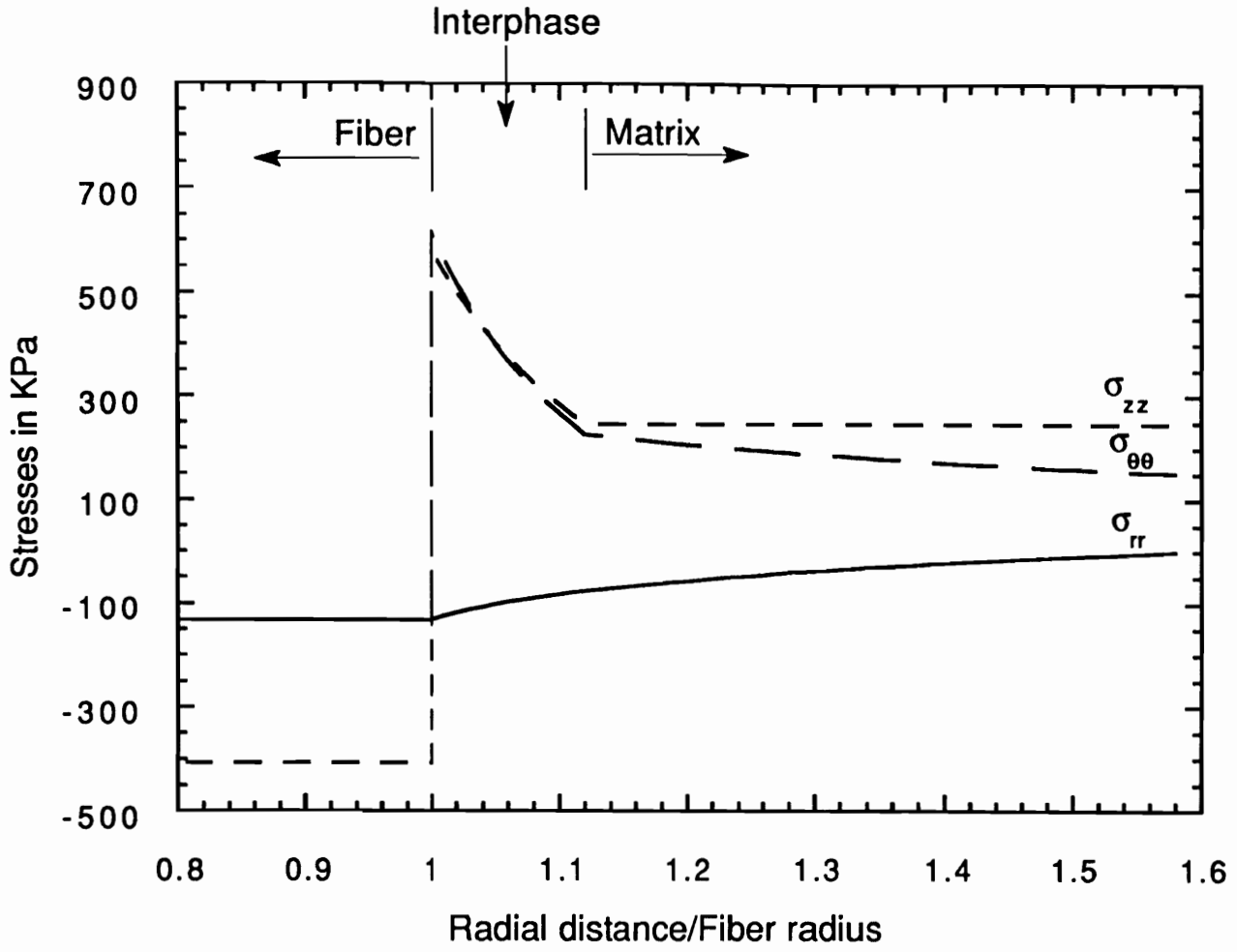

Figure 22. Constituent stresses in a E-glass/IMHS epoxy composite with an interphase possessing gradients in both Young's modulus and coefficient of thermal expansion: $V_f = 0.4$; $\phi = 0.06$; $\xi_y = 3.0$; $E_i = P_y \left(\frac{r}{r_f}\right)^{Q_y}$; $\xi_c = 0.75$; $\alpha_i = P_c \left(\frac{r}{r_f}\right)^{Q_c}$.

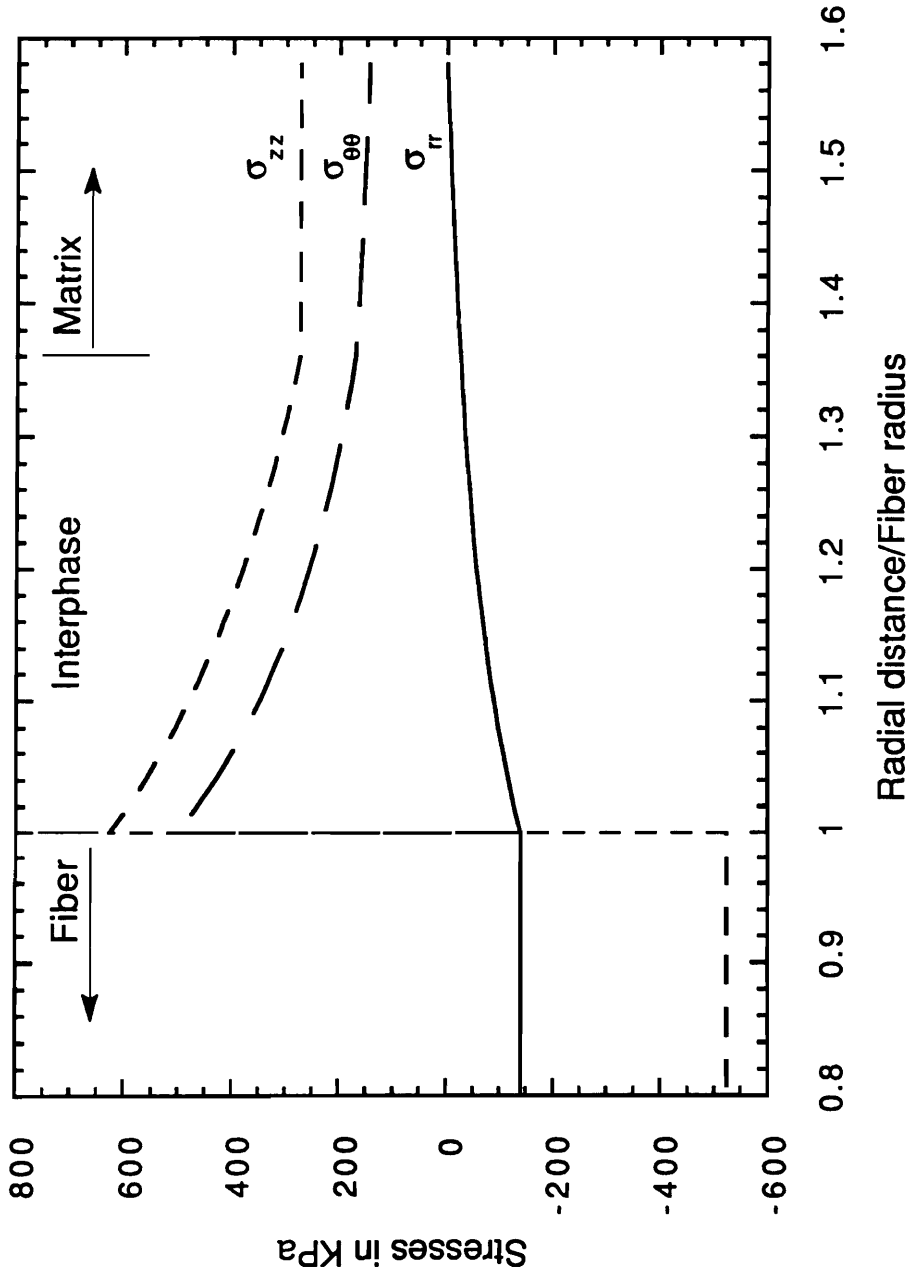

Figure 23. Constituent stresses in a carbon/IMHS epoxy composite modeled by the concentric cylinder assemblage CCA 1: $V_f = 0.4$; $\phi = 0.18$; $\xi_y = 3.0$; $\xi_c = 0.75$.

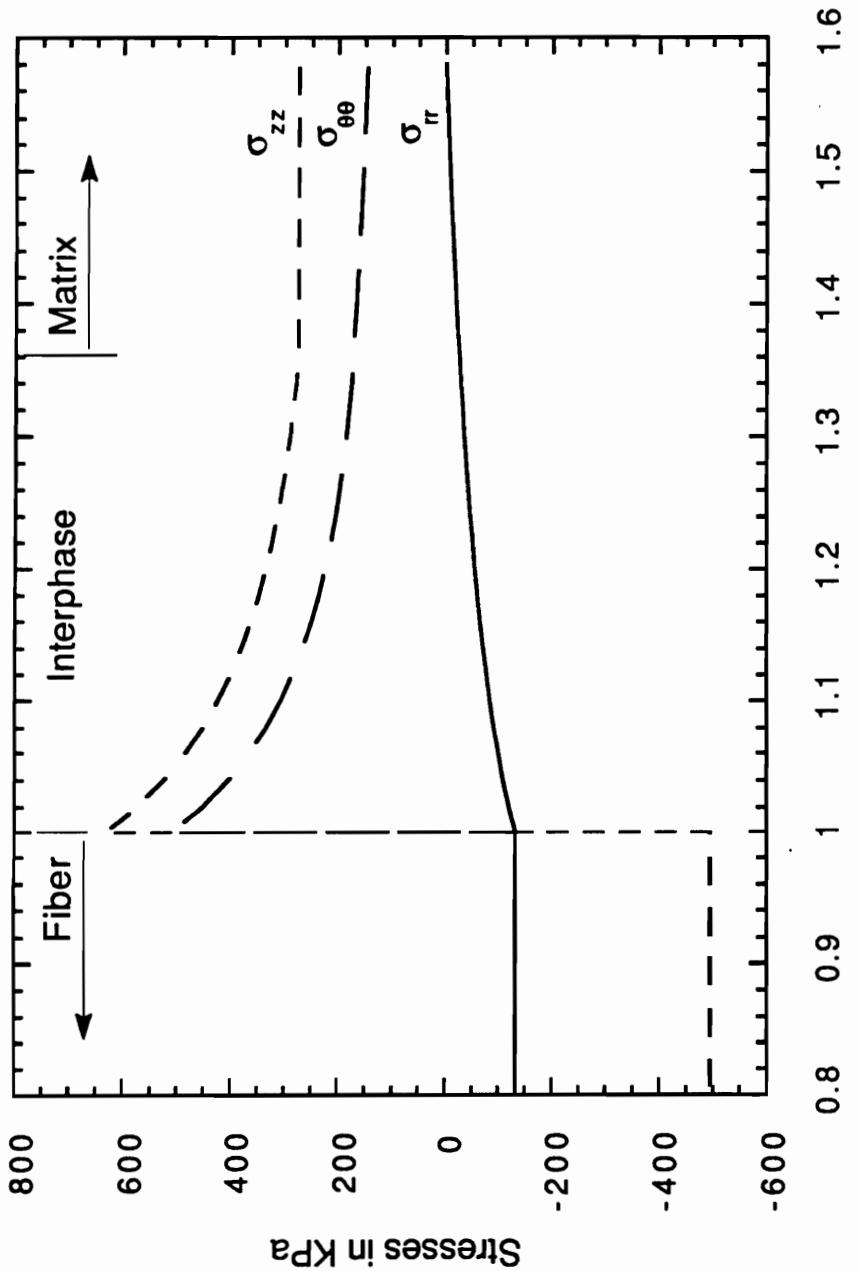

Figure 24. Constituent stresses in a carbon/IMHS epoxy composite modeled by the concentric cylinder assemblage CCA 2: $V_f = 0.4$; $\phi = 0.18$; $\xi_y = 3.0$; $\xi_c = 0.75$.

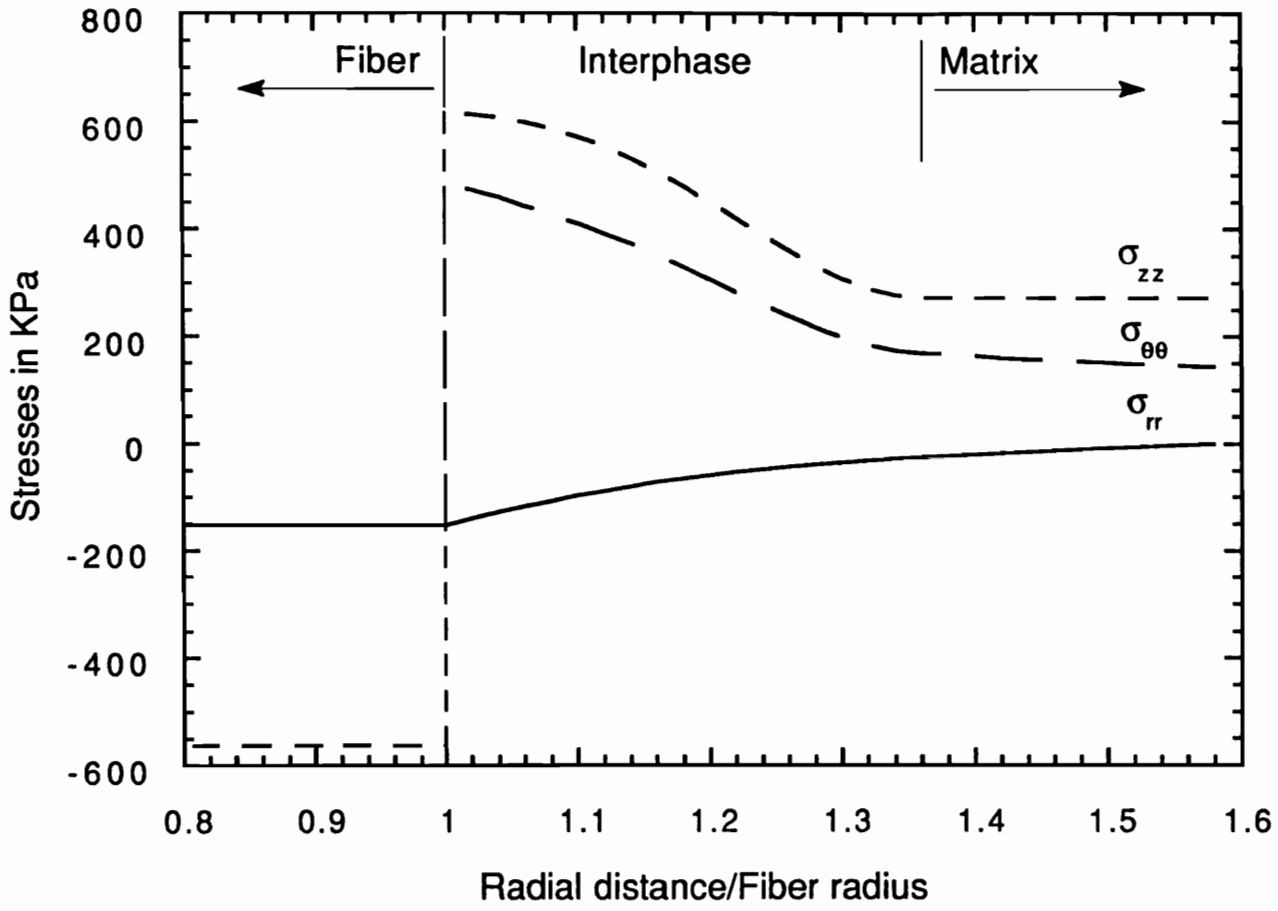

Figure 25. Constituent stresses in a carbon/IMHS epoxy composite modeled by the concentric cylinder assemblage CCA 3: $V_f = 0.4$; $\phi = 0.18$; $\xi_y = 3.0$; $\xi_c = 0.75$.

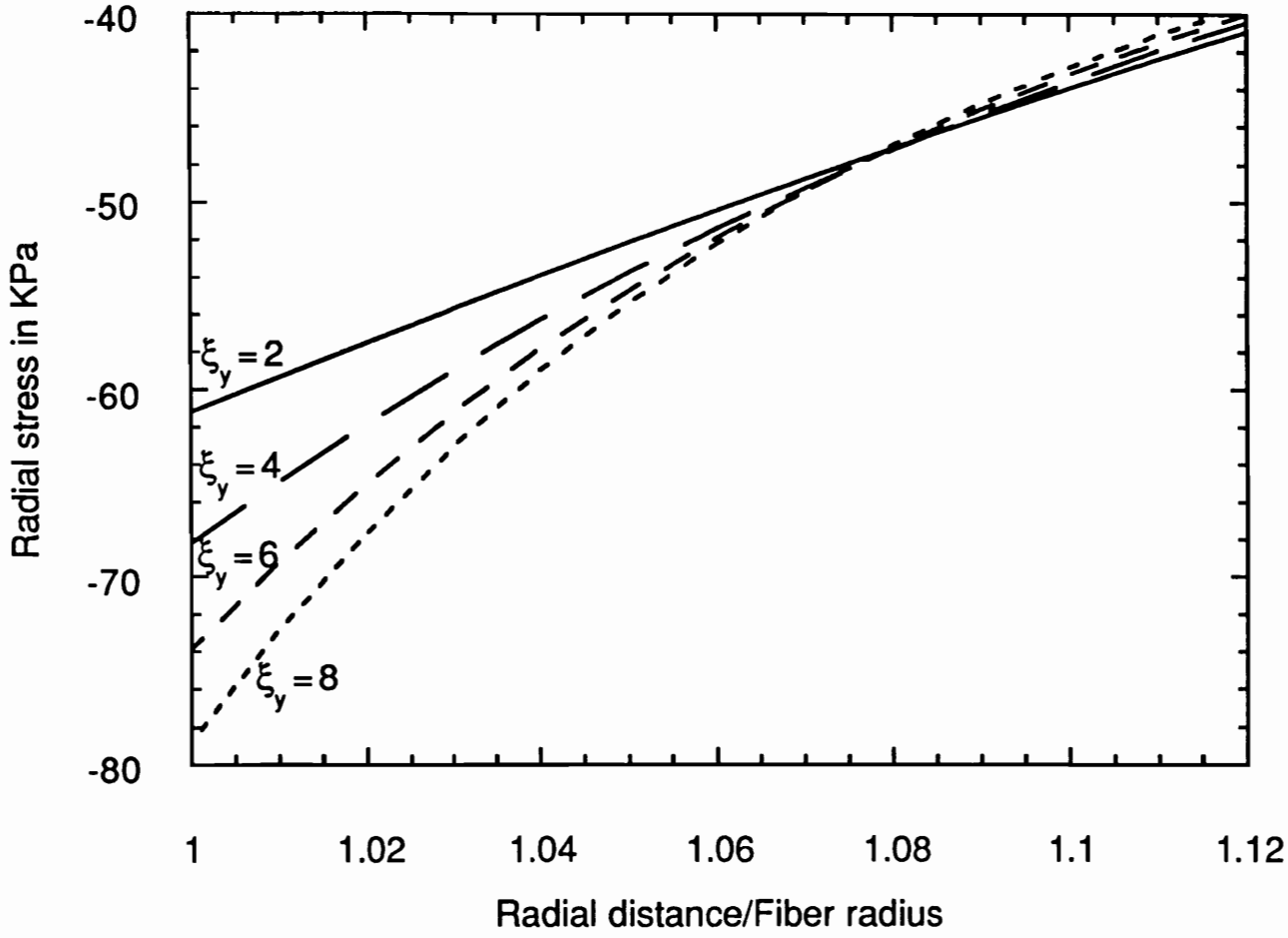

Figure 26. Interphasial radial stress in a Kevlar 49/IMHS epoxy composite modeled by the concentric cylinder assemblage CCA 1 as a function of modulus ratio: $V_f = 0.4$; $\phi = 0.06$; $\xi_c = 0.75$.

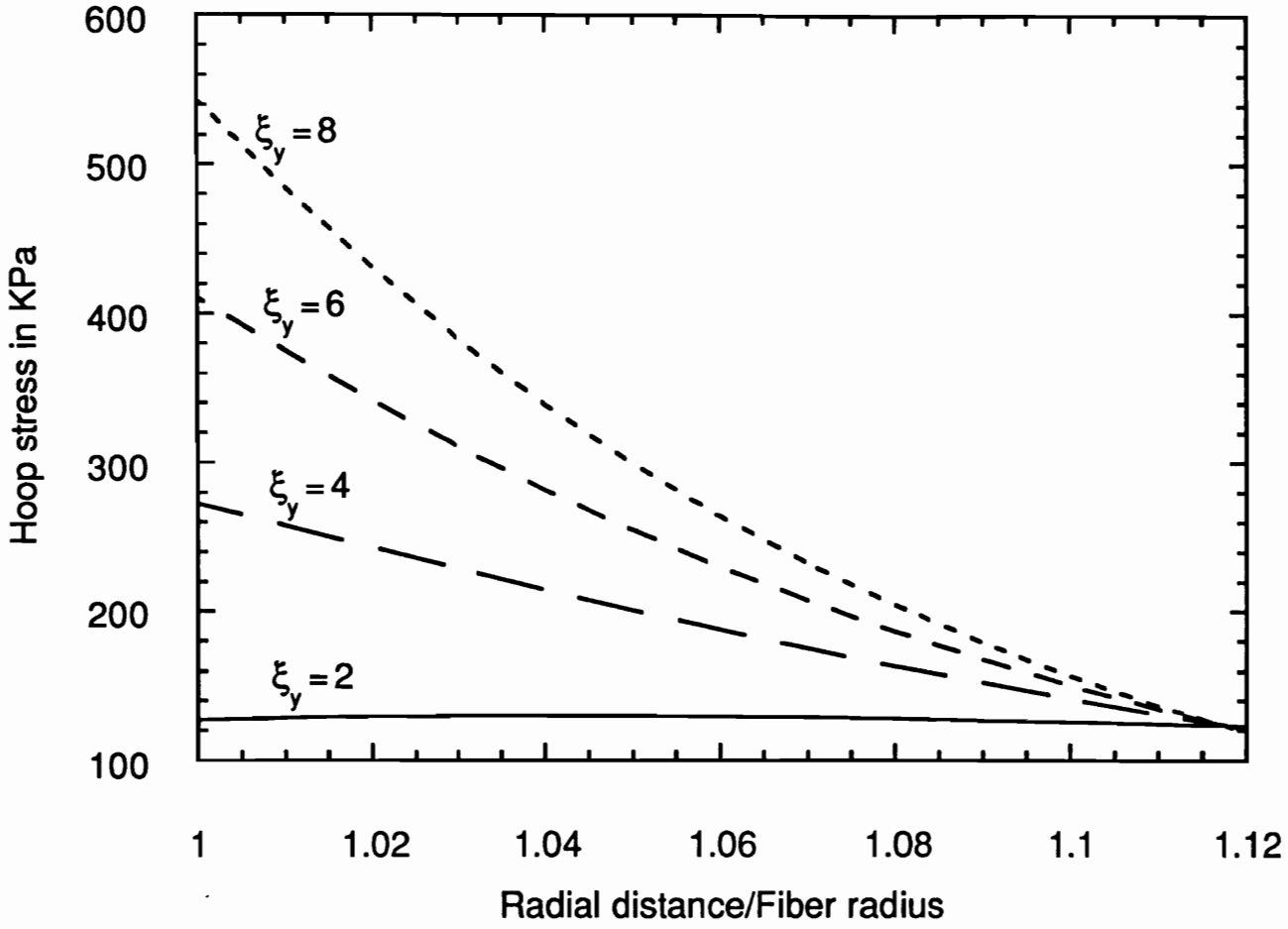

Figure 27. Interphasial hoop stress in a Kevlar 49/IMHS epoxy composite modeled by the concentric cylinder assemblage CCA 1 as a function of modulus ratio: $V_f = 0.4$; $\phi = 0.06$; $\xi_c = 0.75$.

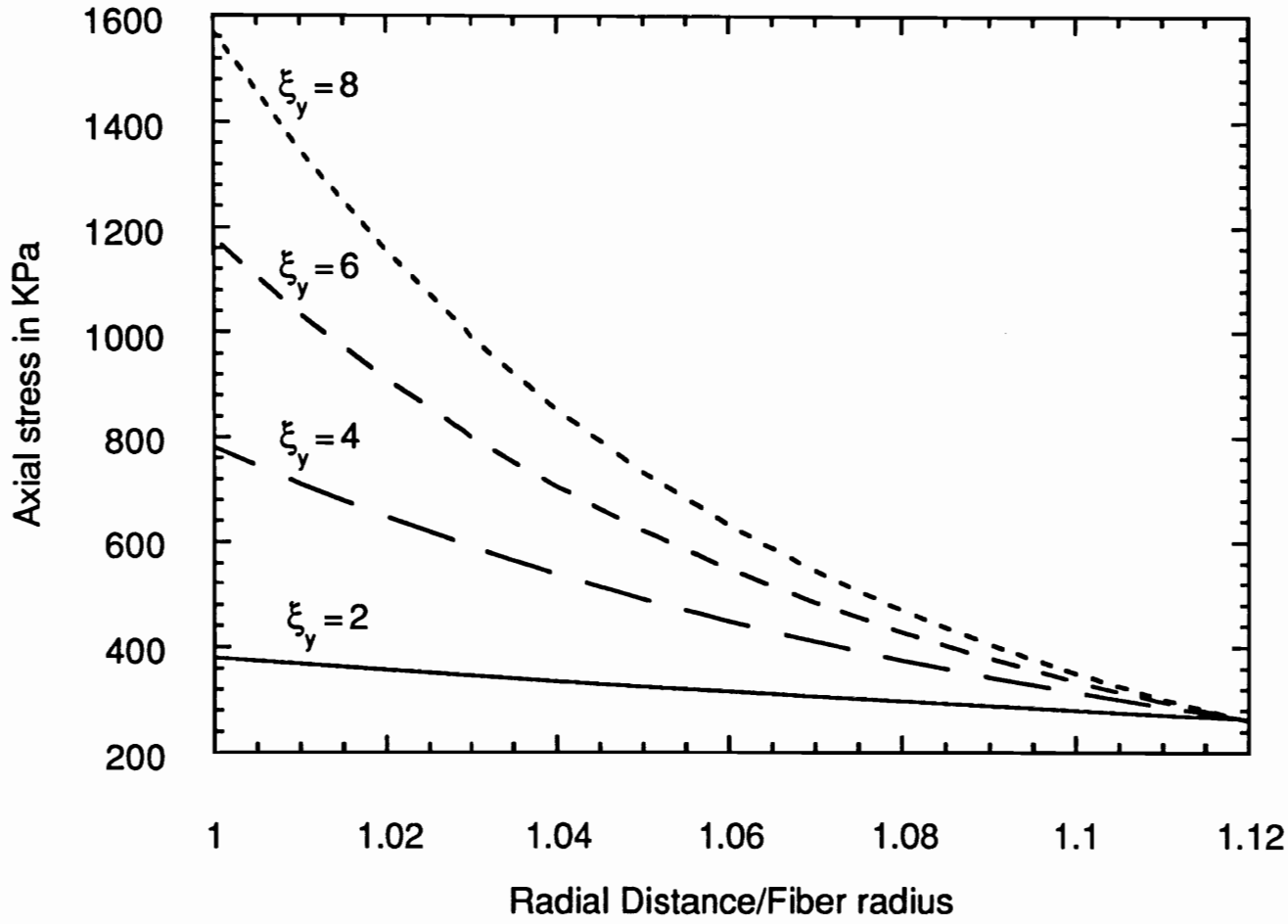

Figure 28. Interphasial axial stress in a Kevlar 49/IMHS epoxy composite modeled by the concentric cylinder assemblage CCA 1 as a function of modulus ratio: $V_f = 0.4$; $\phi = 0.06$; $\xi_c = 0.75$.

6.0 Effect on Local Stress Fields

Stresses in the constituents of a composite subjected to thermo-mechanical loading situations are influenced by:

- the differences in mechanical and thermal properties of the fiber and matrix, and
- the mechanical, thermal and physical properties of the interphase.

Depending on their nature, these stresses influence the strength (or the failure) of a composite. The connection between constituent stresses and composite strength under external loads has been studied by a number of researchers [92-94].

Madhukar and Drzal [92, 93] have investigated the effect of the interphase on the mechanical properties of graphite/epoxy composites. The interphase and consequently the interphasial shear strength was varied by using different surface modifications (no surface treatment, surface treatment, surface treatment and a thin coating of epoxy). The experimental results showed that both in-plane and interlaminar shear strengths of the composite increased approximately in the same ratio as the interphasial shear strength.

Norita, *et al.* [94] have investigated the effect of surface treatment of the carbon fiber on various mechanical properties of carbon fiber/epoxy composites; the interphase modification was achieved through different levels of surface treatment (untreated, and half, once and twice the current production levels). The test results showed gradual improvements in

mechanical properties with increasing levels of surface treatments; however, no improvements were noticed in the case of fibers with twice the production level surface treatment.

In this chapter, the EIAS concept of Benveniste, Dvorak and Chen [58] is employed to evaluate the constituent stresses in a unidirectional fiber-reinforced composite subjected to thermo-mechanical loading situations. The composite consists of three phases — the fiber, interphase and matrix; the interphasial property gradients are defined by the *Power Variation* as outlined in Chapter 4. The general formulation of the ***EIAS concept***, the formulation of the auxiliary problems and their solution methods, the solution methods to the resulting Navier's equations, and the results are presented in the following sections.

6.1 Stress Fields by the "Equivalent Inclusion - Average Stress concept"

The following assumptions are used in the formulation:

- The fiber-interphase assemblage is simulated by two concentric, long, circular cylinders. The radii of the interphase and the fiber are denoted by r_i and r_f, respectively.
- The continuous fiber composite is represented by a material system consisting of an infinite matrix in which the fibers are aligned and distributed in a statistically homogeneous manner.
- A cylindrical coordinate system (r, θ, z) is considered with z as the axial coordinate and r-θ as the transverse plane.
- The temperature change is uniform in all the phases.

The ***Equivalent Inclusion idea*** of Eshelby [59, 60] and the ***Average Stress concept*** of Mori and Tanaka [61] have received wide attention in the micromechanics research community. Many important micromechanics problems have been dealt with using one or both of

the above methods; the reader is urged to refer to Mura [95] for a comprehensive introduction to different topics in micromechanics as related to these problems. Recently, Benveniste [96] has provided a simple reexamination of the ***Equivalent Inclusion idea*** and the ***Average Stress concept***, called the ***EIAS concept***; the formulation for the stress fields given below will closely follow the work of Benveniste [96] and Benveniste, Dvorak and Chen [58].

The cross-section of a unidirectional composite with a distribution of fiber-interphase assemblages in a matrix is shown in Figure 29(a). The boundary conditions for the general thermo-mechanical loading of this composite are given by

$$\lim_{r \to \infty} \sigma_{ij}(r, \theta, z) = \sigma_{ij}^{o} \qquad \underset{\forall\,(r,\theta,z)}{T(r, \theta, z)} = T^{o} \tag{40}$$

where $\sigma_{ij}(r, \theta, z)$ and $T(r, \theta, z)$ are the stress field and uniform temperature change respectively and the superscript "o" indicates known quantities associated with the composite problem. The local stress fields associated with the composite can now be written as

$$\sigma_{ij}^{(n)}(r, \theta, z) = \tilde{M}_{ijkl}^{(n)}(r, \theta, z)\, \sigma_{kl}^{o} + \tilde{N}_{ij}^{(n)}(r, \theta, z)\, T^{o} \qquad n = f, i, m \tag{41}$$

where $\tilde{M}_{ijkl}^{(n)}$ and $\tilde{N}_{ij}^{(n)}$ represent fourth and second order tensors related to the composite, respectively. m, i and f represent quantities related to the matrix, interphase and fiber, respectively. Determination of $\tilde{M}_{ijkl}^{(n)}$ and and $\tilde{N}_{ij}^{(n)}$ in closed-form is difficult due to the interactions of fiber-interphase assemblages. Hence, different models have been introduced in the literature to approximately evaluate $\tilde{M}_{ijkl}^{(n)}$ and $\tilde{N}_{ij}^{(n)}$. The ***EIAS concept*** is one such formulation and can be explained by considering:

- a fiber-interphase assemblage embedded in an infinite matrix medium, and
- a fiber-interphase assemblage embedded in a deformed infinite matrix medium.

Consider a fiber-interphase assemblage embedded in an infinite matrix medium as shown in Figure 29(b). The boundary conditions for the general thermo-mechanical loading of this body is given by

$$\lim_{r \to \infty} \sigma_{ij}(r, \theta, z) = \sigma_{ij}^{d} \qquad \underset{\forall\,(r,\theta,z)}{T(r, \theta, z)} = T^{d} \tag{42}$$

where the superscript "d" indicates known quantities associated with the single fiber-interphase-infinite matrix problem. The stress fields associated with this body can now be written as

$$\sigma_{ij}^{(n)}(r, \theta, z) = \mathbf{M}_{ijkl}^{(n)}(r, \theta, z)\, \sigma_{kl}^{d} + \mathbf{N}_{ij}^{(n)}(r, \theta, z)\, T^{d} \qquad n = f, i, m \tag{43}$$

where $\mathbf{M}_{ijkl}^{(n)}$ and $\mathbf{N}_{ij}^{(n)}$ represent fourth and second order tensors related to the single fiber-interphase embedded in an infinite matrix, respectively; $\mathbf{M}_{ijkl}^{(n)}$ and $\mathbf{N}_{ij}^{(n)}$ can be determined in closed-form for this body under different loading conditions.

Consider a typical fiber-interphase assemblage in the dotted portion of Figure 29(a), which is shown separately in Figure 29(c). The matrix region in this portion of the composite is already deformed and possesses an average stress, σ_{ij}^{av}. Therefore, the boundary conditions for the general thermo-mechanical loading of this portion of the composite can be approximately expressed as

$$\lim_{r \to \infty} \sigma_{ij}(r, \theta, z) = \sigma_{ij}^{av} \qquad \underset{\forall\,(r,\theta,z)}{T(r, \theta, z)} = T^{o} \tag{44}$$

The stress fields associated with this body can now be written as

$$\sigma_{ij}^{(n)}(r, \theta, z) = \mathbf{M}_{ijkl}^{(n)}(r, \theta, z)\, \sigma_{kl}^{av} + \mathbf{N}_{ij}^{(n)}(r, \theta, z)\, T^{o} \qquad n = f, i, m \tag{45}$$

where $\mathbf{M}_{ijkl}^{(n)}$ and $\mathbf{N}_{ij}^{(n)}$ are known once the problem of single fiber-interphase assemblage embedded in an infinite matrix medium, shown in Figure 29(b) is solved.

The volume average stresses in the fiber and interphase are found from Equation (45) as

$$\left\{\sigma_{ij}^{(f)}\right\}_{av} = \left\{\mathbf{M}_{ijkl}^{(f)}\right\}_{av} \sigma_{kl}^{av} + \left\{\mathbf{N}_{ij}^{(f)}\right\}_{av} T^{o} \tag{46}$$

$$\{\sigma_{ij}^{(i)}\}_{av} = \{M_{ijkl}^{(i)}\}_{av}\,\sigma_{kl}^{av} + \{N_{ij}^{(i)}\}_{av}\,T^{o} \tag{47}$$

where the subscript "av" denotes the average values over the volume of the respective constituents. The following relation is then used along with Equations (46) and (47) to determine the average matrix stresses:

$$V_f\{\sigma_{ij}^{(f)}\}_{av} + V_i\{\sigma_{ij}^{(i)}\}_{av} + V_m\,\sigma_{ij}^{av} = \sigma_{ij}^{o} \tag{48}$$

where V_f, V_i and V_m represent the volume fractions of the fiber, interphase and matrix, respectively. Once the average matrix stresses are known, the local stress fields are determined from Equation (45).

6.2 Formulation and Solution Methods for the Auxiliary Problems

The solutions for the auxiliary problems (single fiber-interphase-unbounded matrix assemblage subjected to uniform temperature and boundary loads) are discussed in this section; the application of the ***EIAS concept*** to determine the local stresses follows the description in the previous section. The loading situations under consideration are a uniform temperature change and boundary loads (longitudinal shear stress and transverse shear stress) as shown in Figure 30. Some other cases of boundary loads (axial normal stress in the direction of the fibers, transverse hydrostatic stress perpendicular to the fibers, and transverse normal stress perpendicular to the fibers along either the x or the y coordinate) can be dealt with using the formulation of the three cases described above. Furthermore, since the

general thermo-mechanical loading problem is linear, it can be solved as a superposition of the loading cases mentioned above [58].

The following methodology is used to solve the auxiliary problems:

- A displacement field is assumed based on the loading condition.
- The Navier's (governing differential) equations are found for each of the domains of the problem.
- The governing differential equations are solved to find the the displacements in the constituents in terms of constants.
- The strains and the stresses in the constituents are determined by making use of the strain-displacement and the constitutive relations, respectively.
- The constants are determined by using the boundary and interface conditions.

6.2.1 Uniform Change in Temperature

The composite is assumed to experience an axisymmetric generalized plane-strain. Due to axisymmetry and the absence of shear in the concentric cylinder assemblage model, the displacement field in the n-th domain (n = m, i, f) can be expressed by

$$u_r^{(n)} = u^{(n)}(r)$$

$$u_\theta^{(n)} = 0$$

$$u_z^{(n)} = w^{(n)}(z) \tag{49}$$

where $u_j^{(n)}$ are the components of displacement.

Matrix (n=m) and Fiber (n=f) Domains

The Navier's equations of elasticity are :

$$\frac{d^2w^{(n)}}{dz^2} = 0 \tag{50}$$

$$\frac{d^2u^{(n)}}{dr^2} + \frac{1}{r}\frac{du^{(n)}}{dr} - \frac{u^{(n)}}{r^2} = 0 \tag{51}$$

The general solution to Equation (50) is given by

$$w^{(n)}(z) = C^{(n)}z + D^{(n)} \tag{52}$$

and the general solution to Equation (51) is found by the Cauchy-Euler method (See section on "Solution Methods for the Governing Differential Equations") to be

$$u^{(n)}(r) = A^{(n)}r + \frac{B^{(n)}}{r} \tag{53}$$

$A^{(n)}$, $B^{(n)}$, $C^{(n)}$ and $D^{(n)}$ are unknown constants which will be determined by the boundary/interface conditions. The expressions for $u_r^{(m)}$ and $u_r^{(f)}$ are consistent with the work of Hashin and Rosen [85].

Interphasial Domain (n=i)

The Navier's equations of elasticity are:

$$\frac{d^2w^{(i)}}{dz^2} = 0 \tag{54}$$

$$\frac{d^2u^{(i)}}{dr^2} + \left[\frac{Q_y + 1}{r}\right]\frac{du^{(i)}}{dr} + \left[\frac{Q_y \dfrac{\nu_i}{1-\nu_i} - 1}{r^2}\right]u^{(i)} + \left[\frac{\nu_i}{1-\nu_i}\frac{Q_y}{r}\right]\frac{dw^{(i)}}{dz}$$

$$- \left[\frac{1+\nu_i}{1-\nu_i}\frac{P_c(Q_y + Q_c)r^{Q_c - 1}}{r_f^{Q_c}}\right]T^d = 0 \tag{55}$$

The general solution to Equation (54) is given by

$$w^{(i)}(z) = C^{(i)}z + D^{(i)} \tag{56}$$

and the general solution to Equation (55) is found by the Cauchy-Euler method to be

$$u^{(i)}(r) = A^{(i)}r^{m_1} + B^{(i)}r^{m_2} - C^{(i)}\nu_i r + \frac{\dfrac{1+\nu_i}{1-\nu_i}P_c(Q_y + Q_c)r^{Q_c+1}T^d}{\left\{Q_c{}^2 + 2Q_c + Q_yQ_c + Q_y + Q_y\dfrac{\nu_i}{1-\nu_i}\right\}r_f^{Q_c}} \tag{57}$$

where

$$m_1, m_2 = \frac{1}{2}\left[-Q_y \pm \sqrt{\frac{Q_y{}^2(1-\nu_i) - 4\nu_i(Q_y + 1) + 4}{1-\nu_i}}\right]$$

$A^{(i)}$, $B^{(i)}$, $C^{(i)}$ and $D^{(i)}$ are unknown constants which will be determined by the boundary/interface conditions.

Solution Method

The boundary and interface conditions for this loading situation are given by

$$\lim_{r\to\infty} \frac{1}{\pi r^2}\left[2\pi\int_0^{r_f}\sigma_{zz}^{(f)}rdr + 2\pi\int_{r_f}^{r_i}\sigma_{zz}^{(i)}rdr + 2\pi\int_{r_i}^{r}\sigma_{zz}^{(m)}rdr\right] = 0 \tag{58}$$

$$\lim_{r\to\infty}\sigma_{xx}^{(m)} = 0 \quad \equiv \quad \lim_{r\to\infty}\sigma_{yy}^{(m)} = 0 \quad \equiv \quad \lim_{r\to\infty}\sigma_{rr}^{(m)} = 0 \tag{59}$$

$$u^{(m)} = u^{(i)} \quad w^{(m)} = w^{(i)} \quad \sigma_{rr}^{(m)} = \sigma_{rr}^{(i)} \quad at \quad r = r_i \tag{60}$$

$$u^{(i)} = u^{(f)} \quad w^{(i)} = w^{(f)} \quad \sigma_{rr}^{(i)} = \sigma_{rr}^{(f)} \quad at \quad r = r_f \tag{61}$$

where σ_{rr} and σ_{zz} represent the radial and axial stresses, respectively.

The required end conditions are given by:

$$\sigma_{zz}^{(m)}(r, \pm l/2) = \sigma_{zz}^{(i)}(r, \pm l/2) = \sigma_{zz}^{(f)}(r, \pm l/2) = 0 \tag{62}$$

where l is the length of the cylinder assemblage. Since end conditions (62) are difficult to enforce, condition (58) "equivalent in the St.Venant sense" to conditions (62) is enforced. Equation (58) will be satisfied if $\sigma_{zz}^{(m)} = 0$ is imposed. The boundaries of the matrix, parallel to the fiber direction, are stress free; boundary condition (59) is a direct consequence of this assumption. Interface conditions (60) and (61) are dictated by the assumption of perfect bonding at the fiber-interphase and interphase-matrix interfaces.

The interface conditions on w dictate that $C^{(m)} = C^{(i)} = C^{(f)} = C$ and $D^{(m)} = D^{(i)} = D^{(f)} = D$. Since D represents a rigid body displacement, it can be set to zero without loss of generality. Thus, we have

$$w^{(m)}(z) = w^{(i)}(z) = w^{(f)}(z) = Cz \tag{63}$$

$B^{(f)}$ must be set equal to zero, since $|u^{(f)}(0)| < \infty$. The remaining six boundary/interface conditions are used to solve for the remaining constants $A^{(m)}$, $A^{(i)}$, $A^{(f)}$, $B^{(m)}$, $B^{(i)}$ and C. The displacements, the strains and the stresses in each of the constituents are determined using the values of the above constants.

6.2.2 Longitudinal Shear Load

The displacement field in the n-th domain (n = m, i, f) can be expressed by

$$u_r^{(n)} = 0$$

$$u_\theta^{(n)} = 0$$

$$u_z^{(n)} = w^{(n)}(r) \sin\theta \tag{64}$$

where $u_j^{(n)}$ are the components of displacement.

Matrix (n=m) and Fiber (n=f) Domains

The Navier's equation of elasticity is:

$$\frac{d^2 w^{(n)}}{dr^2} + \frac{1}{r}\frac{dw^{(n)}}{dr} - \frac{w^{(n)}}{r^2} = 0 \tag{65}$$

The general solution to Equation (65) is found by the Cauchy-Euler method to be

$$w^{(n)}(r) = A^{(n)} r + \frac{B^{(n)}}{r} \tag{66}$$

$A^{(n)}$ and $B^{(n)}$ are unknown constants which will be determined by the boundary/interface conditions. The expressions for $u_z^{(m)}$ and $u_z^{(f)}$ are consistent with the work of Benveniste, Dvorak and Chen [58].

Interphasial Domain (n=i)

The Navier's equation of elasticity is:

$$\frac{d^2w^{(i)}}{dr^2} + \left[\frac{Q_y + 1}{r}\right]\frac{dw^{(i)}}{dr} - \frac{w^{(n)}}{r^2} = 0 \tag{67}$$

The general solution to Equation (67) is found by the Cauchy-Euler method to be

$$w^{(i)}(r) = A^{(i)}r^{m_1} + B^{(i)}r^{m_2} \tag{68}$$

where

$$m_1, m_2 = \frac{1}{2}\left[-Q_y \pm \sqrt{Q_y{}^2 + 4}\right]$$

$A^{(i)}$ and $B^{(i)}$ are unknown constants which will be determined by the boundary/interface conditions.

Solution Method

The boundary and interface conditions for this loading situation are given by

$$\lim_{r\to\infty} \sigma_{yz}^{(m)} = \sigma^d \quad \equiv \quad \frac{E_m}{2(1+\nu_m)} A^{(m)} = \sigma^d \tag{69}$$

$$w^{(m)} = w^{(i)} \quad \sigma_{rz}^{(m)} = \sigma_{rz}^{(i)} \quad at \quad r = r_i \tag{70}$$

$$w^{(i)} = w^{(f)} \quad \sigma_{rz}^{(i)} = \sigma_{rz}^{(f)} \quad at \quad r = r_f \tag{71}$$

where σ_{yz} and σ_{rz} represent the shear stresses.

Boundary condition (69) is a direct consequence of the fact that the boundaries of the matrix, parallel to the fiber direction, experience the applied stress. Interface conditions (70) and (71) are dictated by the assumption of perfect bonding at the fiber-interphase and interphase-matrix interfaces. $B^{(f)}$ must be set equal to zero, since $|u^{(f)}(0)| < \infty$. The five boundary/interface conditions are used to solve for the remaining constants $A^{(m)}$, $A^{(i)}$, $A^{(f)}$, $B^{(m)}$ and $B^{(i)}$. The displacements, the strains and the stresses in each of the constituents are determined using the values of the above constants.

6.2.3 Transverse Shear Load

The composite is assumed to experience plane strain and the state of stress applied to the composite at infinity is pure shear. The displacement field in the n-th domain (n = m, i, f) can be expressed by

$$u_r^{(n)} = u^{(n)}(r) \cos 2\theta$$

$$u_\theta^{(n)} = v^{(n)}(r) \sin 2\theta$$

$$u_z^{(n)} = 0 \tag{72}$$

where $u_j^{(n)}$ are the components of displacement.

Matrix (n=m) Domain

The Navier's equations of elasticity are :

$$\frac{d^2u^{(m)}}{dr^2}+\frac{1}{r}\frac{du^{(m)}}{dr}+\frac{5\nu_m-3}{1-\nu_m}\frac{u^{(m)}}{r^2}+\frac{1}{1-\nu_m}\frac{1}{r}\frac{dv^{(m)}}{dr}+\frac{4\nu_m-3}{1-\nu_m}\frac{v^{(m)}}{r^2}=0$$

$$\frac{d^2v^{(m)}}{dr^2}+\frac{1}{r}\frac{dv^{(m)}}{dr}+\frac{10\nu_m-9}{1-2\nu_m}\frac{v^{(m)}}{r^2}-2\frac{1}{1-2\nu_m}\frac{1}{r}\frac{du^{(m)}}{dr}+2\frac{4\nu_m-3}{1-2\nu_m}\frac{u^{(m)}}{r^2}=0 \qquad (73)$$

The general solution to Equations (73) is found by the general solution of Pagano [97] (See section on "Solution Methods for the Governing Differential Equations") to be

$$u^{(m)}=A^{(m)}r^3+\frac{B^{(m)}}{r^3}+C^{(m)}r+\frac{D^{(m)}}{r} \qquad (74)$$

$$v^{(m)}=-\frac{3-2\nu_m}{2\nu_m}A^{(m)}r^3+\frac{B^{(m)}}{r^3}-C^{(m)}r+\frac{2\nu_m-1}{2(1-\nu_m)}\frac{D^{(m)}}{r} \qquad (75)$$

$A^{(m)}$, $B^{(m)}$, $C^{(m)}$ and $D^{(m)}$ are unknown constants which will be determined by the boundary/interface conditions.

Fiber (n=f) Domain

The Navier's equations of elasticity are :

$$\frac{d^2u^{(f)}}{dr^2}+\frac{1}{r}\frac{du^{(f)}}{dr}+\frac{2C_{23f}-3C_{22f}}{C_{22f}}\frac{u^{(f)}}{r^2}+\frac{C_{22f}+C_{23f}}{C_{22f}}\frac{1}{r}\frac{dv^{(f)}}{dr}+\frac{C_{23f}-3C_{22f}}{C_{22f}}\frac{v^{(f)}}{r^2}=0$$

$$\frac{d^2v^{(f)}}{dr^2}+\frac{1}{r}\frac{dv^{(f)}}{dr}+\frac{C_{23f}-9C_{22f}}{C_{22f}-C_{23f}}\frac{v^{(f)}}{r^2}-2\frac{C_{22f}+C_{23f}}{C_{22f}-C_{23f}}\frac{1}{r}\frac{du^{(f)}}{dr}+2\frac{C_{23f}-3C_{22f}}{C_{22f}-C_{23f}}\frac{u^{(f)}}{r^2}=0 \qquad (76)$$

where C_{ij_f} refer to fiber stiffnesses. The general solution to Equations (76) is found by the general solution of Pagano [97] to be

$$u^{(f)} = A^{(f)} r^3 + \frac{B^{(f)}}{r^3} + C^{(f)} r + \frac{D^{(f)}}{r} \tag{77}$$

$$v^{(f)} = -\frac{3C_{22f} + C_{23f}}{2C_{23f}} A^{(f)} r^3 + \frac{B^{(f)}}{r^3} - C^{(f)} r + \frac{C_{23f} - C_{22f}}{2C_{22f}} \frac{D^{(f)}}{r} \tag{78}$$

where C_{ij_f} refer to fiber stiffnesses. $A^{(f)}$, $B^{(f)}$, $C^{(f)}$ and $D^{(f)}$ are unknown constants which will be determined by the boundary/interface conditions. The expressions for $u_r^{(m)}$, $u_\theta^{(m)}$, $u_r^{(f)}$ and $u_\theta^{(f)}$ are consistent with the work of Christensen and Lo [98] and Theocaris and Varias [75].

Interphase (n=i) Domain

The Navier's equations of elasticity are :

$$\frac{d^2u^{(i)}}{dr^2} + \frac{Q_y + 1}{r}\frac{du^{(i)}}{dr} + \frac{5\nu_i - 3 + Q_y\nu_i}{1-\nu_i}\frac{u^{(i)}}{r^2} + \frac{1}{1-\nu_i}\frac{1}{r}\frac{dv^{(i)}}{dr} + \frac{4\nu_i - 3 + 2Q_y\nu_i}{1-\nu_i}\frac{v^{(i)}}{r^2} = 0$$

$$\frac{d^2v^{(i)}}{dr^2} + \frac{Q_y + 1}{r}\frac{dv^{(i)}}{dr} + \frac{10\nu_i - 9 - Q_y(1-2\nu_i)}{1-2\nu_i}\frac{v^{(i)}}{r^2} - 2\frac{1}{1-2\nu_i}\frac{1}{r}\frac{du^{(i)}}{dr}$$

$$+ 2\frac{4\nu_i - 3 - Q_y(1-2\nu_i)}{1-2\nu_i}\frac{u^{(i)}}{r^2} = 0 \tag{79}$$

The general solution to Equations (79) is found by the general solution of Pagano [97] to be

$$u^{(i)} = \mathbb{R}_r^{(i)}(A^{(i)}, B^{(i)}, C^{(i)}, D^{(i)}, r) \tag{80}$$

$$v^{(i)} = \mathbb{R}_\theta^{(i)}(A^{(i)}, B^{(i)}, C^{(i)}, D^{(i)}, r) \tag{81}$$

where $\mathbb{R}_r^{(i)}$ and $\mathbb{R}_\theta^{(i)}$ are functions of the radial distance and constants. $A^{(i)}$, $B^{(i)}$, $C^{(i)}$ and $D^{(i)}$ are unknown constants which will be determined by the boundary/interface conditions.

Solution Method

The boundary and interface conditions for this loading situation are given by

$$\lim_{r\to\infty} \sigma_{xx}^{(m)} = \sigma^d \quad \equiv \quad \lim_{r\to\infty} \sigma_{yy}^{(m)} = -\sigma^d \quad \equiv \quad \frac{E_m}{1+\nu_m} C^{(m)} = \sigma^d \tag{82}$$

$$u_r^{(m)} = u_r^{(i)} \quad u_\theta^{(m)} = u_\theta^{(i)} \quad \sigma_{rr}^{(m)} = \sigma_{rr}^{(i)} \quad \sigma_{r\theta}^{(m)} = \sigma_{r\theta}^{(i)} \quad \text{at} \quad r = r_i \tag{83}$$

$$u_r^{(i)} = u_r^{(f)} \quad u_\theta^{(i)} = u_\theta^{(f)} \quad \sigma_{rr}^{(i)} = \sigma_{rr}^{(f)} \quad \sigma_{r\theta}^{(i)} = \sigma_{r\theta}^{(f)} \quad \text{at} \quad r = r_f \tag{84}$$

where σ_{xx} and σ_{yy} represent the normal stresses, and $\sigma_{r\theta}$ represents the shear stress.

Boundary condition (82) is a direct consequence of the fact that the boundaries of the matrix, parallel to the fiber direction, experience the applied stress. Interface conditions (83) and (84) are dictated by the assumption of perfect bonding at the fiber-interphase and interphase-matrix interfaces. $B^{(f)}$ and $D^{(f)}$ must be set equal to zero, since $|u^{(f)}(0)| < \infty$. $A^{(m)}$ must be set equal to zero, since $|\lim_{r\to\infty} \sigma_{xx}^{(m)}| < \infty$ and $|\lim_{r\to\infty} \sigma_{yy}^{(m)}| < \infty$. The nine boundary/interface conditions are used to solve for the remaining constants $A^{(i)}$, $A^{(f)}$, $B^{(m)}$, $B^{(i)}$, $C^{(m)}$, $C^{(i)}$, $C^{(f)}$, $D^{(m)}$ and $D^{(i)}$. The displacements, the strains and the stresses in each of the constituents are determined using the values of the above constants.

6.3 Solution Methods for the Governing Differential Equations

Equations (51), (55), (65), and (67) are solved by the Cauchy-Euler method. The equations are transformed into equations with constant coefficients after making a change of variables

$$r = e^x \tag{85}$$

where x is the transformed independent variable. The differential equations are then solved by one of the basic methods [86].

The solution of Equations (73), (76) and (79) follows the general solution of Pagano [97] for a cylindrically anisotropic body under two dimensional surface tractions and involves the following steps:

- The following functional forms are assumed for u and v:

$$u = \mathbb{P}r^p \quad v = \mathbb{Q}r^p \tag{86}$$

  where $\mathbb{P}$ and $\mathbb{Q}$ are constants.

- u and v are substituted into Navier's equations (73), (76) and (79) resulting in two algebraic equations in $\mathbb{P}$ and $\mathbb{Q}$ for each constituent.
- The determinant of the coefficients ($\mathbb{P}$ and $\mathbb{Q}$) of the algebraic equations is found for each of the constituents. They are given by:

$$D_m = D_m(p, E_m, \nu_m)$$

$$D_l = D_l(p, Q_y, \nu_l)$$

$$D_f = D_f(p, C_{ijf}) \tag{87}$$

- The determinant is set to zero, in each case, resulting in a fourth order equation in p; the roots of this equation (p_1, p_2, p_3 and p_4) are determined.
- Relationships between $\mathbb{P}_k$ ($k = 1, 2, 3, 4$) and $\mathbb{Q}_k$ ($k = 1, 2, 3, 4$) are also determined from the algebraic equations.

The expression for Q_y can be written as

$$Q_y = \frac{\ln\left(\frac{1}{\xi_y}\right)}{\ln\left(1 + \frac{2c}{d}\right)} \tag{88}$$

The determinant of the coefficients for the interphase is dependent on Q_y (and hence c and ξ_y) and ν_i ($= \nu_m = 0.35$, in this case). A three-dimensional plot of $D_i(p, Q_y)$ vs. p vs. Q_y is shown in Figure 31(a); the top surface of the plot represents the zero value of the determinant. Figure 31(b) shows the top surface of the three-dimensional plot as a contour plot and the roots (p_1, p_2, p_3 and p_4) can be determined for a given value of Q_y. Clearly, the roots p_k ($k = 1, 2, 3, 4$) for the interphase are imaginary for some Q_y values (for example, $Q_y = 5$); these values of Q_y correspond to interphases for which the displacement fields cannot be expressed in the form of Equation (72). Furthermore, it is interesting to note that the roots for the fiber and matrix ($Q_y = 0$) domains can also be found from this plot. The symbolic software package MATHEMATICA [99] was used for drawing the plots.

6.4 Results and Discussion

E-glass/IMHS epoxy, carbon/IMHS epoxy and Kevlar 49/IMHS epoxy are considered in this discussion; typical material property values are given in Table 4. Parametric studies were performed by varying the parameter ξ_y and the fiber volume fraction, V_f and the results are presented.

Figures 32, 33, and 34 present the constituent stresses under different loading conditions as follows:

- Figure 32 — carbon/IMHS epoxy — uniform temperature change of 1 °C.
- Figure 33 — E-glass/IMHS epoxy — longitudinal shear load of 1 MPa.
- Figure 34 — Kevlar 49/IMHS epoxy — transverse shear load of 1 MPa.

Comparison of Figure 32 with Figure 23 shows that the signs of all the constituent stresses in Figure 32 are the opposite of the signs in Figure 23. This reversal is caused by the reversal in the sign of T°. Figures 33 and 34 show the distribution of stresses as a function of radial distance only, for the purpose of clarity. As can be seen, the Mori-Tanaka analyses provide a simple way to calculate the approximate stress state in composites with interphasial regions.

Figures 35, 36, and 37 show the distribution of shear stresses in carbon/IMHS epoxy as a function of ξ_y under longitudinal and transverse shear loading conditions. It is clearly seen that changing the interphase stiffness changes the stress distribution in all the constituents. Hence, optimizing the interphasial stiffness is an attractive option for optimizing composite materials for specific mechanical requirements.

Figures 38 and 39 show the constituent stresses in a Kevlar 49/IMHS epoxy composite under a uniform temperature change of 1 °C for volume fractions 0.4 and 0.6, respectively. Comparisons are made between the results of concentric cylinder assemblage (CCA) analysis and the results of Mori-Tanaka analysis. It is seen that the Mori-Tanaka analysis takes into account fiber-fiber interaction through the average matrix stresses.

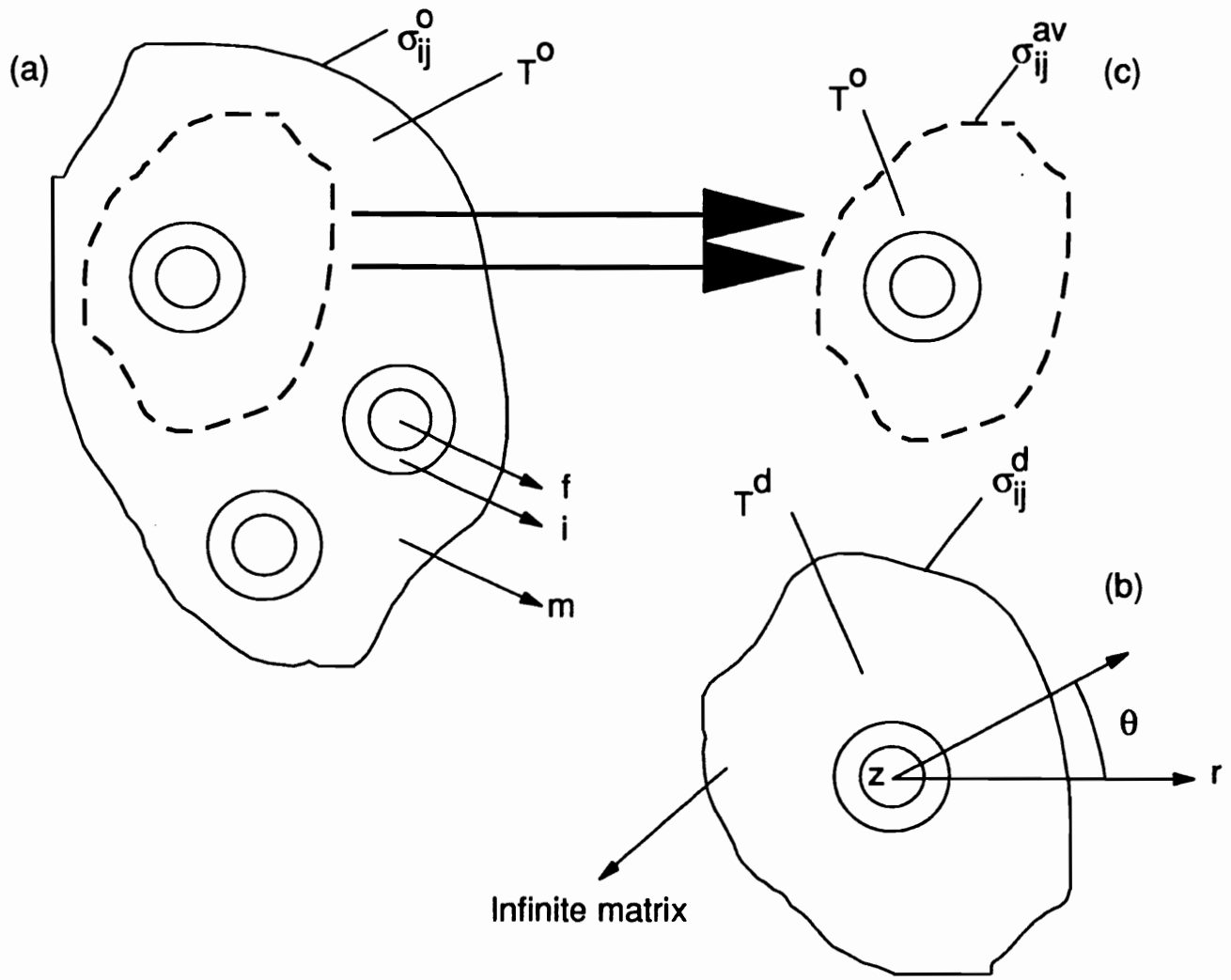

Figure 29. Schematic representations depicting the idea behind the Mori-Tanaka analysis.

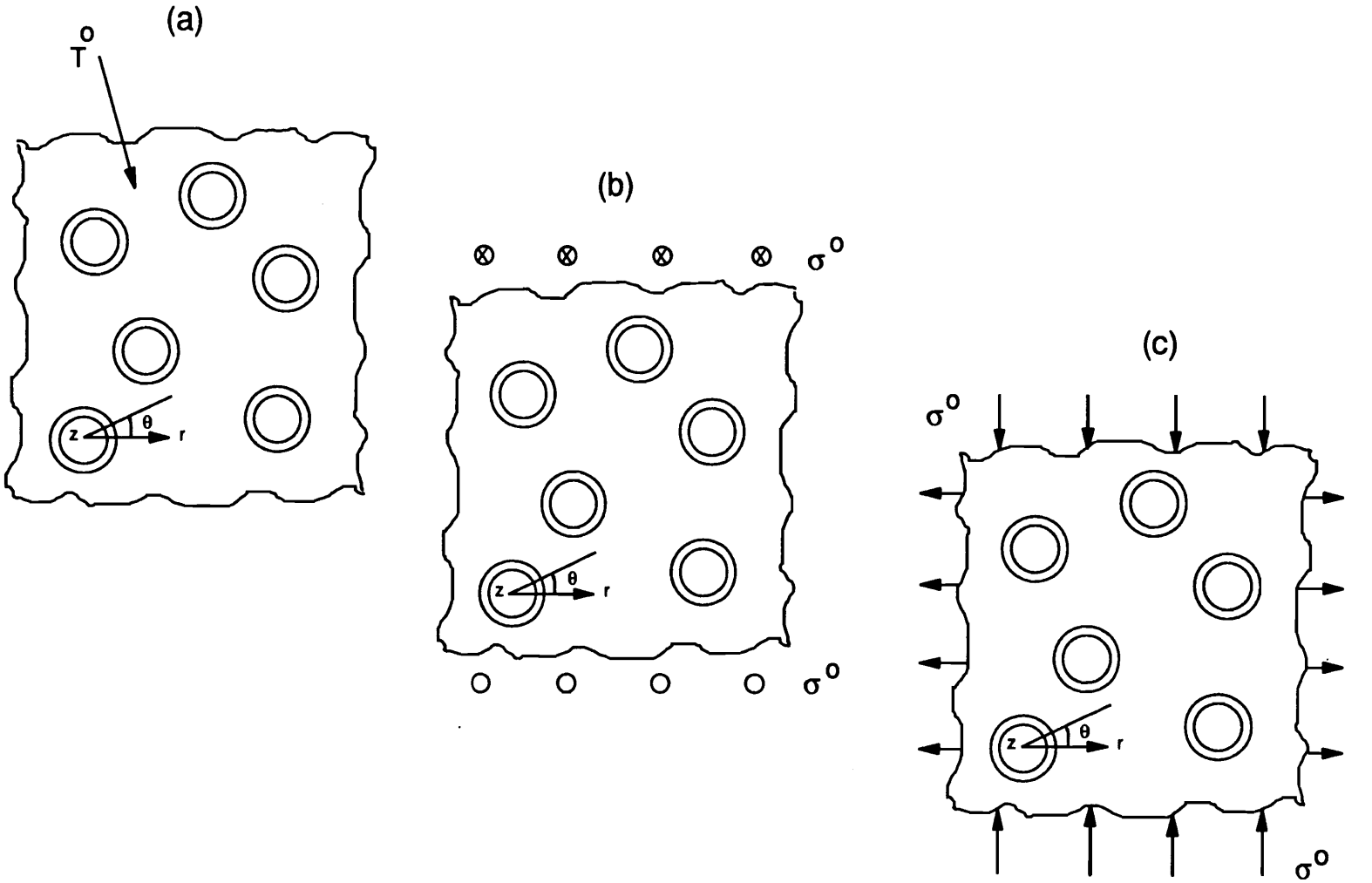

Figure 30. Loading configurations under consideration: (a) Uniform temperature change, (b) Applied longitudinal shear, and (c) Applied transverse shear.

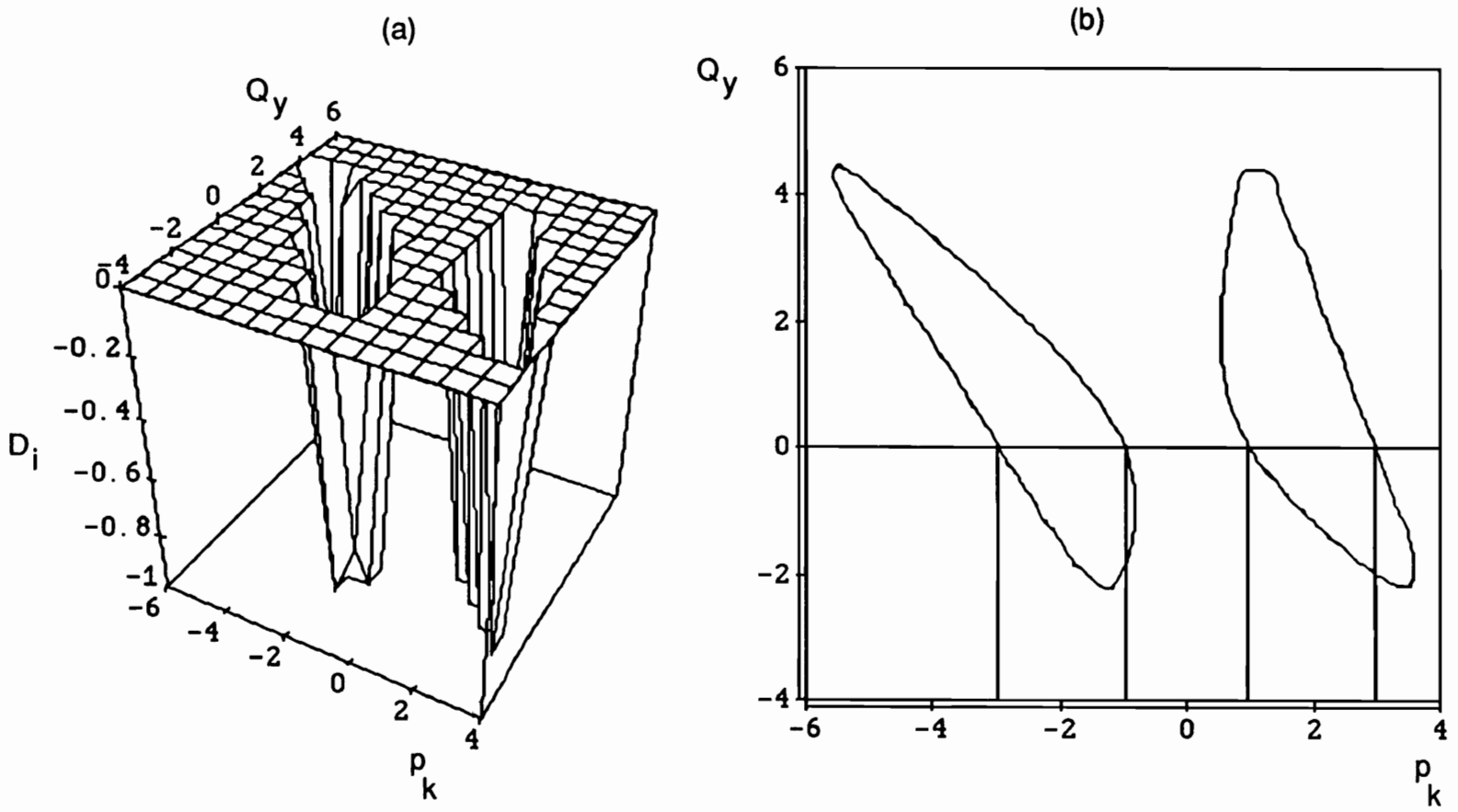

Figure 31. A three-dimensional plot and a contour plot showing the roots of the characteristic equation encountered in the solution of the transverse shear problem.

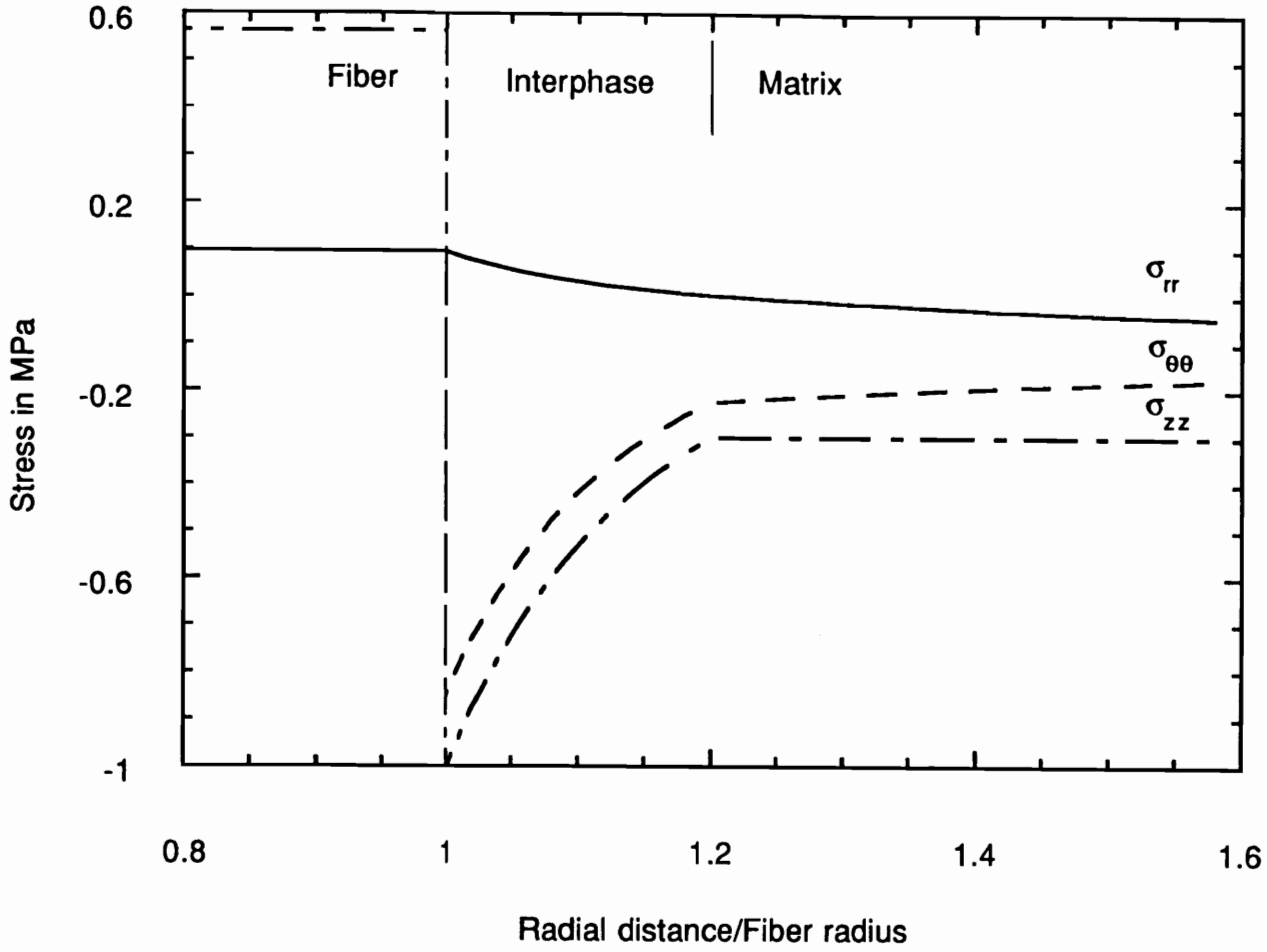

Figure 32. Constituent stresses in a carbon/IMHS epoxy composite under a uniform temperature change of 1 degree C: $V_f = 0.4$; $\phi = 0.1$; $\xi_y = 4.5$; $\xi_c = 0.75$.

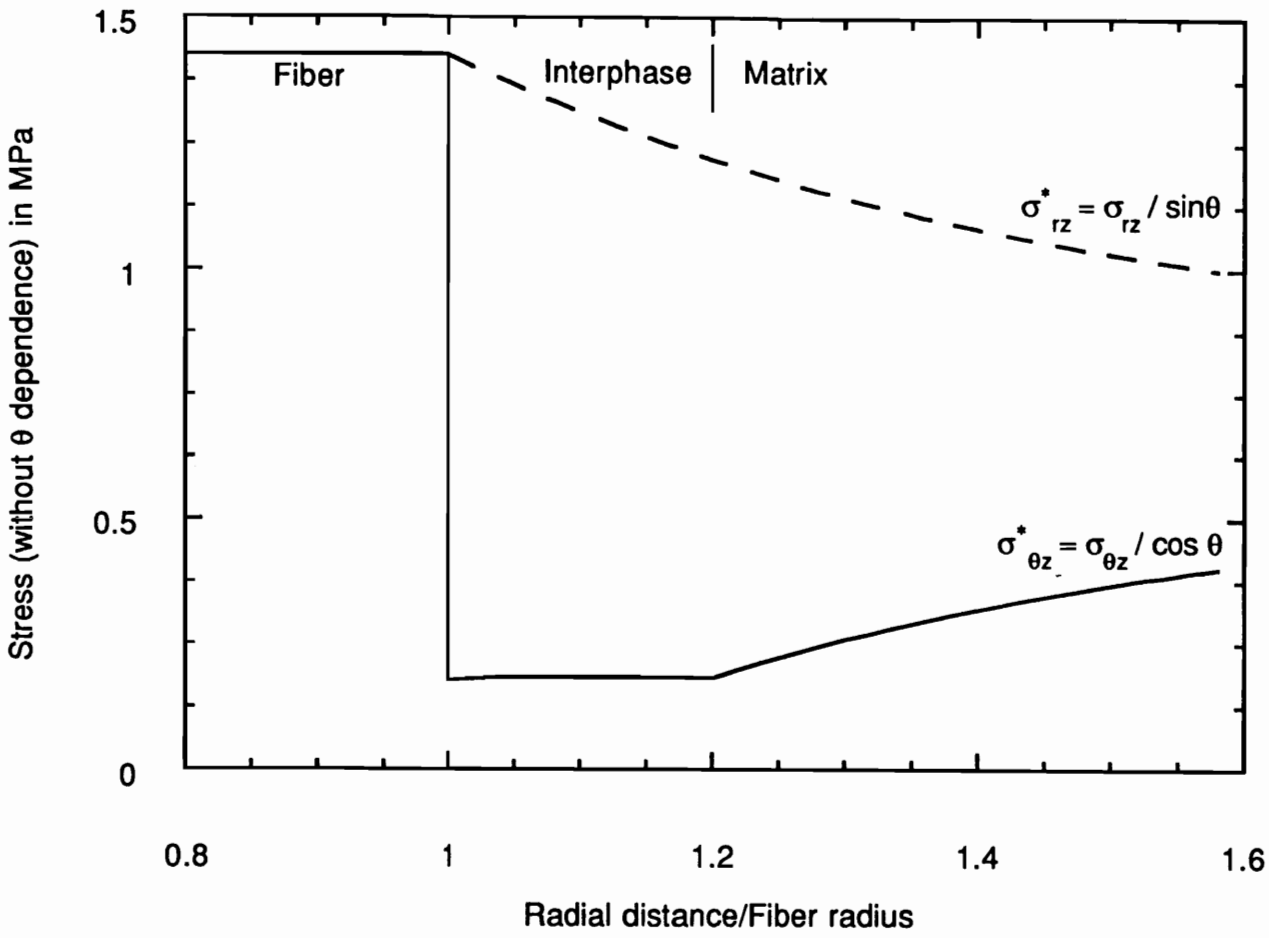

Figure 33. Constituent stresses in a E-glass/IMHS epoxy composite under a longitudinal shear load of 1 MPa: $V_f = 0.4$; $\phi = 0.1$; $\xi_y = 3$.

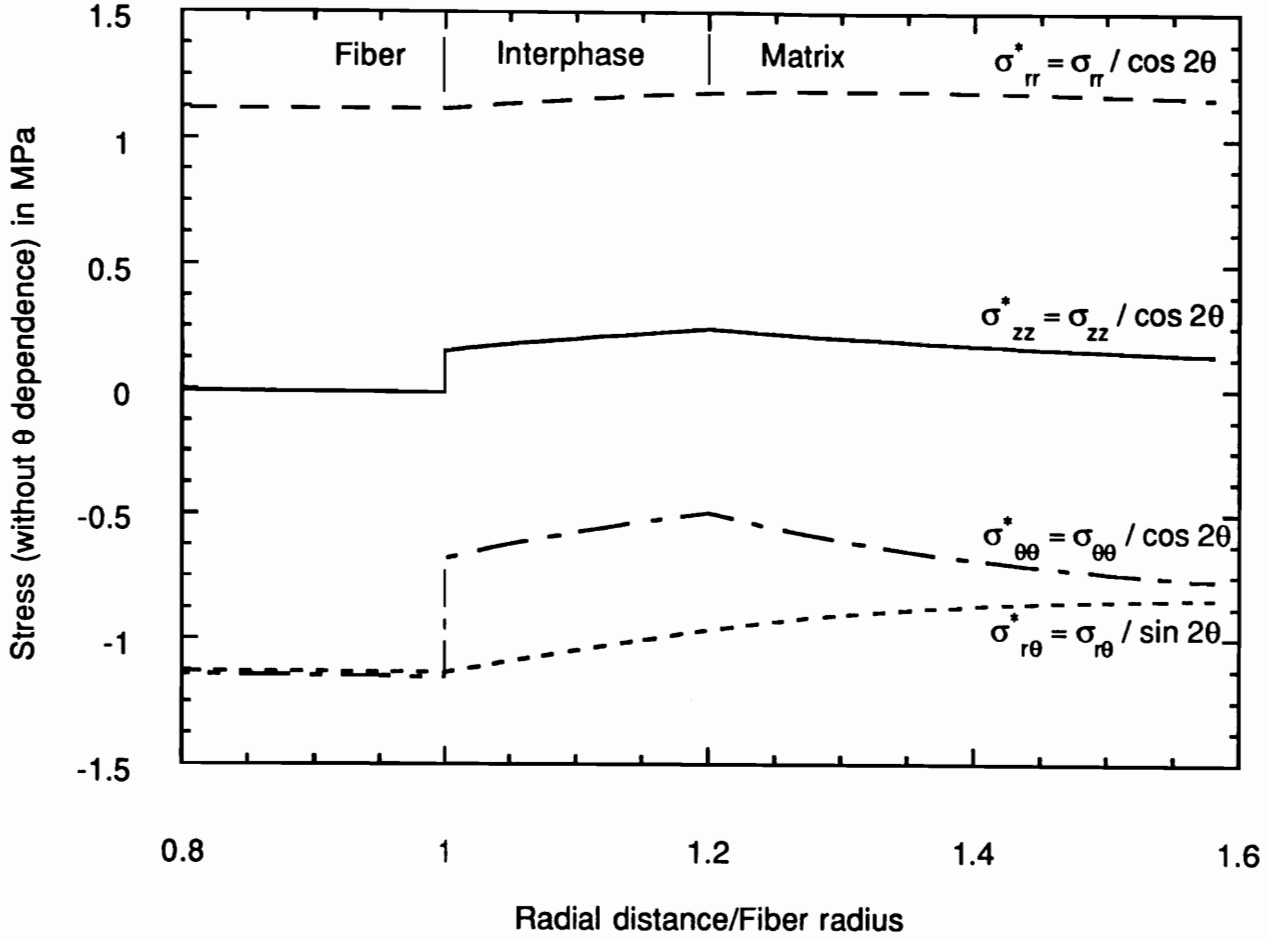

Figure 34. Constituent stresses in a Kevlar 49/IMHS epoxy composite under a transverse shear load of 1 MPa: $V_f = 0.4$; $\phi = 0.15$; $\xi_y = 1.49$.

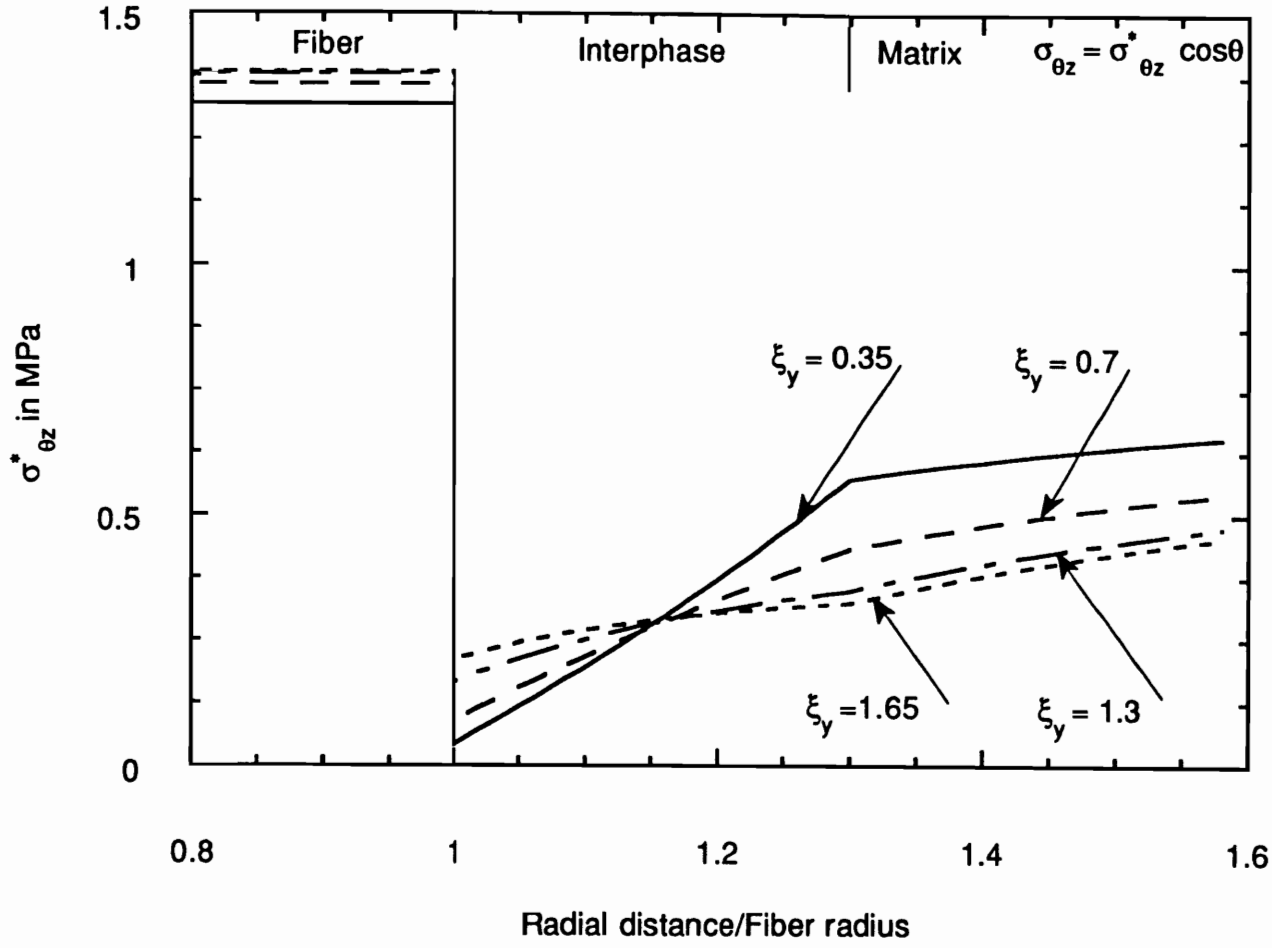

Figure 35. Shear stress as a function of modulus ratio in a carbon/IMHS epoxy composite under a longitudinal shear load of 1 MPa: $V_f = 0.4$; $\phi = 0.1$.

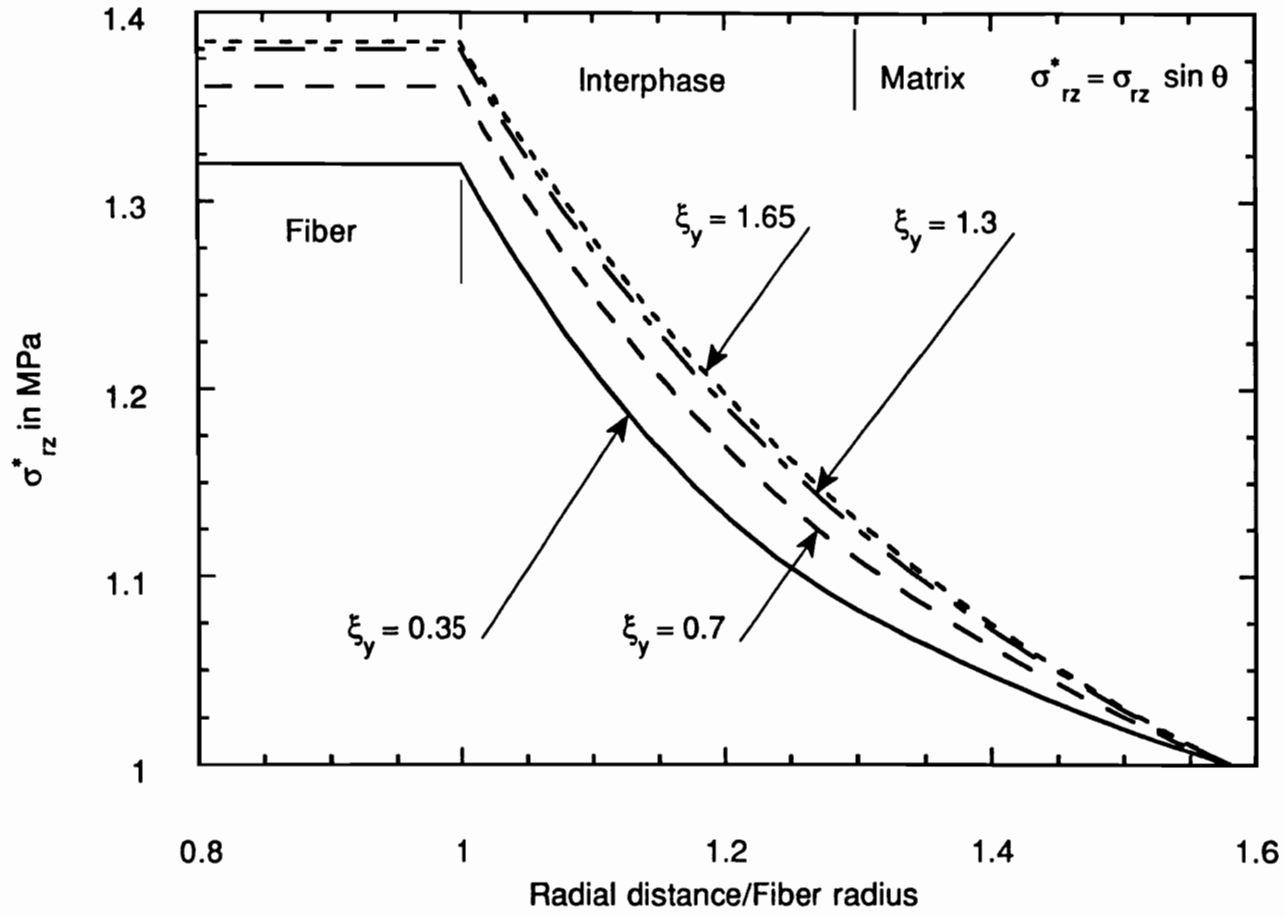

Figure 36. Shear stress as a function of modulus ratio in a carbon/IMHS epoxy composite under a longitudinal shear load of 1 MPa: $V_f = 0.4$; $\phi = 0.15$.

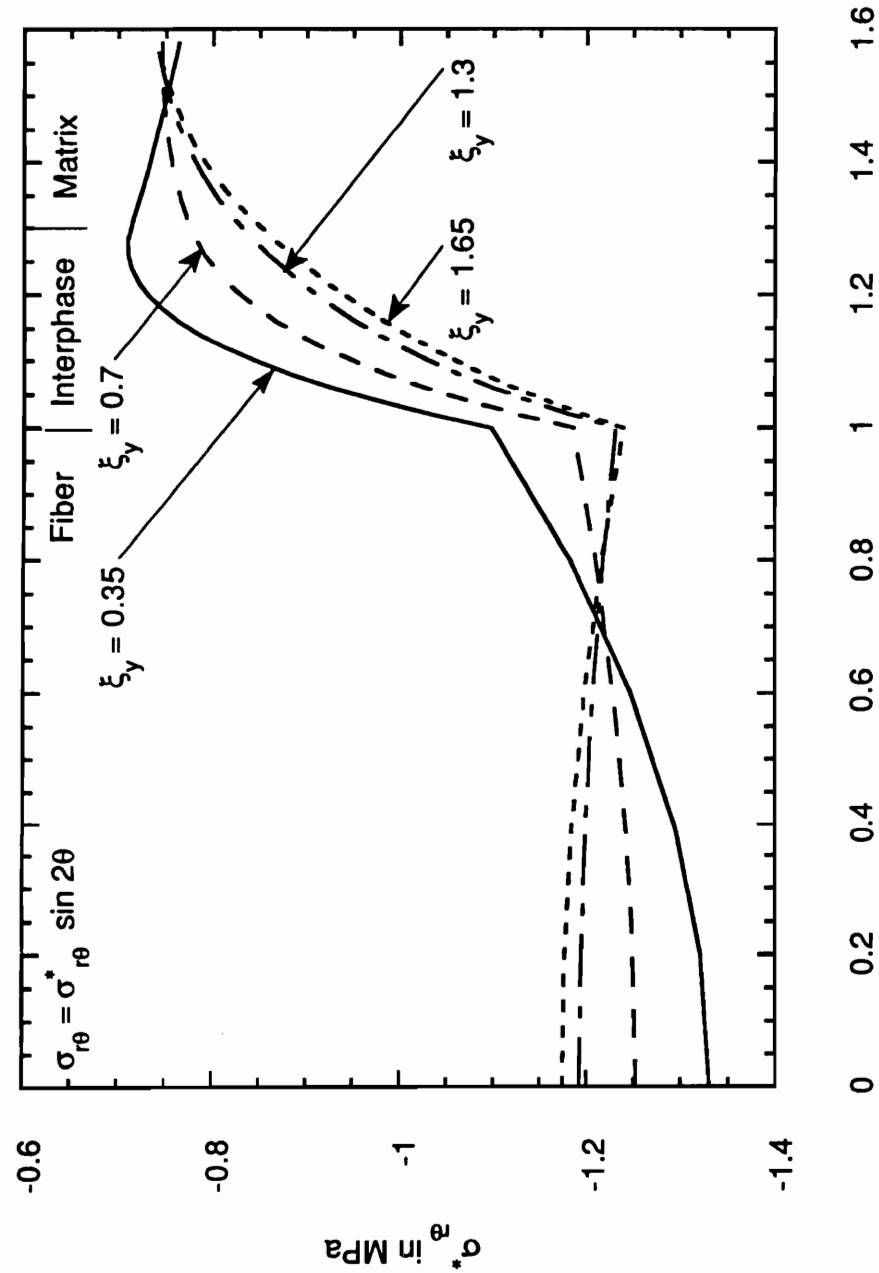

Figure 37. Shear stress as a function of modulus ratio in a carbon/IMHS epoxy composite under a transverse shear load of 1 MPa: $V_f = 0.4$; $\phi = 0.15$.

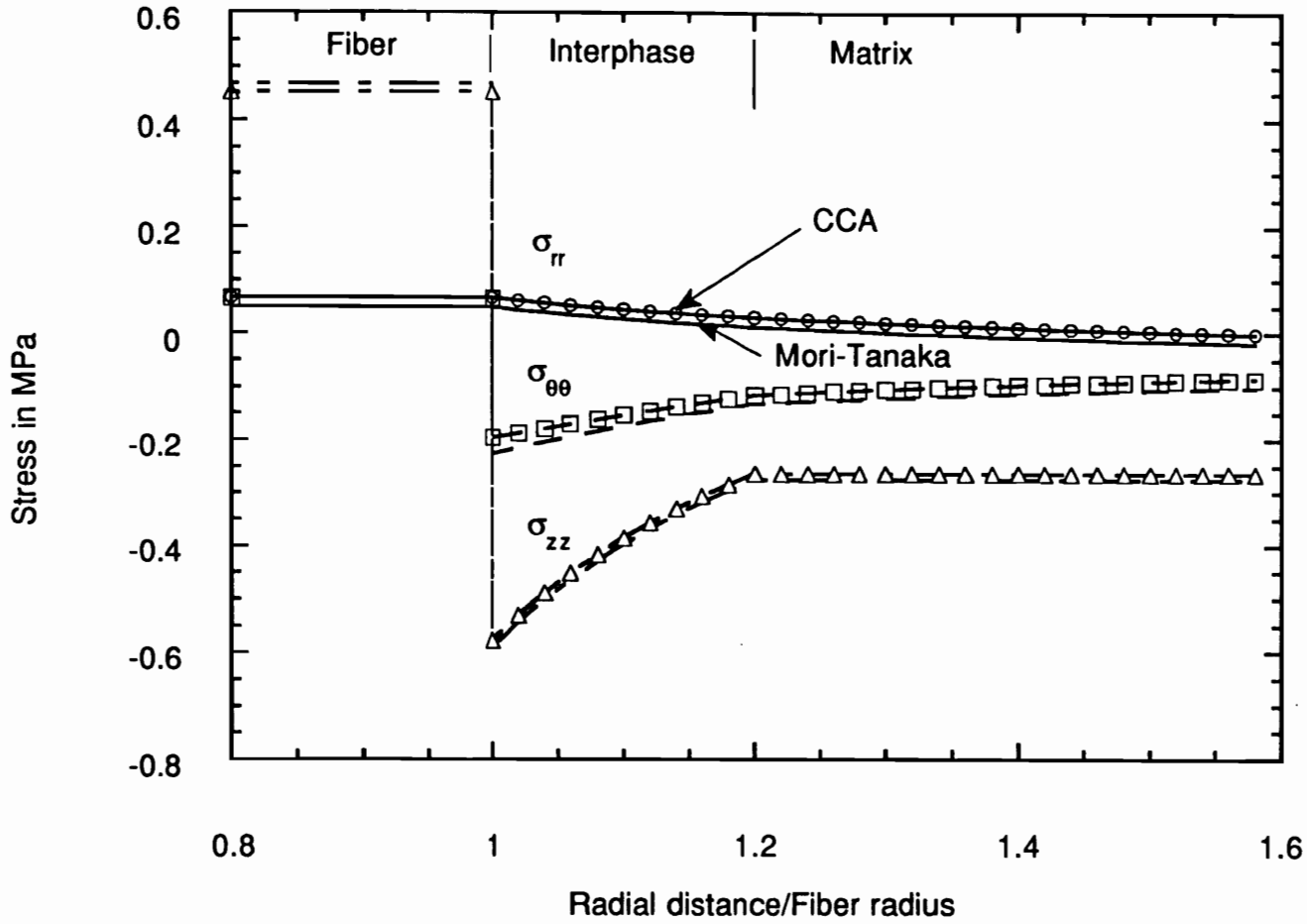

Figure 38. Constituent stress comparison between concentric cylinder assemblage and Mori-Tanaka analyses for a Kevlar 49/IMHS epoxy composite under a uniform temperature change of 1 degree C: $V_f = 0.4$; $\phi = 0.1$; $\xi_y = 3$; $\xi_c = 0.75$.

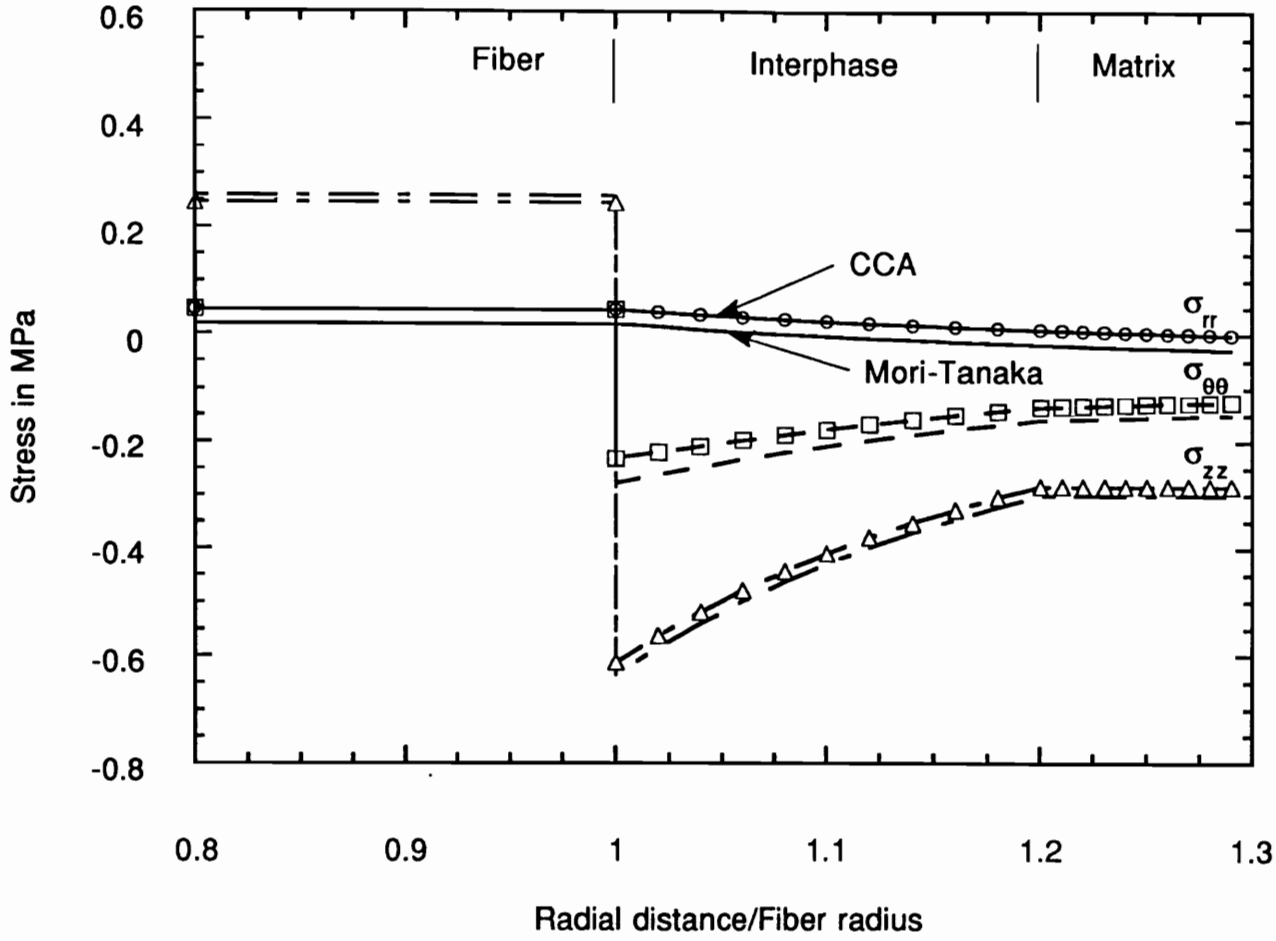

Figure 39. Constituent stress comparison between concentric cylinder assemblage and Mori-Tanaka analyses for a Kevlar 49/IMHS epoxy composite under a uniform temperature change of 1 degree C: $V_f = 0.6$; $\phi = 0.1$; $\xi_y = 3$; $\xi_c = 0.75$.

7.0 Experimental Study

A novel method is discussed in this section for the experimental study of the interphasial effects. The method requires the use of the following:

- Preparation of the model composite,
- Production of modulus gradients at the fiber-matrix interface of the model composite, and
- Use of Moire interferometry to measure displacements in the gradient region of the model composite.

A model composite system consisting of a coated glass rod embedded in Epon 828 was considered; coatings were applied to the glass rod in succession to simulate two different interphase types. Different coatings were synthesized by the addition of epoxy modifiers to Epon 828. These modifiers increased the Young's modulus of Epon 828 in direct proportion to the amount added. The model composite specimens were loaded in transverse compression and transverse shear, and the resulting in-plane displacements were measured by the use of the Moire interferometry technique. Differences in the displacement fields in the gradient regions of the various specimens were identified.

7.1 Model Composite Preparation

A model composite may be thought of as a composite material system with the constituents scaled up in size for one of the following reasons:

- isolation of the phenomena involved at the fiber-matrix interphase,
- control of the fiber packing arrangement,
- measurement of the displacements and stresses in the interphase region, and
- verification of theoretical predictions of local stresses.

Typically, model composite studies [100-103] have been used to evaluate the residual curing stresses in composite material systems.

Koufopoulos and Theocaris [100] have undertaken a two-dimensional, photoelastic study of the shrinkage stresses in a composite. Circular discs (diameter 30 mm and thickness 5 mm) of completely cured, unplasticized, cold-setting epoxy were arranged in a square array in a mold; the mold was then filled with plasticized epoxy and cured. Specimens with different center-to-center distances between discs and different plasticizer percentages in the matrix were studied. The magnitude of stresses at various points in the matrix were evaluated; comparisons to theoretical stress values showed good agreements. Daniel and Durelli [101] have also used two-dimensional photoelasticity to study the shrinkage stresses in a composite. Circular glass discs (diameter 0.25 in and thickness 0.25 in) were cured in epoxy to produce single and double inclusions in epoxy. Shrinkage stresses were evaluated and were shown to agree well with theoretical predictions.

Marloff and Daniel [102] have utilized the stress-freezing technique to determine the three-dimensional stress distributions in the matrix of unidirectional fiber-reinforced composite models. The model consisting of a square array of polycarbonate rods (diameter 0.375 in) in an epoxy matrix simulated a boron-epoxy composite with a fiber volume fraction of 0.5. One of the specimens was subjected to compressive loads and the other was allowed to develop stresses due to matrix shrinkage. Both specimens were subjected to a stress freezing

cycle and the stresses were calculated based on the fringe order. Excellent agreement was found between the theoretical and experimental stress concentration values at the fiber-matrix interface and at the midpoint between fibers. Asamoah and Wood [103] have used photothermoelasticity to analyze the residual stresses at the fiber-matrix interface in continuous, unidirectional model composites. Aluminum rods of 0.5 in diameter were arranged in a hexagonal geometry in a mold; the mold was then filled with epoxy and cured. Specimens with different center-to-center distances between the rods, representing different fiber volume fractions, were studied. Comparisons were made between the experimental results and the results of finite element analyses and good agreements were found.

The model composite under consideration here is a single fiber/matrix composite, similar to the square array composite that has been used by Ifju [104] to investigate the local behavior of a composite under transverse compression. It consists of the following materials:

- Fiber — Pyrex glass rod 2 mm in diameter,
- Matrix — Epon 828, and
- Curing Agent — "A", a room temperature curing agent

Curing agent A was specifically chosen to avoid the buildup of large residual curing stresses in the composite. The properties of the fiber and matrix are given in Table 6.

The methodology used to make samples is outlined below:

- Epon 828 was mixed with curing agent A (6 to 7 parts per hundred resin) in a glass container.
- The mixture was degased in a vacuum chamber and poured gently into a tank made of poly methyl methacrylate.
- An index plate, with a glass rod fixed to its center, was lowered gently into the tank as shown in Figure 40. Care was taken to ensure that the glass rod slides into the center of the tank.
- Cure was accomplished in 24 hours at room temperature.
- The sides of the tank were pried apart and the sample was removed.

- Slices were cut out of the cured sample using a Buehler Isomet low speed saw (Figure 41). The slices were then machined to make specimens.

7.2 Interphase Simulation Using Coatings

Garton, *et al.* [105, 106, 107] have developed a range of additives for epoxy resins which can increase the tensile modulus of the cured polymer up to about 60%. These additives are mixed with the epoxy resin and curing agent and the mixture is then cured in the conventional fashion. One of these additives, namely EPPHAA (epoxyphenoxypropane + 4 hydroxy acetanilide) is considered in this study; more details about the additive can be found elsewhere [106]. Typical stress-strain curves for Epon 828 crosslinked with MDA (methylene dianiline) are shown in Figure 42; an increase in tensile modulus from 2.5 GPa to about 4.0 GPa is seen with an increase in the amount of EPPHAA. The increase in modulus is achieved through a reduction in free volume of the epoxy: the reduction in free volume hinders polymer segmental motion and hence increases the modulus.

Epoxy additives offer the potential for constructing modulus gradients in model composite systems; this was achieved as follows:

- Different epoxy-crosslinking agent-additive mixtures with a sequentially varying percentage of additive were prepared at about 70 °C.
- The glass rods were sequentially coated with these epoxy-crosslinking agent-additive mixtures. The coating was applied to different locations of the glass rod through a syringe and the glass rod was rotated to help spread the coating evenly. The glass rod was then held vertical until the coating layer was cured at room temperature. Holding the glass rod vertical causes some sliding in the coating layer, resulting in a thicker coating at the bottom of the glass rod than at the top.

- Care was taken to ensure that a coating layer was nearly cured before the next coating layer was applied. It was necessary to optimize the extent of cure of the coating layers: Over-curing a layer will result in poor adhesion between the over-cured layer and the succeeding layer, while under-curing a layer will result in the additive equilibrating between the under-cured layer and the succeeding layer.

Using this methodology three different interphase types were simulated:

- Specimen A/Interphase Type 1 — The glass rod was in direct contact with the matrix.
- Specimen B/Interphase Type 2 — The Young's modulus of the interphase was a gradient as shown in Figure 43. The thicknesses and the moduli of the coating layers for this interphase are given in Table 7.
- Specimen C/Interphase Type 3 — The Young's modulus of the interphase was a gradient as shown in Figure 44. The thicknesses and the moduli of the coating layers for this interphase are given in Table 8.

It should be emphasized here that the thicknesses, moduli values and the number of coatings considered for specimen B and C would at best represent the linear property variation for the interphase used by Sottos, *et al.* [15]. Simulation of interphase property variations discussed in Chapter 4 is currently not possible as this would require smaller coating thicknesses and a smoother modulus variation.

7.3 Moire Interferometry

Moire interferometry [108, 109, 110] is a full-field, optical technique that utilizes coherent light and features sub-wavelength displacement sensitivity and high spatial resolution. The technique supplies both the horizontal (U) and vertical (V) displacement information on the entire face of the specimen in the form of fringe patterns; strains can then be calculated from the displacement patterns.

The principle of Moire interferometry can be explained with the help of Figure 45. A crossed-line diffraction grating is replicated on the surface of the specimen; the grating is thin, compliant and deforms freely with the loaded specimen. Input beams of collimated coherent light, A_1 and A_2, in a horizontal plane interfere with each other and produce an interference pattern called the virtual reference grating. The virtual reference grating in this work has a frequency (f) of 2400 lines/mm. The specimen grating and the virtual reference grating interact to form a Moire pattern which is a null field (uniform intensity and devoid of fringes) before loads are applied to the specimen. After loading, the Moire fringe pattern produced is a contour map of the in-plane U displacements. This is photographed by a camera which is focused on the surface of the specimen. Beams B_1 and B_2, in the vertical plane produce the in-plane V displacement fringes.

The fringe patterns are contour maps in which the fringe order is proportional to the in-plane displacements as shown below:

$$U = \frac{N_x}{f}; \qquad V = \frac{N_y}{f} \tag{89}$$

N_x and N_y are the fringe orders when lines of the reference grating are perpendicular to the x and y directions, respectively. The normal strains, ε_x and ε_y, and the shear strain γ_{xy} can be determined from the displacement fields by the small strain relationships given by

$$\varepsilon_x = \frac{\partial U}{\partial x} = \frac{1}{f}\frac{\partial N_x}{\partial x} \tag{90}$$

$$\varepsilon_y = \frac{\partial V}{\partial y} = \frac{1}{f}\frac{\partial N_y}{\partial y} \tag{91}$$

$$\gamma_{xy} = \frac{\partial U}{\partial y} + \frac{\partial V}{\partial x} = \frac{1}{f}\left(\frac{\partial N_x}{\partial y} + \frac{\partial N_y}{\partial x}\right) \tag{92}$$

7.4 Testing

7.4.1 Loading Fixture

The loading fixture shown in Figure 46 was used in both the compression and shear tests; the fixture was developed and used by Ifju [104] to study the local behavior of a square array composite. The fixture consists of a single piece body as shown, with calibrated strain gages attached to the columns for the measurement of applied compressive load. The specimen (in the case of compression test) or the test fixture (in the case of shear test) is held between two blocks, which are rectangular in cross-section. Block A is fixed to the top of the body, while block B is supported by wedge A through a semi-circular cylindrical piece and screw. The semi-circular cylindrical piece helps to apply approximate point loads along the center line of the specimen, while the screw helps to keep block B horizontal. Wedge A moves up or down in vertical grooves on the sides of the body and rests on wedge B. Wedge B moves left or right in horizontal grooves at the bottom of the body and its movement is controlled by screws. A compressive load is applied by moving wedge B to the right which in turn raises wedge A.

7.4.2 Compression Test

The specimen configuration for the compression test and the compressive stress produced by the given load arrangement are shown in Figures 47 (a) and 47 (b), respectively. Specimen A was tested at different load levels until a failure load (4000 N) was identified. An applied load (2560 N) well below the failure load was chosen and specimens B and C were

tested at this load level. Moire fringe patterns depicting the U and V displacements for each specimen were photographed.

7.4.3 Shear Test

The specimen configuration for the shear test is shown in Figure 48; the center piece is machined from the sample and the end pieces are attached by means of an adhesive. The shear test is accomplished through a four-point asymmetrical loading arrangement shown in Figure 49 [111]. The exterior supports are separated by a distance a and the interior supports are separated by a distance b. The load is applied through semi-circular cylindrical pieces as shown. The test fixture shown in Figure 49 is placed between blocks A and B in the loading fixture for the shear test.

The loads on the specimen and the resultant shear force and bending moment diagrams are shown in Figure 50. The shear force is constant and the bending moment changes sign in the region between the interior load points. The bending moment is zero and the specimen is in pure shear at the center of the specimen. The shear stress distribution across the depth of the specimen, in the region between the notches, is reasonably uniform [111] and hence the shear stress produced by the given load arrangement is as shown in Figure 50.

Specimen A was tested at different load levels until a failure load (1560 N) was identified. An applied load (890 N) well below the failure load was chosen and specimens B and C were tested at this load level. Moire fringe patterns depicting the U and V displacements for each specimen were photographed.

7.5 Results and Discussion

Figures 51 and 52 show the U and V displacements near the interphasial region for all three specimens under compression; a quarter of the displacement contour is shown in each case. Figures 53 and 54 show the U and V displacements near the interphasial region for all three specimens under shear; one-half of the displacement contour is shown in each case. The following observations can be made based on Figures 51, 52, 53 and 54:

- Comparisons between displacement contours under the same loading condition show that only small changes are introduced in the fringe patterns due to the presence of the interphasial regions; these changes are well within the bounds of experimental error.
- Strains in the fiber are nearly constant.
- Strains in the matrix are larger than the strains in the fiber.
- Strain transitions between the fiber and the matrix are abrupt.
- Magnification of the region near the glass rod does not show the presence of multiple fringes required to calculate pointwise displacements.

Some improvements that may lead to pointwise displacement measurement in the interphase/coating regions are discussed below:

- Higher sensitivity of Moire interferometry — Sensitivity can be improved by either increasing the frequency of the virtual reference grating or by considering ultra-high sensitivity Moire interferometry [112]. A reference grating frequency of 4000 lines/mm has been achieved [109] without any specialized equipment. Further, Han [112] has demonstrated ultra-high sensitivity Moire interferometry, where a reference grating frequency of 57600 lines/mm has been achieved through an optical/digital fringe multiplication method.
- Larger coating thicknesses — The thicknesses of the individual coatings can be increased thereby providing a larger region over which displacements have to be measured. A

higher diameter glass rod can be used in this case to preserve the interphase thickness to fiber diameter ratio.

- Higher applied load — Higher applied loads may cause higher strains in the coatings resulting in a better fringe pattern next to the glass rod. Toughened epoxy can be used as a matrix material in order to apply higher loads to the specimens.
- Steeper modulus gradients in the interphase region.

Table 6. Material properties for the fiber and matrix used in the model composite sample.

Property	Pyrex glass	Epon-828
E (GPa)	62.78	2.90
ν	0.20	0.34

Table 7. The thicknesses and the Young's moduli of the coating layers in specimen B.

	Property	Coating 1	Coating 2	Coating 3	Coating 4
	E (GPa)	2.800	3.400	3.900	4.200
	ν	0.300	0.300	0.300	0.300
Coating Thickness in mm	25 mm from the base	0.032	0.053	0.074	0.073
	50 mm from the base	0.030	0.057	0.068	0.066
	75 mm from the base	0.020	0.061	0.059	0.056
	100 mm from the base	0.009	0.036	0.054	0.034

Table 8. The thicknesses and the Young's moduli of the coating layers in specimen C.

	Property	Coating 1	Coating 2	Coating 3	Coating 4
	E (GPa)	4.200	3.900	3.400	2.800
	ν	0.300	0.300	0.300	0.300
Coating Thickness in mm	25 mm from the base	0.058	0.102	0.061	0.056
	50 mm from the base	0.041	0.094	0.061	0.047
	75 mm from the base	0.045	0.074	0.067	0.033
	100 mm from the base	0.033	0.056	0.069	0.021

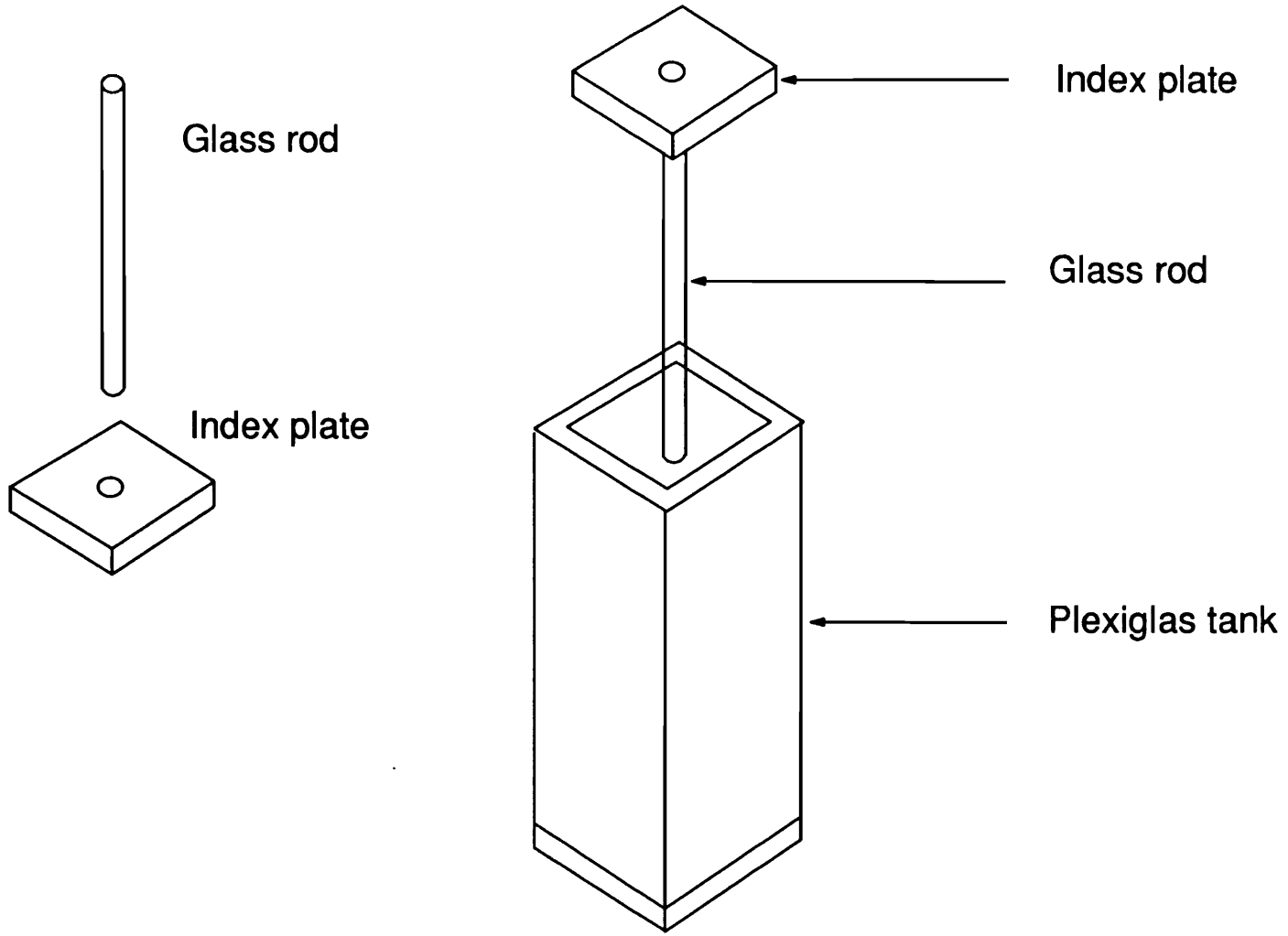

Figure 40. Making the model composite sample.

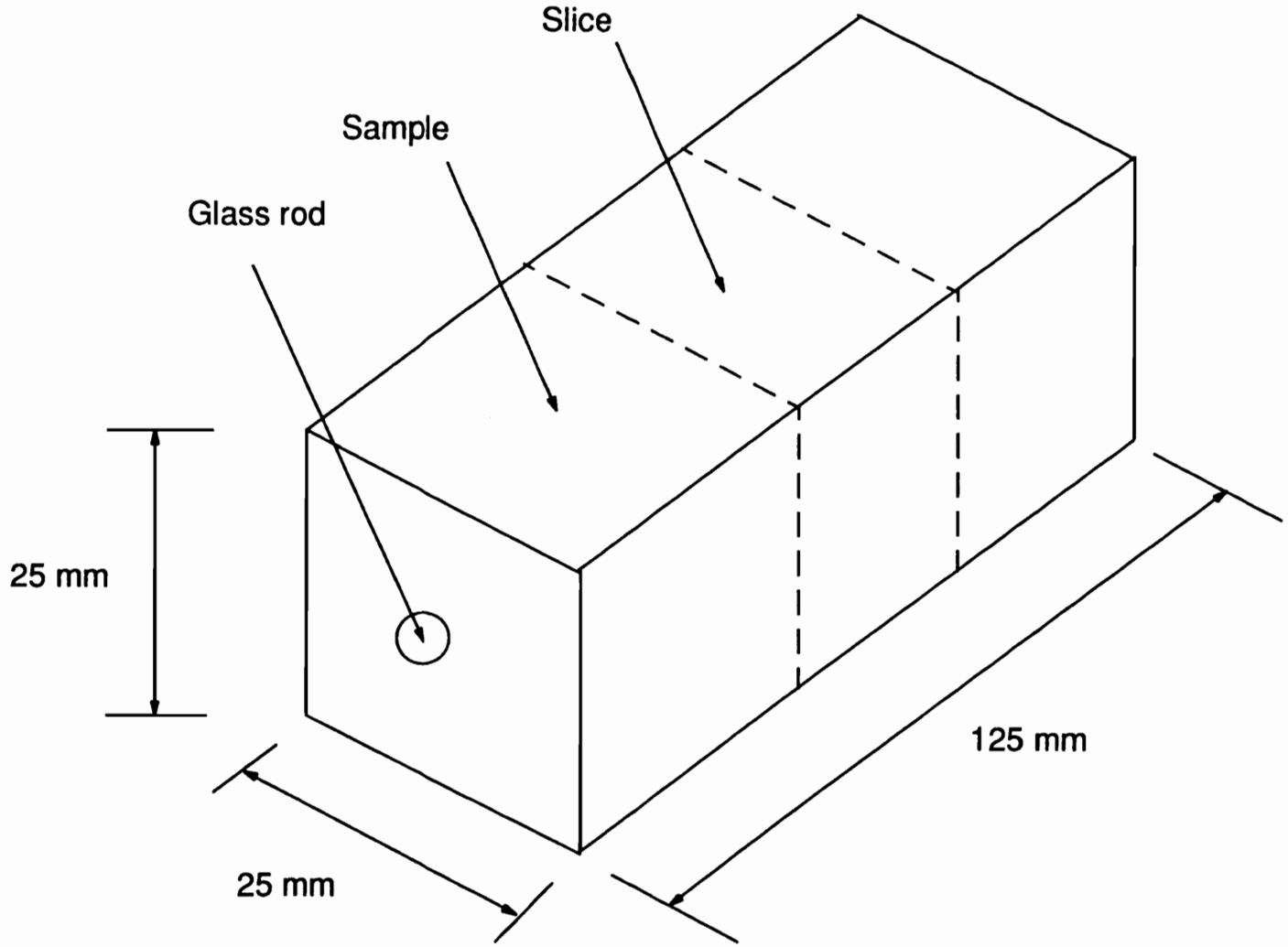

Figure 41. Cutting slices from the sample to make specimens.

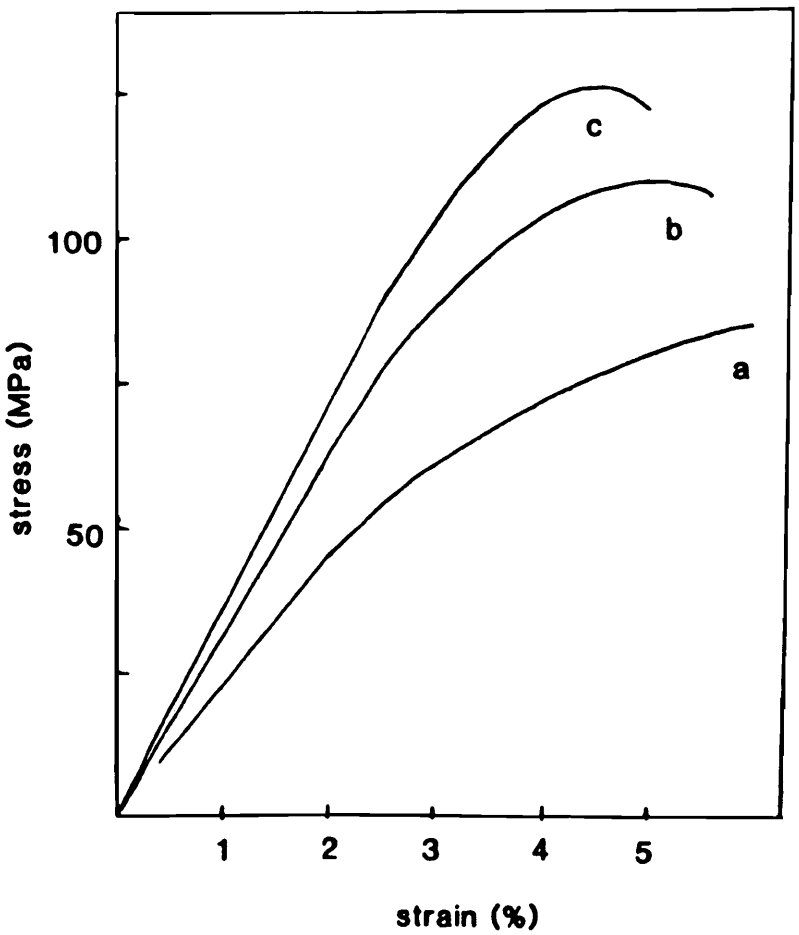

Figure 42. Tensile stress versus strain curves at 25 degrees C and 2 mm/min for Epon 828 crosslinked with MDA: (a) control, (b) 20 phr EPPHAA and (c) 30 phr EPPHAA.

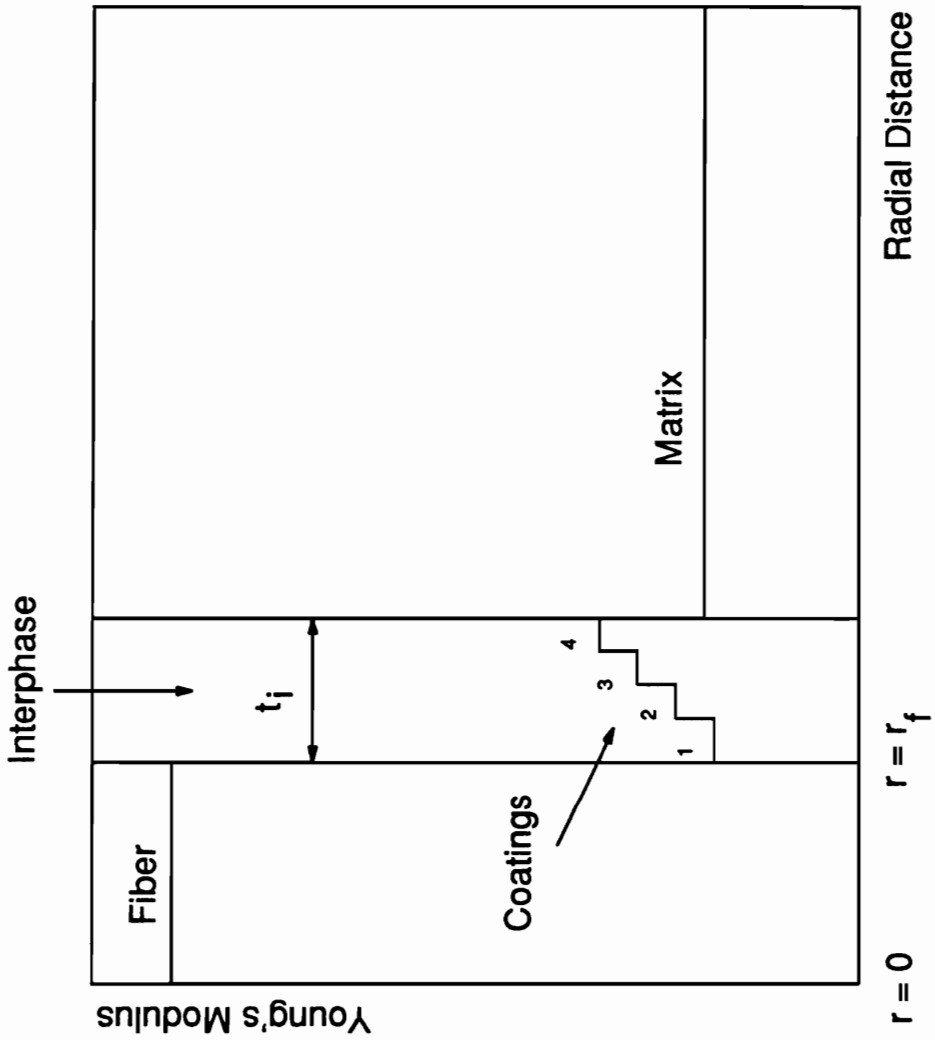

Figure 43. Schematic of the Young's moduli variation in the interphase for specimen B.

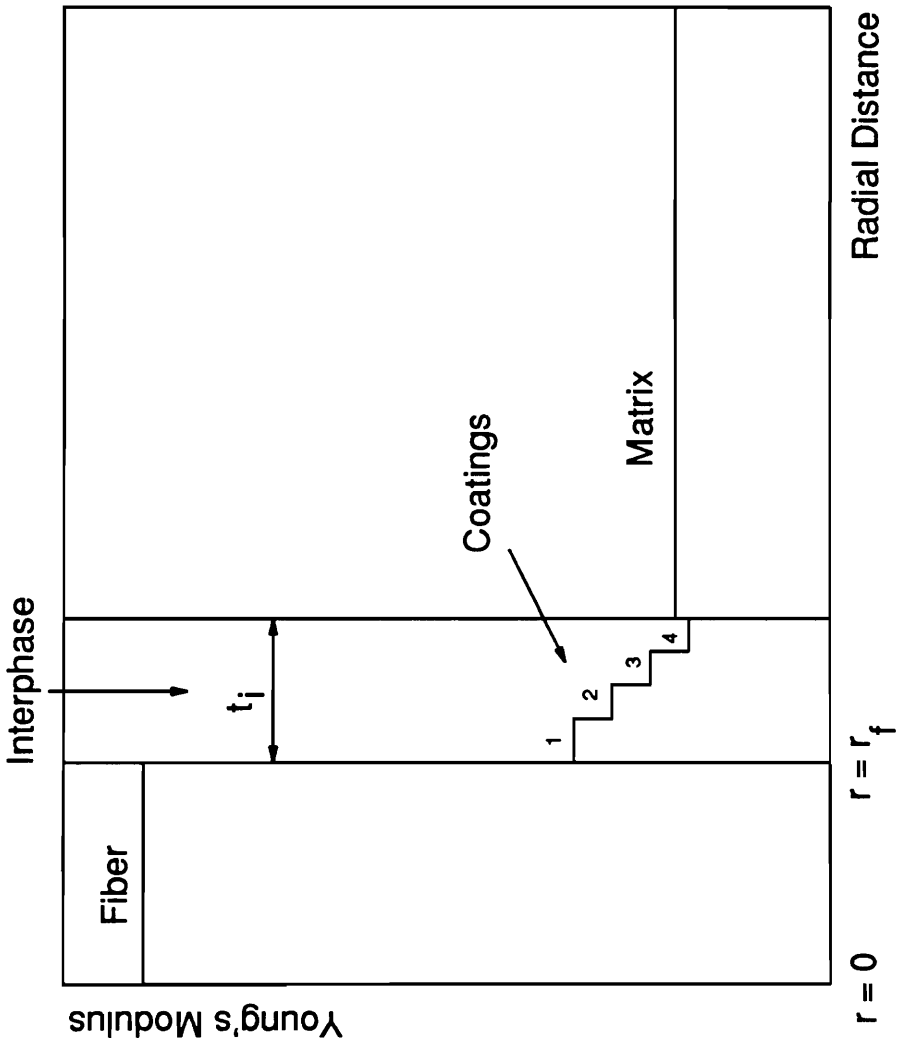

Figure 44. Schematic of the Young's moduli variation in the interphase for specimen C.

$$f = \frac{2}{\lambda}\sin\alpha$$

$$U = \frac{1}{f}N_x \qquad V = \frac{1}{f}N_y$$

$$\varepsilon_x = \frac{\partial U}{\partial x} = \frac{1}{f}\frac{\partial N_x}{\partial x} \qquad \varepsilon_y = \frac{\partial V}{\partial y} = \frac{1}{f}\frac{\partial N_y}{\partial y}$$

$$\gamma_{xy} = \frac{\partial U}{\partial y} + \frac{\partial V}{\partial x} = \frac{1}{f}\left[\frac{\partial N_x}{\partial y} + \frac{\partial N_y}{\partial x}\right]$$

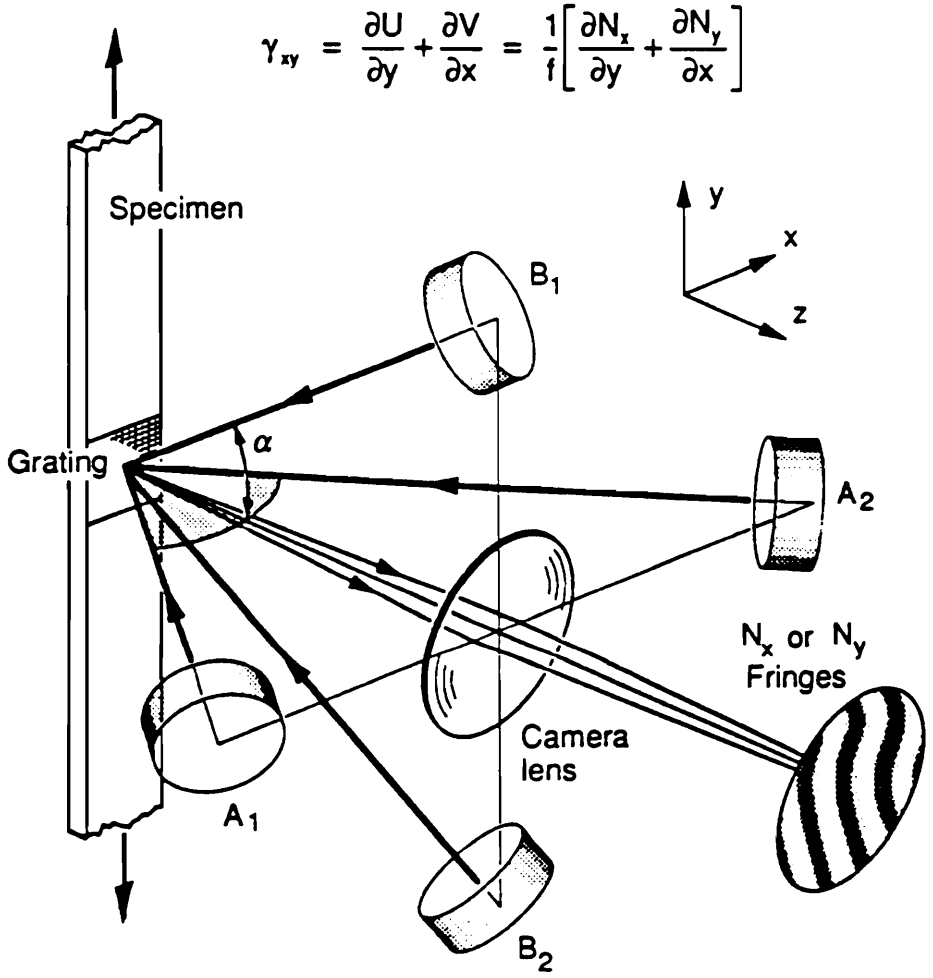

Figure 45. Schematic of the principle behind the Moire interferometry technique.

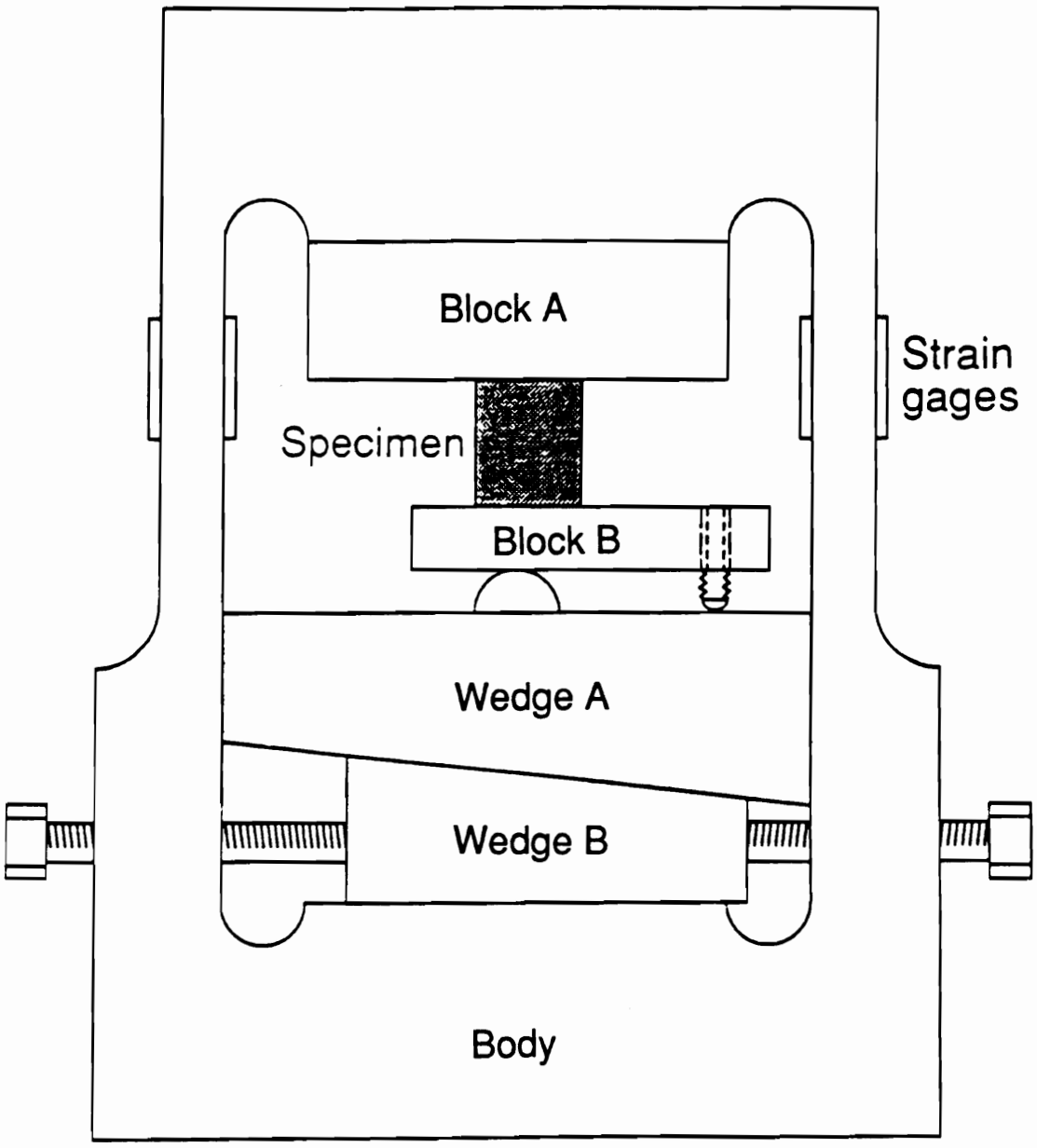

Figure 46. Loading fixture used in the compression and shear test.

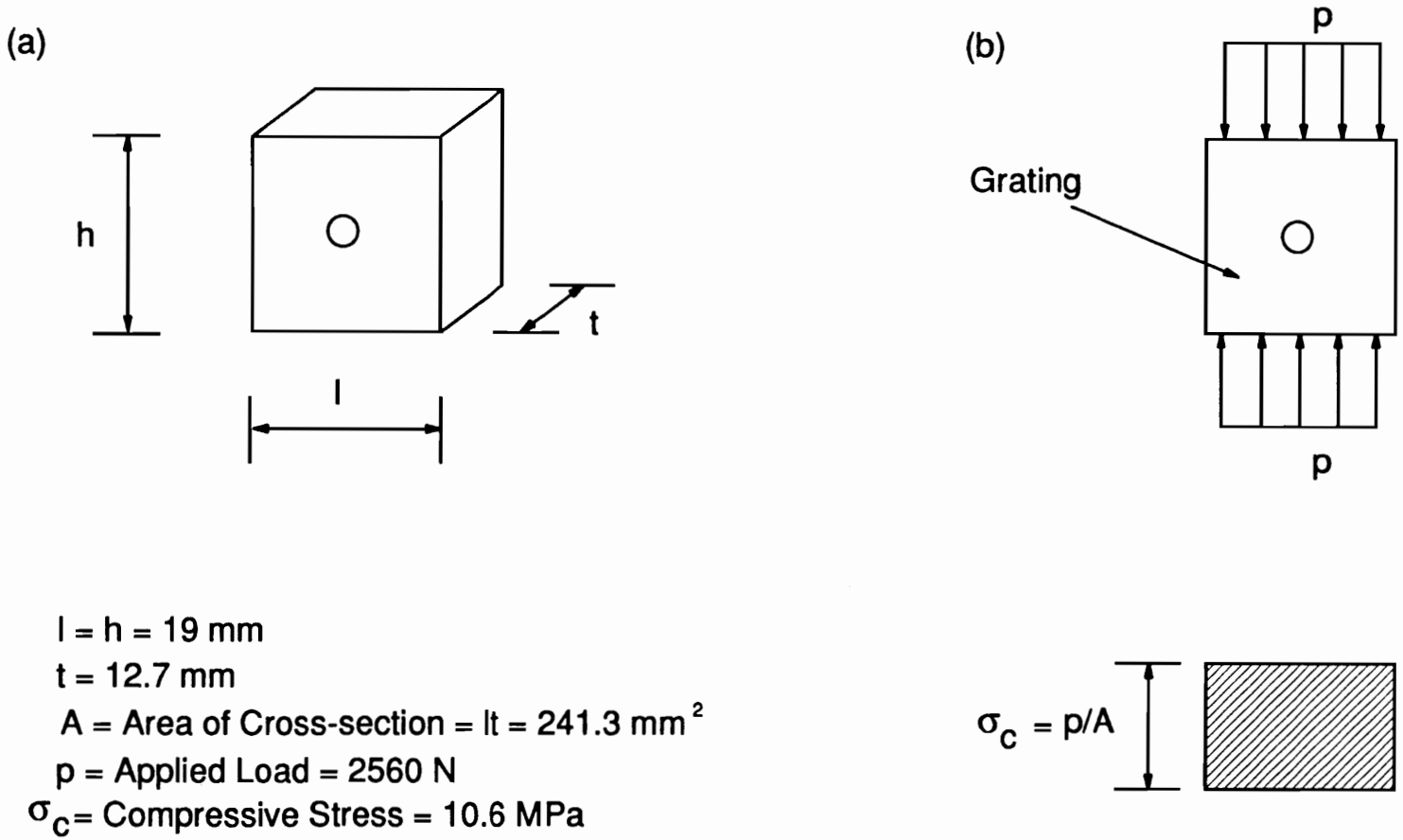

l = h = 19 mm
t = 12.7 mm
A = Area of Cross-section = lt = 241.3 mm^2
p = Applied Load = 2560 N
σ_c = Compressive Stress = 10.6 MPa

Figure 47. Specimen configuration for the compression test.

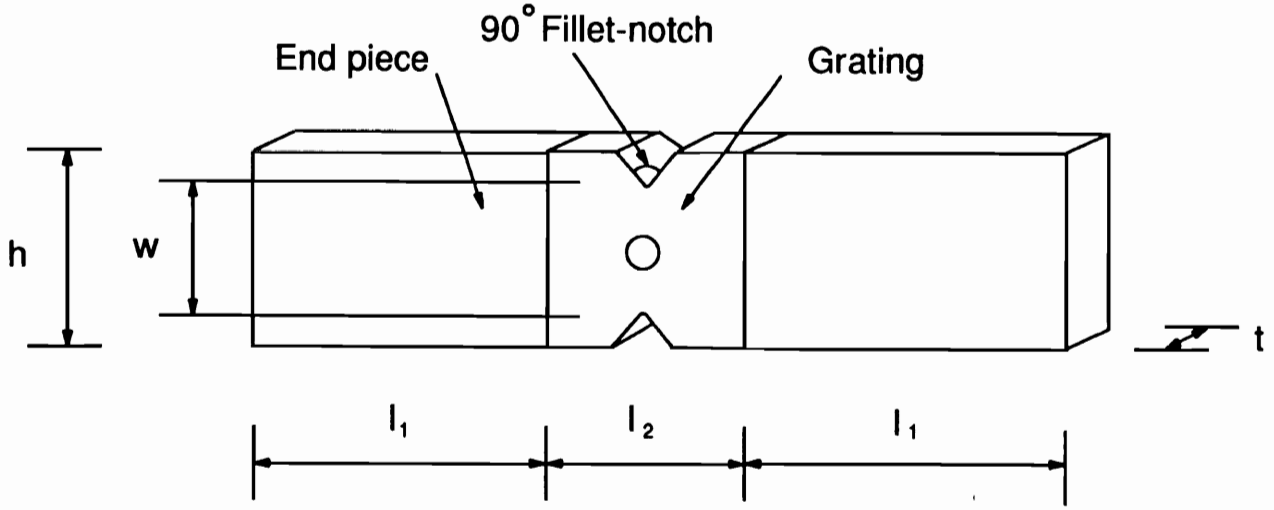

h = 19 mm
l_1 = 28.6 mm
l_2 = 19 mm
t = 6.4 mm
w = 11.4 mm
A = Area of Cross-section = wt = 73 mm^2

Figure 48. Specimen configuration for the shear test.

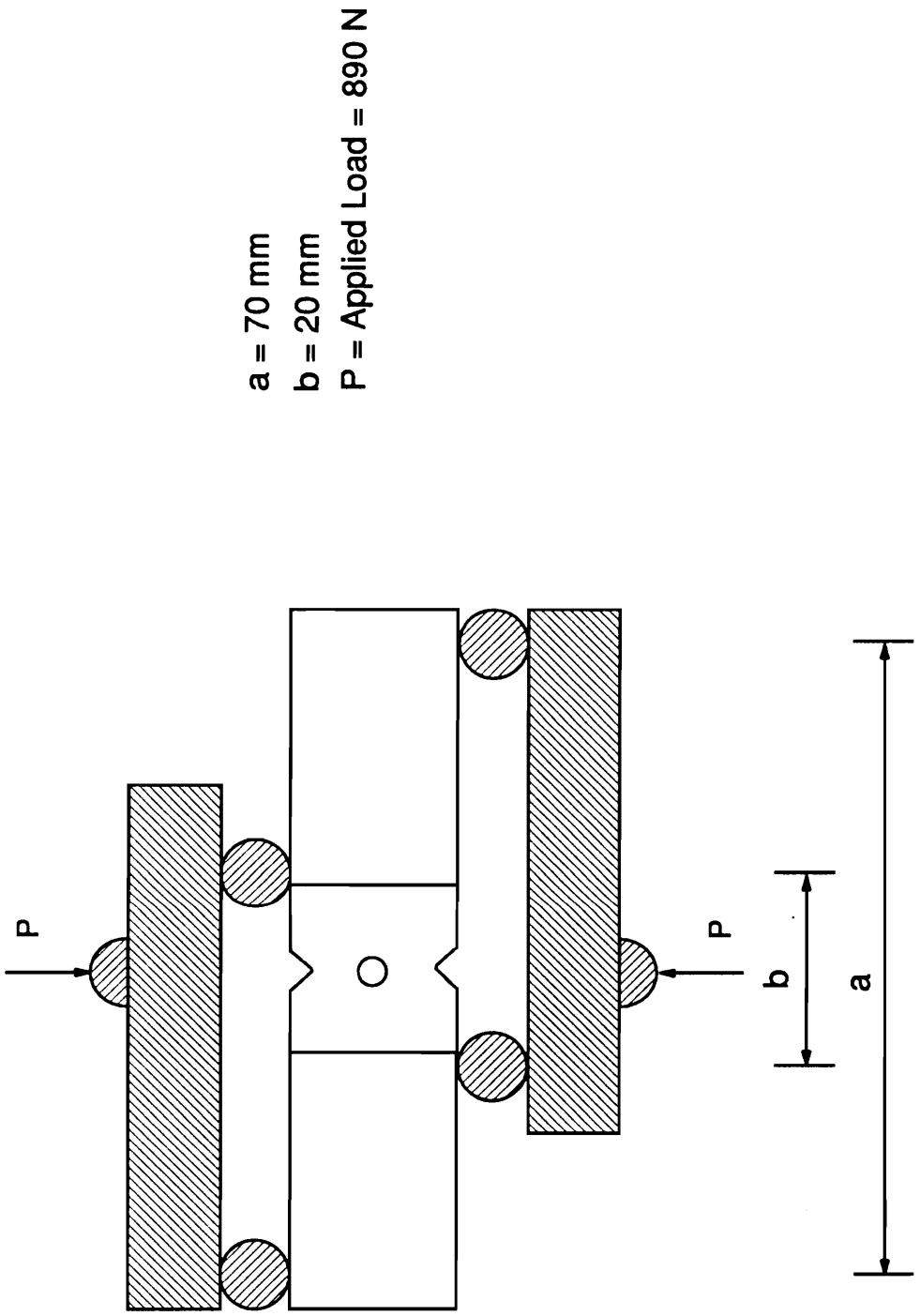

Figure 49. Schematic of the four-point asymmetrical test fixture used for the shear test.

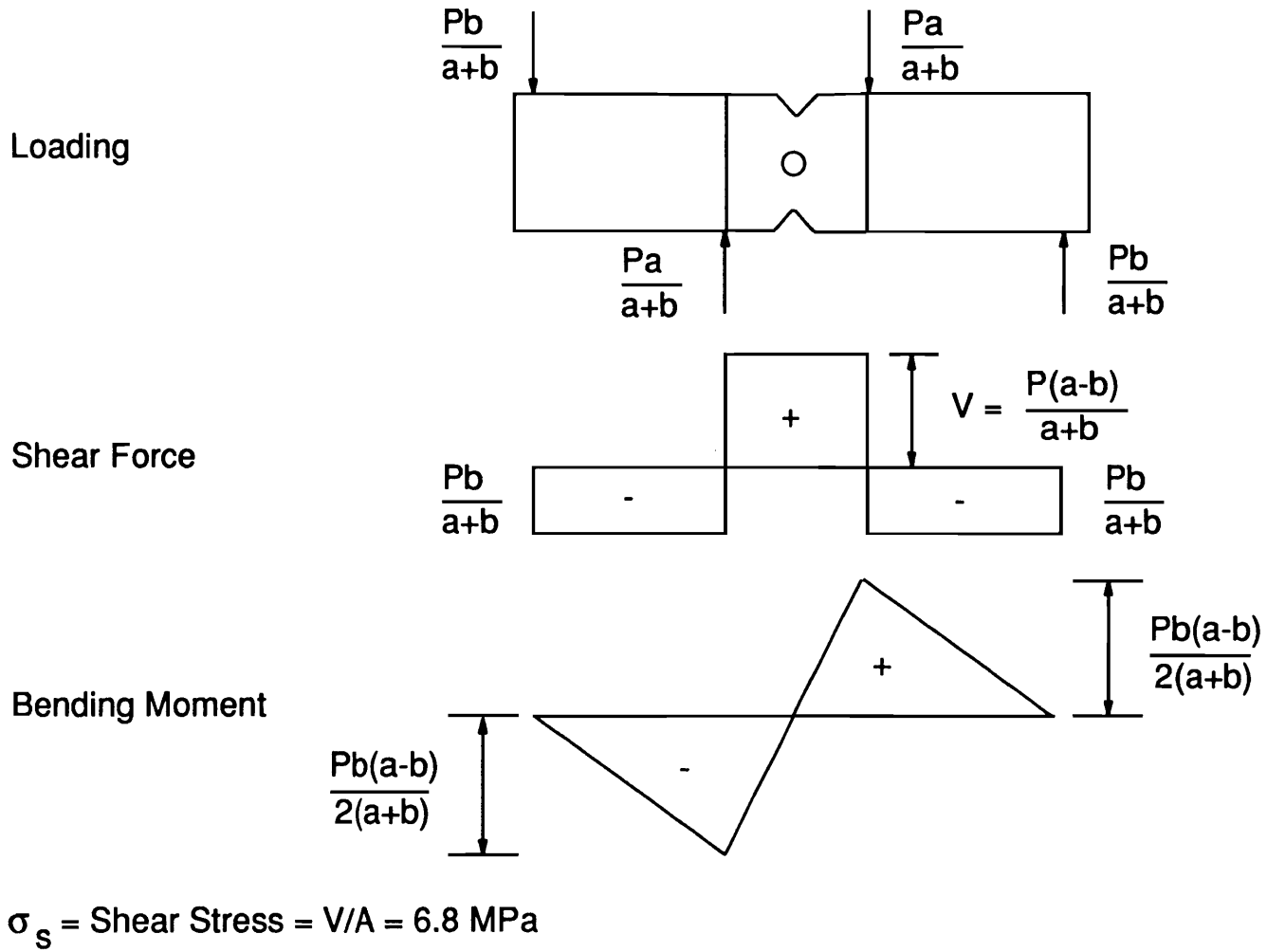

σ_s = Shear Stress = V/A = 6.8 MPa

Figure 50. Loading, shear force and bending moment diagrams for the shear test.

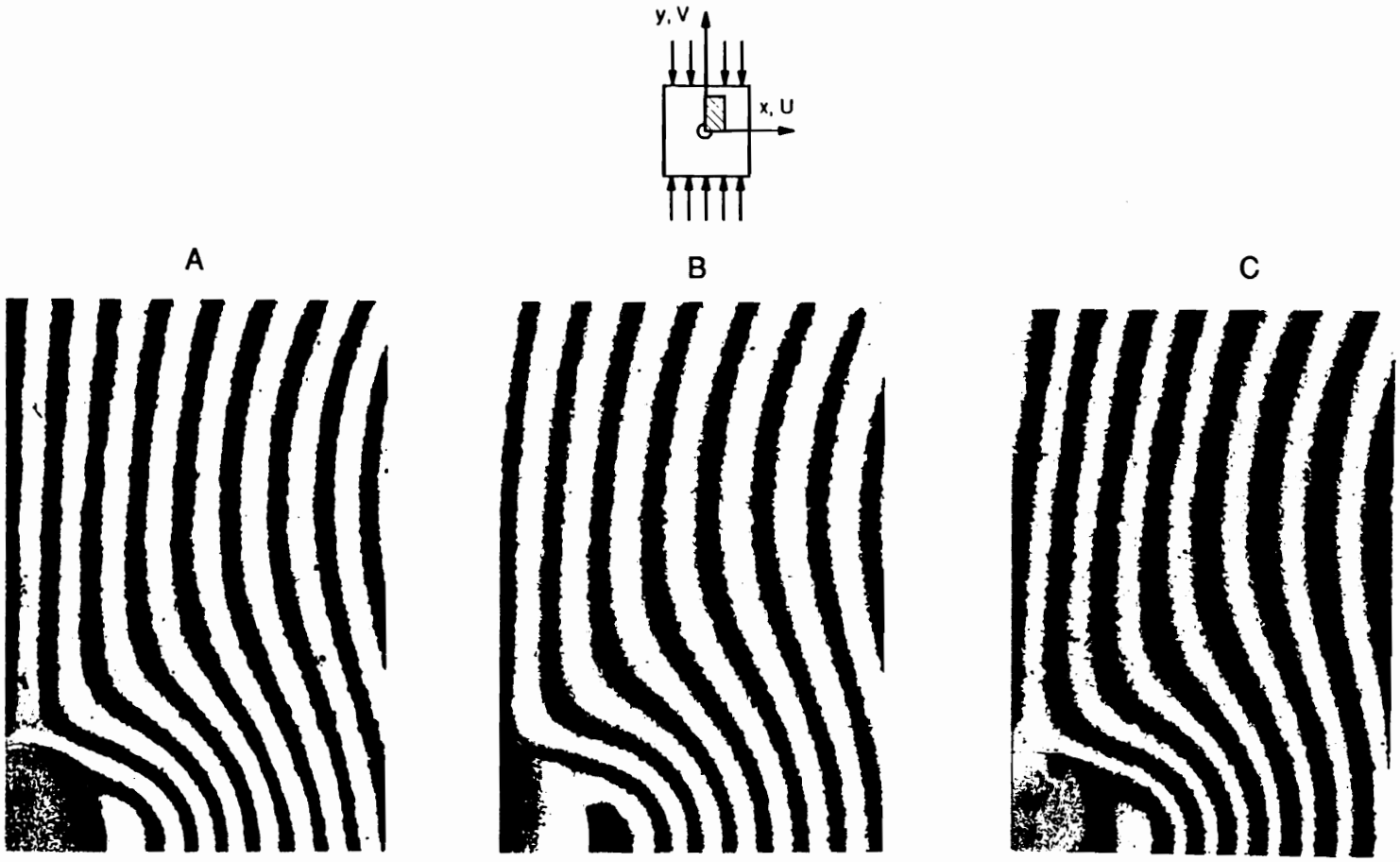

Figure 51. Fringe pattern depicting the horizontal displacement (U) for all three specimens under compression; a quarter of the displacement contour is shown in each case.

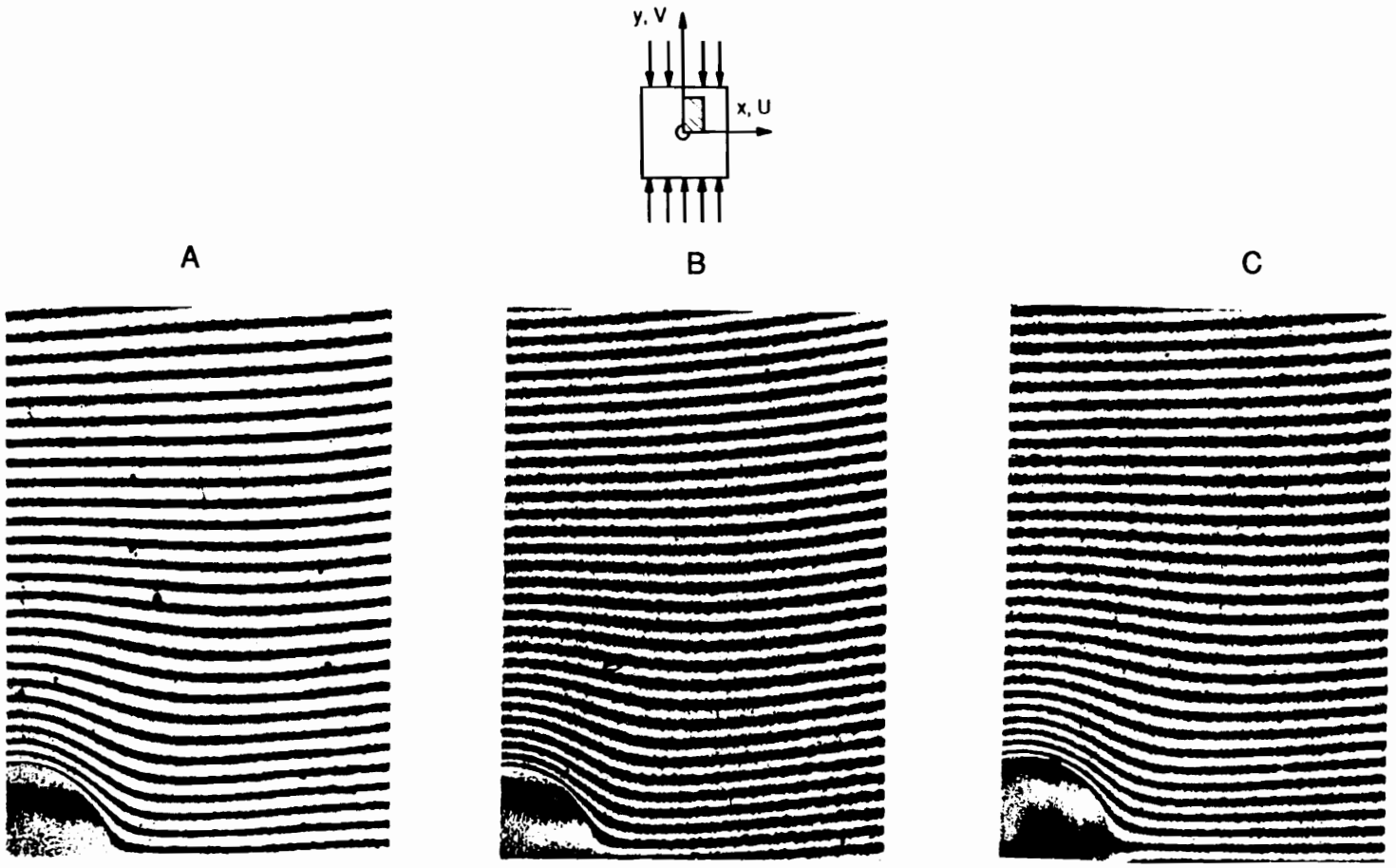

Figure 52. Fringe pattern depicting the vertical displacement (V) for all three specimens under compression; a quarter of the displacement contour is shown in each case.

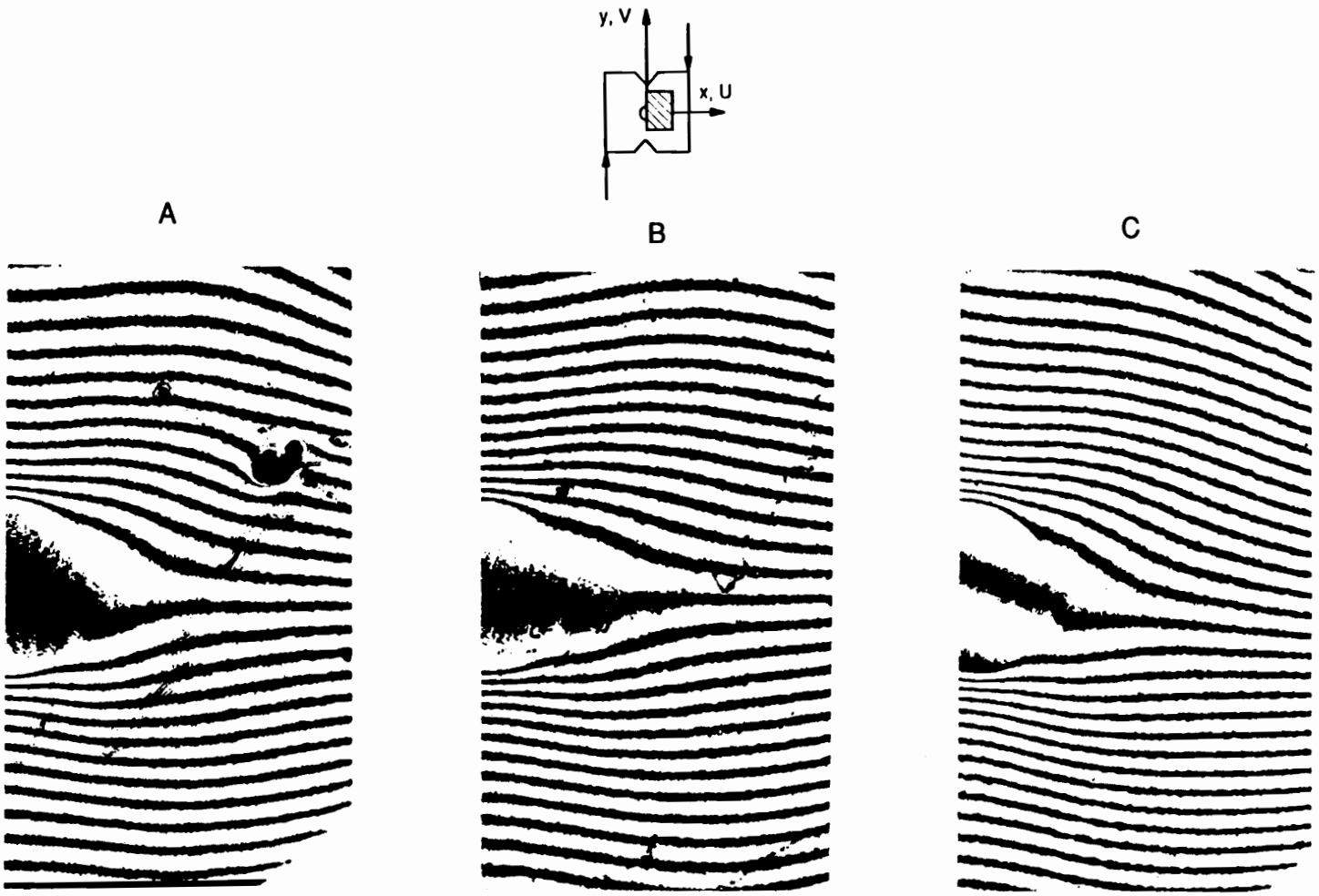

Figure 53. Fringe pattern depicting the horizontal displacement (U) for all three specimens under shear; one-half of the displacement contour is shown in each case.

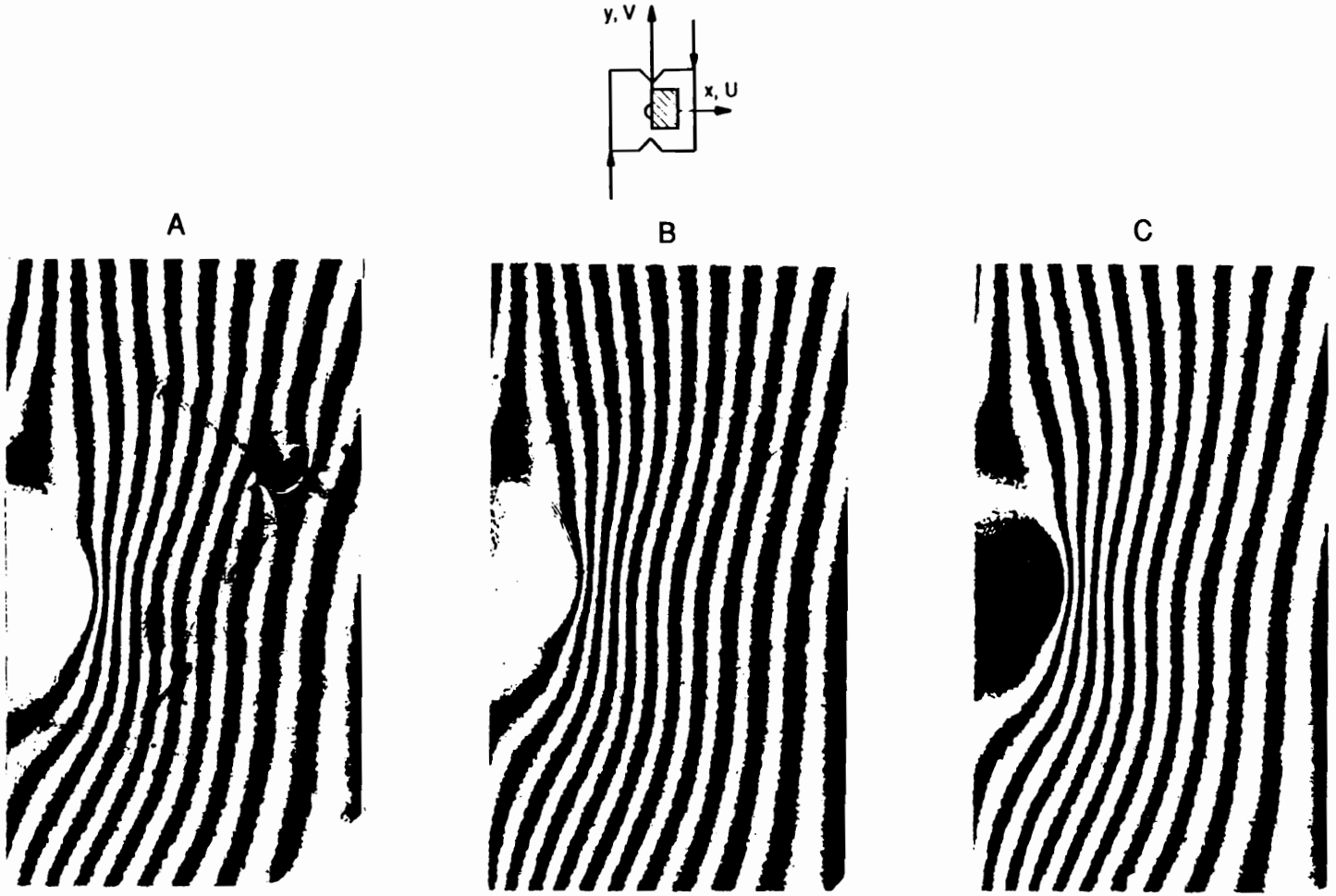

Figure 54. Fringe pattern depicting the vertical displacement (V) for all three specimens under shear; one-half of the displacement contour is shown in each case.

8.0 Closure

8.1 Conclusions

A survey of available literature on interphase definition, characterization and modeling (Chapters 1, 2 and 3) indicates that the interaction between the fiber and matrix in a composite may result in property gradients in the interphase. The interphasial properties that are affected include the elastic moduli and the coefficients of thermal expansion among others.

In the absence of definitive data on the property gradients in the interphase, a model was proposed in Chapter 4 for the interphase properties in fiber-reinforced thermosets. This was a simple model based on the models already available in the literature for polymer matrix composites. The interphase was assumed to be isotropic and its Young's modulus and coefficient of thermal expansion were assumed to be functions of distance from the fiber. Three different functional forms — Power variation, Reciprocal variation and Cubic variation — were considered. The Poisson's ratio of the interphase was assumed to be the same as that of the matrix.

The influence of a distinct interphase region on the residual thermal stresses in a composite was studied in Chapter 5. The residual thermal stresses in the constituents (fiber, interphase, and matrix) of a fiber-reinforced epoxy were predicted using a concentric cylinder assemblage analysis. All three functional forms were considered for the interphase properties. The Navier's equations of elasticity were solved in "closed-form" for each type of property variation. A parametric study was used to demonstrate the fact that changes in the interphase properties can drastically alter the residual thermal stress state in the interphase. This is important to the structural performance of a composite since residual thermal stresses affect fiber/matrix adhesion. It was also shown that changing the type of property variation results in only modest changes in the constituent stress state.

The influence of a distinct interphase region on the local stresses in a composite under thermo-mechanical loading situations was considered in Chapter 6. The *non-dilute* local stresses in the constituents (fiber, interphase, and matrix) of a fiber-reinforced epoxy were predicted using a Mori-Tanaka analysis. The interphase properties were assumed to vary according to the Power variation and the Navier's equations of elasticity were solved in "closed-form" for each loading condition. A parametric study was used to demonstrate the fact that changes in the interphase properties can drastically alter the stress state in the interphase.

An experimental study utilizing model composites was considered in Chapter 7 in an attempt to verify parts of the analysis. A simple linear variation in interphasial Young's modulus was considered. A model composite system consisting of a coated glass rod embedded in Epon 828 was considered. Coatings were applied to the glass rod in succession to simulate two different interphasial regions. The model composite specimens were loaded in compression and shear, perpendicular to the fiber direction, and the resulting in-plane displacements were measured by the use of the Moire interferometry technique. Differences in displacement fields between the various specimens, due to the presence of interphasial regions, were found to be minimal. More experimental work should be performed to be able to measure point-wise displacements in the interphasial (coatings) region.

In summary, a theoretical model which provides a better representation of the interphase properties has been proposed. A simple analytical treatment of a polymer matrix composite under different loading conditions shows the dependency of local stresses on interphasial properties. A proper choice of the interphase thickness, Young's modulus and coefficient of thermal expansion can be used to control local stress components of interest. A novel experiment to study the effect of interphasial properties on local displacements in a model composite was conducted. Preliminary results indicate the need for more sensitive measurements. Thus, the package presented in this dissertation, as summarized schematically in Figure 55, provides a firm foundation for future theoretical and experimental interphase studies.

8.2 Future Work

The interphase property models should be incorporated into stress analyses for composite materials that take into account fiber-fiber interaction through a regular arrangement of fibers (hexagonal or square array) or a random arrangement of fibers. These analyses will provide the means to study the effect of interphasial property gradients in composites with higher (0.5 and more) fiber volume fractions.

It would be highly desirable to measure material properties of the interphase as a function of distance from the fiber. Several recent attempts in this direction appear promising, but much more needs to be done. Advances in the areas of bone mechanics, adhesive joints and tunneling microscopy may serve as starting points for advances in interphasial property measurement.

Model composite experiments along with the Moire interferometry technique remains an attractive option to investigate interphasial displacements. A more sensitive Moire

interferometry technique or specimens with thicker coatings may provide the means to measure pointwise displacements in the coating regions.

The ideas behind the interphase model reported in this study can be

- used to provide guidance for controlling local failures in a composite with interphasial property gradients,
- used for the design and optimization of such material systems,
- used to assess the influence of
  - fiber surface coatings,
  - fiber-matrix chemical interactions, and
  - morphological variations in regions of the matrix material

  on the local stress state, and
- extended to metal matrix and ceramic matrix composites with suitable modifications to the input properties.

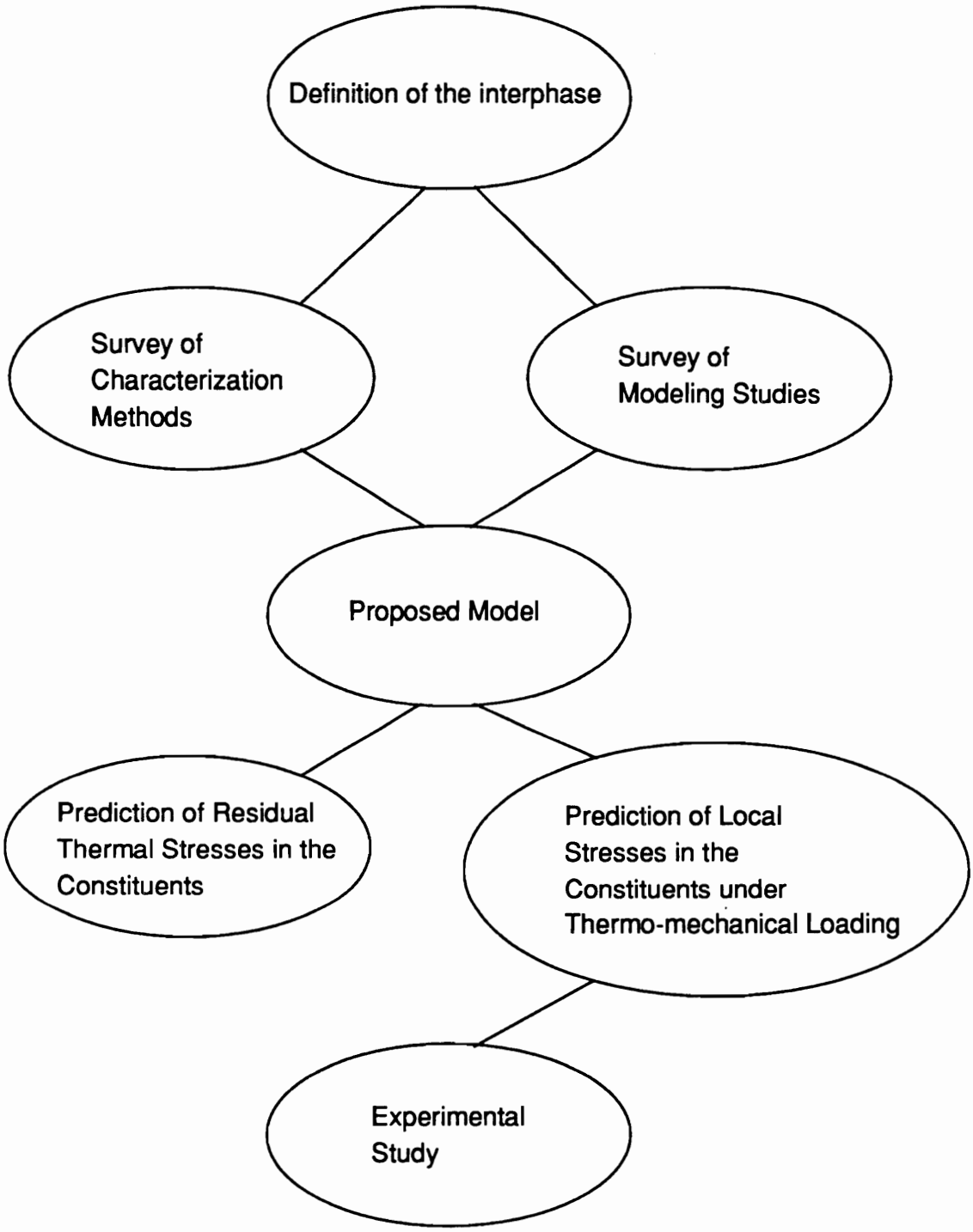

Figure 55. Schematic summary of the nature of this study.

References

1. E. P. Plueddemann, ed., Interfaces in Polymer Matrix Composites, Academic Press, 1974.
2. D. W. Petrasek and J. W. Weeton, "Effects of Alloying on Room-Temperature Tensile Properties of Tungsten-Fiber-Reinforced-Copper-Alloy Composites," *Transactions of the AIME*, Vol. 230, pp. 977-990, 1964.
3. J. J. Brennan, "Interfacial Characterization of Glass and Glass-Ceramic Matrix/Nicalon SiC Fiber Composites," in Tailoring Multiphase and Composite Ceramics, R. E. Tressler, G. L. Messing, C. G. Pantano and R. E. Newnham, eds., Plenum Publishing Co., pp. 549-560, 1985.
4. R. Swain, K. L. Reifsnider, K. Jayaraman and M. El-Zein, "Interface/Interphase Concepts in Composite Material Systems," *Journal of Thermoplastic Composites*, Vol. 3, pp. 13-23, 1990.
5. L. T. Drzal, M. J. Rich and P. F. Lloyd, "Adhesion of Graphite Fibers to Epoxy Matrices: I. The Role of Fiber Surface Treatment," *Journal of Adhesion*, Vol. 16, pp. 1-30, 1982.
6. S. M. Lee, Dictionary of Composite Materials Technology, Technomic Publishing Co., 1989.
7. L. T. Drzal, M. J. Rich, M. F. Koenig and P. F. Lloyd, "Adhesion of Graphite Fibers to Epoxy Matrices: II. The Effect of Fiber Finish," *Journal of Adhesion*, Vol. 16, pp. 133-152, 1983.

8. I. Verpoest, M. Desaeger, J. Ivens, "The Influence of the Fiber-Matrix Interface on Damage Development in Composite Materials," *Proceedings of the Colloquium on Interfaces in Materials*, Brussels, Dec. 1988.

9. L. T. Drzal, "Composite Interphase Characterization," *SAMPE Journal*, Vol.19, pp. 7-13, 1983.

10. A. G. Metcalfe, ed., Interfaces in Metal Matrix Composites, Academic Press, 1974.

11. R. J. Kerans, R. S. Hay, N. J. Pagano and T. A. Parthasarathy, "The Role of Fiber-Matrix Interface in Ceramic Composites," *Ceramic Bulletin*, Vol. 68, pp. 429-442, 1989.

12. P. W. Erickson, A. Volpe and E. R. Cooper, "Effects of Glass Surfaces on Laminating Resins," *Modern Plastics*, pp. 141-146 and 181-184, August 1964.

13. A. G. Metcalfe, "Interaction and Fracture of Titanium-Boron Composites," *Journal of Composite Materials*, Vol. 1, pp. 356-365, 1967.

14. L. H. Sharpe, "Some Thoughts About the Mechanical Response of Composites," *Journal of Adhesion*, Vol. 6, pp. 15-21, 1974.

15. N. R. Sottos, R. L. McCullough and S. I. Güçeri, "Thermal Stresses Due to Property Gradients at the Fiber/Matrix Interface," in Mechanics of Composite Materials and Structures, J. N. Reddy and J. L. Teply, eds., American Society of Mechanical Engineers, pp. 11-20, 1989.

16. H. C. Tsai, A. M. Arocho and L. W. Gause, "Prediction of Fiber-Matrix Interphase Properties and their Influence on Interface Stress, Displacement and Fracture Toughness of Composite Material," *Materials Science and Engineering*, Vol. A126, pp. 295-304, 1990.

17. H. Ishida and J. L. Koenig, eds., Composite Interfaces, Elsevier Science Publishing Co., 1986.

18. H. Ishida, ed., Interfaces in Polymer, Ceramic and Metal Matrix Composites, Elsevier Science Publishing Co., 1988.

19. H. Ishida, ed., Controlled Interphases in Composite Materials, Elsevier Science Publishing Co., 1990.

20. B. A. Lerch, D. R. Hull and T. A. Leonhardt, "Microstructure of a SiC/Ti-15-3 Composite," *Composites*, Vol. 21, pp. 216-224, 1990.

21. J. Peacock, B. Fife, E. Nield and R. A. Crick, "Examination of the Morphology of Aromatic Polymer Composite (APC-2) Using an Etching Technique," in Composite Interfaces, H. Ishida and J. L. Koenig, eds., Elsevier Science Publishing Co., pp. 299-306, 1986.

22. J. J. Brennan, "Interfacial Chemistry and Bonding in Fiber Reinforced Glass and Glass-Ceramic Matrix Composites," in Ceramic Microstructures '86: Role of Interface, J. A. Pask and A. G. Evans, eds., Plenum Publishing, pp. 387-399, 1988.

23. J. J. Brennan, "Interfacial Characteristics of Glass-Ceramic Matrix/SiC Fiber Composites," *Journal De Physique*, Vol. 49, pp. C5-791 to C5-809, 1988.

24. P. K. Hansma and J. Tersoff, "Scanning Tunneling Microscopy," *Journal of Applied Physics*, Vol. 16, No. 2, pp. R1-R23, 1987.

25. L. C. Feldman and J. W. Mayer, Fundamentals of Surface and Thin Film Analysis, Elsevier Science Publishing Co., 1986.

26. T. J. Shaffner, "New Developments in Surface Characterization Techniques for the Semiconductor Industry," *Surface and Interface Analysis*, Vol. 14, pp. 598-606, 1989.

27. E. Occhiello, F. Garbassi, M. Morra, "Spectroscopic Characterization of Interfaces in Polymer Composites," *Composites Science and Technology*, Vol. 36, pp. 133-151, 1989.

28. J. L. Thomason and J. B. W. Morsink, "Investigation of the Interphase in Glass-Fibre-Reinforced Epoxy Composites," in Interfaces in Polymer, Ceramic and Metal Matrix Composites, H. Ishida, ed., Elsevier Science Publishing Co., pp. 503-512, 1988.

29. C. R. Bacon, J. G. Williams and B. C. Cornilsen, "Interphase Chemistry via Micro-Raman Spectroscopy," *Proceedings of the Fifth Technical Conference of the American Society for Composites*, Technomic Publishing Co., pp. 137-143, 1990.

30. C. C. Chamis, "Mechanics of Load Transfer at the Fiber/Matrix Interface," NASA TN D-6588, 1972.

31. B. Z. Jang, L. R. Hwang and Y. K. Lieu, "The Assessment of Interfacial Adhesion in Fibrous Composites," in Interfaces in Metal-Matrix Composites, A. K. Dhingra and S. K. Fishman, eds., Metallurgical Society of the AIME, pp. 95-109, 1986.

32. M. Narkis, E. J. H. Chen and R. B. Pipes, "Review of Methods for Characterization of Interfacial Fiber-Matrix Interactions," *Polymer Composites*, Vol. 9, pp. 245-251, 1988.

33. A. R. Sanadi and M. R. Piggott, "Interfacial Effects in Carbon-Epoxies - Part 1: Strength and Modulus with Short Aligned Fibers," *Journal of Materials Science*, Vol. 20, pp. 421-430, 1985.

34. M. R. Piggott, "The Effect of the Interface/Interphase on Fiber Composite Properties," *Polymer Composites*, Vol. 8, pp. 291-297, 1987.

35. J. F. Mandell, D. H. Grande, T. -H. Tsiang and F. J. McGarry, "Modified Microdebonding Test for Direct *in-situ* Fiber/Matrix Bond Strength Determination in Fiber Composites," in Composite Materials: Testing and Design, ASTM STP 893, J. M. Whitney, ed., American Society for Testing and Materials, pp. 87-108, 1986.

36. El. M. Asloun, M. Nardin and J. Schultz, "Stress Transfer in Single-Fiber Composites: Effect of Adhesion, Elastic Modulus of Fiber and Matrix, and Polymer Chain Mobility," *Journal of Materials Science*, Vol. 24, pp. 1835-1844, 1989.

37. N. R. Sottos, W. R. Scott and R. L. McCullough, "Micro-Interferometry for Measurement of Thermal Displacements at Fiber/Matrix Interfaces," *Experimental Mechanics*, Vol. 31, pp. 98-103, 1991.

38. N. R. Sottos, The Influence of Interphase Regions on Local Thermal Stresses and Deformations in Composites, Ph.D. Dissertation, Department of Mechanical Engineering, University of Delaware, Newark, Delaware, 1990.

39. M. R. James, W. L. Morris and B. N. Cox, "A High Accuracy Automated Strain-field Mapper," *Experimental Mechanics*, Vol. 30, pp. 60-67, 1990.

40. M. R. James, W. L. Morris, B. N. Cox and M. S. Dadkhah, "Description and Application of Displacement Measurements Based on Digital Image Processing," AMD-Vol. 102, Micro-

mechanics: Experimental Techniques, W. N. Sharpe, Jr., ed., The American Society of Mechanical Engineers, pp. 89-99, 1989.

41. J. G. Williams, M. E. Donnellan, M. R. James and W. L. Morris, "Elastic and Inelastic Deformations in the Interphase in Organic Matrix Composites," *Proceedings of the Fifth Technical Conference of the American Society for Composites*, Technomic Publishing Co., pp. 127-136, 1990.
42. J. G. Williams, M. E. Donnellan, M. R. James and W. L. Morris, "Properties of the Interphase in Organic Matrix Composites," *Materials Science and Engineering*, Vol. A126, pp. 305-312, 1990.
43. J. F. Mandell, K. C. C. Hong and D. H. Grande, "Interfacial Shear Strength and Sliding Resistance in Metal and Glass-Ceramic Matrix Composites," *Ceramic Engineering and Science Proceedings*, Vol. 8, pp. 937-940, 1987.
44. G. C. Knollman, "Variation of Shear Modulus Through the Interfacial Bond Zone of an Adhesive," *International Journal of Adhesion and Adhesives*, Vol. 5, pp. 137-141, 1985.
45. W. C. Van Buskirk, S. C. Cowin and R. N. Ward, "Ultrasonic Measurement of Orthotropic Elastic Constants of Bovine Femoral Bone," *Journal of Biomechanical Engineering*, Vol. 103, pp. 67-72, 1981.
46. I. Jasiuk and Y. Tong, "The Effect of Interface on the Elastic Stiffness of Composites," in Mechanics of Composite Materials and Structures, J. N. Reddy and J. L. Teply, ed., American Society of Mechanical Engineers, pp. 49-54, 1989.
47. J. D. Achenbach and H. Zhu, "Effect of Interphases on Micro and Macromechanical Behavior of Hexagonal-Array Fiber Composites," *Journal of Applied Mechanics*, Vol. 57, pp. 956-963, 1990.
48. J. A. Nairn, "Thermoelastic Analysis of Residual Stresses in Unidirectional, High-Performance Composites," *Polymer Composites*, Vol. 6, pp. 123-130, 1985.
49. K. H. Lo, R. W. Schmitz and W. G. Gottenberg, "Determination of Flexible Interlayer Thickness for Fiber Reinforced Composites," *Proceedings of the Materials Research Society Symposium*, Materials Research Society, Vol. 170, pp. 55-58, 1990.

50. W. Zhang, "Computation of Stress Fields in Unidirectional n-Phase Fibrous Composites under Longitudinal and Transverse Loads," *Computers and Structures*, Vol. 34, pp. 647-653, 1990.

51. D. E. Bowles, "Micromechanics Thermal Stress Analysis of Composites for Space Structure Applications," *Proceedings of the Symposium on the Mechanics of Composites at Elevated and Cryogenic Temperatures*, American Society of Mechanical Engineers, 1991.

52. B. J. Sullivan and Z. Hashin, "Determination of Mechanical Properties of Interfacial region Between Fiber and Matrix in Organic Matrix Composites," Controlled Interphases in Composite Materials, H. Ishida, ed., Elsevier Science Publishing Co., pp. 521-537, 1990.

53. Y. P. Qiu and G. J. Weng, "Elastic Modulus of Thickly Coated Particle and Fiber-Reinforced Composites," *Journal of Applied Mechanics*, Vol. 58, pp. 388-398, 1991.

54. Y. Mikata and M. Taya, "Stress Field in a Coated Continuous Fiber Composite Subjected to Thermo-Mechanical Loadings," *Journal of Composite Materials*, Vol. 19, pp. 554-578, 1985.

55. G. P. Tandon and N. J. Pagano, "A Study of Fiber-Matrix Interfacial Modeling," *Proceedings of the Fourth Japan-U.S. Conference on Composite Materials*, Technomic Publishing Co., pp. 191-200, 1988.

56. N. J. Pagano and G. P. Tandon, "Elastic Response of Multidirectional Coated-fiber Composites," *Composites Science and Technology*, Vol. 31, pp. 273-293. 1988.

57. N. J. Pagano and G. P. Tandon, "Thermo-elastic Model for Multidirectional Coated-Fiber Composites: Traction Formulation," *Composites Science and Technology*, Vol. 38, pp. 247-269, 1991.

58. Y. Benveniste, G. J. Dvorak and T. Chen, "Stress Fields in Composites with Coated Inclusions," *Mechanics of Materials*, Vol. 7, pp. 305-317, 1989.

59. J. D. Eshelby, "The Determination of the Elastic Field of an Ellipsoidal Inclusion, and Related Problems," *Proceedings of the Royal Society of London*, Vol. A241, pp. 376-396, 1957.

60. J. D. Eshelby, "The Elastic Field Outside an Ellipsoidal Inclusion," *Proceedings of the Royal Society of London*, Vol. A252, pp. 561-569, 1959.

61. T. Mori and K. Tanaka, "Average Stress in Matrix and Average Elastic Energy of Materials with Misfitting Inclusions," *Acta Metallurgica*, Vol. 21, pp. 571-574, 1973.

62. Y. Tong and I. Jasiuk, "Transverse Elastic Moduli of Composites Reinforced With Cylindrical Coated Fibers: Successive Iteration Method," *Proceedings of the Fifth Technical Conference of the American Society for Composites*, Technomic Publishing Co., pp. 117-126, 1990.

63. M. Vedula, R. N. Pangborn and R. A. Queeney, "Modifications of Residual Thermal Stress in a Metal-Matrix Composite With the Use of a Tailored Interfacial Region," *Composites*, Vol. 19, pp. 133-137, 1988.

64. S. M. Arnold, V. K. Arya and M. M. Melis, "Elastic/Plastic Analyses of Advanced Composites Investigating the Use of the Compliant Layer Concept in Reducing Residual Stresses Resulting from Processing," NASA TM-103204, 1990.

65. L. J. Ghosn and B. A. Lerch, "Optimum Interface Properties for Metal Matrix Composites," NASA TM-102295, 1989.

66. J. J. Caruso, C C. Chamis and H. C. Brown, "Parametric Studies to Determine the Effect of Compliant Layers on Metal Matrix Composite Systems," NASA TM-102465, 1990.

67. M. Morel, D. A. Saravanos and C. C. Chamis, "Interphase Layer Optimization for Metal Matrix Composites With Fabrication Considerations," NASA TM-105166, 1991.

68. P. W. Erickson, A. Volpe and E. R. Cooper, "Effects of Glass Surfaces on Laminating Resins," *Modern Plastics*, pp. 141-146 and 184-188, August 1964.

69. G. A. Van Fo Fy, "A Study of the Effect of Fiber Treatment on Stress Distribution in Glass-Reinforced Plastic Structures," *Prikladnaya Mekhanika*, Vol. 3, pp. 106-112, 1967.

70. L. T. Drzal, M. J. Rich, M. F. Koenig and P. F. Lloyd, "Adhesion of Graphite Fibers to Epoxy Matrices: II. The Effect of Fiber Finish," *Journal of Adhesion*, Vol. 16, pp. 133-152, 1983.

71. P. S. Theocaris, "On the Evaluation of Adhesion between Phases in Fiber Composites," *Colloid and Polymer Science*, Vol. 262, pp. 929-938, 1984.

72. Y. Lipatov, Physical Chemistry of Filled Polymers, Rubber and Plastics Research Association of Great Britain, United Kingdom, 1979.

73. P. S. Theocaris, E. P. Sideridis and G. C. Papanicolaou, "The Elastic Longitudinal Modulus and Poisson's Ratio of Fiber Composites," *Journal of Reinforced Plastics and Composites*, Vol. 4, pp. 396-418, 1985.

74. P. S. Theocaris, G. C. Papanicolaou and G. D. Spathis, "Physical Model For the Thermal Expansion Behaviour of Fibre-Reinforced Viscoelastic Composites," *Fibre Science and Technology*, Vol. 15, pp. 187-197, 1981.

75. P. S. Theocaris and A. G. Varias, "Accurate Evaluation of the Transverse Shear Modulus in Unidirectional Fibrous Composites, " *Rheologica Acta*, Vol. 26, pp. 182-192, 1987.

76. P. S. Theocaris and A. G. Varias, "The Shear Modulus in the Fiber Direction of Unidirectional Fiber Composites Based on the Concept of Mesophase, " *Rheologica Acta*, Vol. 26, pp. 322-327, 1987.

77. E. Sideridis, "The In-plane Shear Modulus of Fiber Reinforced Composites as Defined By the Concept of Interphase," *Composites Science and Technology*, Vol. 31, pp. 35-53, 1988.

78. P. S. Theocaris, "Synergism Phenomena Between Phases in Composites: The Mesophase," *Colloid and Polymer Science*, Vol. 265, pp. 461-480, 1987.

79. G. R. Palmese, Origin and Influence of Interphase Material Property Gradients in Thermosetting Composites, Ph.D. Dissertation, Department of Chemical Engineering, University of Delaware, Newark, Delaware, 1991.

80. L. Penn, F. Bystry, W. Karp and S. Lee, "Aramid/Epoxy vs. Graphite/Epoxy: Origin of the Difference in Strength at the Interface," in *Molecular Characterization of Composite Interfaces*, H. Ishida and G. Kumar, eds., Plenum Press, New York, pp. 93-109, 1985.

81. B. Z. Jang, L. R. Hwang and Y. K. Lieu, "The Assessment of Interfacial Adhesion in Fibrous Composites," in *Interfaces in Metal-Matrix Composites*, A. K. Dhingra and S. K. Fishman, eds., Metallurgical Society of the AIME, pp. 95-109, 1986.

82. J. Kalantar and L. T. Drzal, "The Bonding Mechanism of Aramid Fibres to Epoxy Matrices: Part II - An Experimental Investigation," *Journal of Materials Science*, Vol. 25, pp. 4194-4202, 1990.

83. J. Banbaji, "On a More Generalized Theory of the Pull-Out Test from an Elastic Matrix: Part I - Theoretical Considerations," *Composites Science and Technology*, Vol. 32, pp. 183-193, 1988.

84. J. Banbaji, "On a More Generalized Theory of the Pull-Out Test from an Elastic Matrix: Part II - Application to a Polypropylene-Cement System," *Composites Science and Technology*, Vol. 32, pp. 195-207, 1988.

85. Z. Hashin and B. W. Rosen, "The Elastic Moduli of Fiber-Reinforced Materials," *Journal of Applied Mechanics*, Vol. 31, pp. 223-232, 1964; Errata, Vol. 32, p. 219, 1965.

86. S. L. Ross, *Differential Equations*, Blaisdell Publishing Company, New York, 1964.

87. D. E. Johnson and J. R. Johnson, *Mathematical Methods in Engineering and Physics*, Prentice-Hall, Inc., Englewood Cliffs, NJ, 1982.

88. MACSYMA, *A Computer Algebra System and Programming Environment*, Symbolics, Inc., Burlington, MA, 1988.

89. J. J. Caruso and C. C. Chamis, "Assessment of Simplified Composite Micromechanics Using Three-Dimensional Finite Element Analysis," *Journal of Composites Technology & Research*, Vol. 8, pp. 77-83, 1986.

90. *Data Manual for Kevlar 49 Aramid*, E. I. Du Pont de Nemours & Co., Inc., 1986.

91. S. Rojstaczer, D. Cohn and G. Marom, "Thermal Expansion of Kevlar Fibres and Composites," *Journal of Materials Science Letters*, Vol. 4, pp. 1233-1236, 1985.

92. M. S. Madhukar and L. T. Drzal, "Fiber-Matrix Adhesion and Its Effect on Composite Mechanical Properties: I. Inplane and Interlaminar Shear Behavior of Graphite/Epoxy Composites," *Journal of Composite Materials*, Vol. 25, pp. 932-957, 1991.

93. M. S. Madhukar and L. T. Drzal, "Fiber-Matrix Adhesion and Its Effect on Composite Mechanical Properties: II. Longitudinal (0°) and Transverse (90°) Tensile and Flexure Behavior of Graphite/Epoxy Composites," *Journal of Composite Materials*, Vol. 25, pp. 958-991, 1991.

94. T. Norita, J. Matsui and H. S. Matsuda, "Effect of Surface Treatment of Carbon Fiber on Mechanical Properties of CFRP," in Composite Interfaces, H. Ishida and J. L. Koenig, eds., Elsevier Science Publishing Co., pp. 123-132, 1986.

95. T. Mura, *Micromechanics of Defects in Solids*, Martinus-Nijhoff Publishers, The Hague, 1982.

96. Y. Benveniste, "A New Approach to the Application of Mori-Tanaka's Theory in Composite Materials," *Mechanics of Materials*, Vol. 6, pp. 147-157, 1987.

97. N. J. Pagano, "The Stress Field in a Cylindrically Anisotropic Body under Two-Dimensional Surface Tractions," *Journal of Applied Mechanics*, Vol. 39, pp. 791-796, 1972.

98. R. M. Christensen and K. H. Lo, "Solutions for Effective Shear Properties in Three Phase Sphere and Cylinder Models," *Journal of the Mechanics and Physics of Solids*, Vol. 27, pp. 315-330, 1979.

99. MATHEMATICA, *A System for Doing Mathematics by Computer*, Wolfram Research, Inc., Champaign, IL, 1988.

100. T. Koufopoulos and P. S. Theocaris, "Shrinkage Stresses in Two-Phase Materials," *Journal of Composite Materials*, Vol. 3, pp. 308-320, 1968.

101. I. M. Daniel and A. J. Durelli, "Shrinkage Stresses Around Rigid Inclusions," *Experimental Mechanics*, Vol. 2, pp. 240-244, 1962.

102. R. H. Marloff and I. M. Daniel, "Three-dimensional Photoelastic Analysis of a Fiber-Reinforced Composite Model," *Experimental Mechanics*, Vol. 9, pp. 156-162, 1969.

103. N. K. Asamoah and W. G. Wood, "Thermal Self-Straining of Fibre-Reinforced Materials," *Journal of Strain Analysis*, Vol. 5, pp. 88-97, 1970.

104. P. Ifju, "Experimental Investigation of a Square Array Fiber-Reinforced Composite Model With Transverse Compression," Project Report, Virginia Polytechnic Institute and State University, Blacksburg, Virginia, 1990.

105. P. D. McLean, A. Garton and W. T. K. Stevenson, "Improved Epoxy-Amine Matrices for Composites," *Polymer Composites*, Vol. 7, pp. 330-336, 1986.

106. A. Garton and G. S. Haldankar, "Modification of Free Volume in Epoxy Adhesive Formulations," *Journal of Adhesion*, Vol. 29, pp. 13-26, 1989.

107. A. Garton, G. S. Haldankar and E. Shockey, "The Production of Modulus Gradients at Interfaces," Proceedings of the Materials Research Society Symposium, Vol. 170, pp. 291-296, 1990.

108. P. Ifju, The Shear Gage and Compact Shear Specimen for Shear Property Measurements of Composite Materials, Ph. D. Dissertation, Materials Engineering Science Program, Virginia Polytechnic Institute and State University, Blacksburg, Virginia, 1992.

109. D. Post, "Moire Interferometry," in Handbook on Experimental Mechanics, A. S. Kobayashi, ed., Society for Experimental Mechanics, pp. 314-387, 1987.

110. D. Post, "Moire Interferometry for Composites," in Manual on Experimental Methods for Mechanical Testing of Composites, R. E. Pendleton and M. E. Tuttle, eds., Society for Experimental Mechanics, pp. 67-80, 1989.

111. J. M. Slepetz, T. F. Zagaeski and R. F. Novello, "In-plane Shear Test for Composite Materials," AMMRC TR 78-30, 1978.

112. B. Han, Extension of Moire Interferometry into the Ultra-high Sensitivity Domain, Ph. D. Dissertation, Department of Engineering Science and Mechanics, Virginia Polytechnic Institute and State University, Blacksburg, Virginia, 1991.

Vita

The author was born to Saraswathy and Rajagopalan Jayaraman on 13th May 1962, in Tiruchirapalli, Tamil Nadu, India. He grew up in Thanjavur, Tamil Nadu, where he received his elementary and high school education.

He attended P. S. G. College of Technology, Coimbatore, Tamil Nadu, which was affiliated to the University of Madras. He obtained a Bachelor's degree in Mechanical Engineering with honors in May 1984. Subsequently, he entered Howard University, Washington, D. C. and obtained a Master's degree in Mechanical Engineering (Applied Mechanics) in December 1986.

The author has been enrolled in the Ph. D. program in Engineering Mechanics at Virginia Polytechnic Institute & State University, Blacksburg, VA since January 1987. He plans to do postdoctoral research in Engineering Mechanics at Virginia Polytechnic Institute & State University after graduation.